UNIVERSIDADE ESTADUAL PAULISTA
"Julio de Mesquita Filho"
INSTITUTO DE BIOCIÊNCIAS DE BOTUCATU

EFEITO DO IMUNOMODULADOR P-MAPA ASSOCIADO À INTERLEUCINA-12 SOBRE A VIA DE SINALIZAÇÃO DOS RECEPTORES *TOLL-LIKE* E AGRESSIVIDADE DAS CÉLULAS SKOV-3 DE CARCINOMA OVARIANO HUMANO

LUIZ ANTONIO LUPI JÚNIOR

BOTUCATU – SP
2020

Programa de Pós-graduação em Biologia Geral e Aplicada
Instituto de Biociências de Botucatu/ UNESP
Rua Professor Doutor Antonio Celso Wagner Zanin, 250 - CEP 18618-689 - Botucatu - SP - Brasil
Tel (14) 3880-0781 posgraduacao@ibb.unesp.br

Instituto de Biociências

UNIVERSIDADE ESTADUAL PAULISTA
"JÚLIO DE MESQUITA FILHO"
Campus de Botucatu

PG-BGA

EFEITO DO IMUNOMODULADOR P-MAPA ASSOCIADO À INTERLEUCINA-12 SOBRE A VIA DE SINALIZAÇÃO DOS RECEPTORES *TOLL-LIKE* E AGRESSIVIDADE DAS CÉLULAS SKOV-3 DE CARCINOMA OVARIANO HUMANO

LUIZ ANTONIO LUPI JÚNIOR

PROF. DR. LUIZ GUSTAVO DE ALMEIDA CHUFFA

PROFª. DRª. FLÁVIA KARINA DELELLA

Tese apresentada ao Instituto de Biociências, Campus de Botucatu, UNESP, para obtenção do título de Doutor no Programa de Pós-Graduação em Biologia Geral e Aplicada, Área de concentração Biologia Celular e Estrutural

Orientador: Prof. Dr. Luiz Gustavo de Almeida Chuffa

BOTUCATU – SP

2020

Programa de Pós-graduação em Biologia Geral e Aplicada
Instituto de Biociências de Botucatu/ UNESP
Rua Professor Doutor Antonio Celso Wagner Zanin, 250 - CEP 18618-689 - Botucatu - SP - Brasil
Tel (14) 3880-0781 posgraduacao@ibb.unesp.br

FICHA CATALOGRÁFICA ELABORADA PELA SEÇÃO TÉC. AQUIS. TRATAMENTO DA INFORM.
DIVISÃO TÉCNICA DE BIBLIOTECA E DOCUMENTAÇÃO - CÂMPUS DE BOTUCATU - UNESP
BIBLIOTECÁRIA RESPONSÁVEL: ROSEMEIRE APARECIDA VICENTE-CRB 8/5651

Lupi Júnior, Luiz Antonio.
Efeito do imunomodulador P-MAPA associado à interleucina-12 sobre a via de sinalização dos receptores toll-like e agressividade das células SKOV-3 de carcinoma ovariana humano / Luiz Antonio Lupi Júnior. - Botucatu, 2020

Tese (doutorado) - Universidade Estadual Paulista "Júlio de Mesquita Filho", Instituto de Biociências de Botucatu
Orientador: Luiz Gustavo de Almeida Chuffa
Coorientador: Flávia Karina Delella
Capes: 20000006

1. Ovários - Tumores. 2. Interleucinas. 3. Receptores Toll-like. 4. Fatores imunológicos.

Palavras-chave: Câncer de ovário; IL-12; P-MAPA; SKOV-3; TLR.

Dedicatória

Dedico este trabalho àqueles que são a base da minha existência e alimentam diariamente minha força de vontade: Deus, meu filho Lorenzo, minha esposa Marcilene, minha mãe Cecília e para meu maior exemplo, que olha por todos nós diariamente ao lado de Deus, meu querido pai Lupi.

Agradecimentos

A Deus, por ter sempre me abençoado com disposição, energia, inteligência e saúde para produzir tudo que fosse necessário e mostrar o melhor caminho para que eu alcançasse meus objetivos.

Ao meu pai, por ter me dado educação, por ter investido tempo e dinheiro em meus sonhos, sempre acreditando que eu seria bem sucedido. Obrigado por ser exemplo, por sempre ter cuidado de mim e continuar olhando por nós e por toda a nossa família daí de cima. Você sempre será lembrado com muito amor.

À minha mãe, que ao lado de meu pai, me providenciou a melhor educação possível e foi meu porto seguro, sempre garantindo que tudo daria certo e que nada faltaria para mim e para minha família amada. Obrigado por ajudar a superar todo e qualquer momento de dificuldade e estar continuamente à disposição para qualquer chamado. Espero um dia poder retribuir toda a ajuda, o carinho e amor que nos deu.

À minha esposa Marcilene, minha companheira de lutas diárias, meu amor. Obrigado por acompanhar diariamente minha jornada, por abdicar de tudo para cuidar de mim e do nosso filho, por aceitar a aventura de viver em família. Obrigado por aceitar e superar as inúmeras dificuldades, as restrições e por dividir e comemorar as alegrias e conquistas comigo. Obrigado por me fazer ter certeza de que, independente de qualquer coisa, sempre posso contar com você para me dizer que tudo vai dar certo e que dias muito melhores virão. Obrigado por respeitar minhas escolhas e por viver cada dia na certeza de que Deus sempre irá nos abençoar.

Ao meu filho Lorenzo, essa criança iluminada, que eu amo com todas as minhas forças, muito além do que eu imaginei que poderia amar um dia. Obrigado por ser uma benção, por ser tão atento, delicado, amoroso, colaborativo, inteligente, curioso e aventureiro. Obrigado por me ensinar a ser mais simples, a amar mais, a observar mais os detalhes e a entender a importância de cada segundo, de cada sorriso, de cada gesto e atitude, de cada palavra e de cada aventura. Você é minha inspiração!

Às minhas irmãs, cunhados e sobrinhos queridos, que sempre acompanharam e apoiaram minhas escolhas e meu caminho. Obrigado por ser família, por fazerem eu me sentir apoiado e admirado sempre que precisei de uma palavra positiva ou de um gesto de carinho. Tenho certeza que posso contar com vocês para tudo.

Ao meu mestre, orientador, professor e amigo prof. Luiz Gustavo Chuffa. Obrigado por aceitar o desafio de ter um doutorando como seu primeiro orientado de pós-graduação. Obrigado por transformar minha carreira, por dar a oportunidade de fazer, produzir e saber mais. Por sempre se preocupar em ser melhor e fazer de nós cada vez melhores. O melhor líder é aquele

que lidera pelo exemplo e não existem dúvidas que se um dia eu tiver um pouco da sua sabedoria, da sua disposição e da sua capacidade de execução e produção estarei satisfeito.

À minha co-orientadora, professora Flávia Delella e sua equipe, por me acolher em seu laboratório de cultura celular e aceitar o desafio de ensinar as técnicas de cultivo desde o início, além de sempre contribuir para o crescimento do meu trabalho.

A todos os professores e servidores do departamento de Anatomia, que sempre foram companhia diária, sempre garantiram convivência leve e agradável e sempre proporcionaram muita sabedoria. Agradeço especialmente ao prof. Wílson, que me acolheu e orientou durante a iniciação científica e mestrado, me ensinando a base de ser bom aluno, escritor, pesquisador, colega e amigo, com ensinamentos que levarei para sempre.

Aos meus colegas de pós-graduação pela convivência diária, por todos os aprendizados e compartilhamento dos desafios diários, principalmente ao nosso grupo de pesquisa: Maira, Henrique, Letícia e Roberta. Especialmente agradeço ao meu grande companheiro Henrique, sempre disposto a ajudar, aprender e a oferecer uma palavra amiga ou garantir uma boa risada.

A todos os parceiros, amigos e colegas que cruzaram meu caminho e, de alguma forma, me ensinaram sobre a ciência, sobre a educação, o aprendizado, a sala de aula ou sobre a vida. Seria incapaz de ser quem eu sou, mesmo que pequeno, sem a passagem de vocês por minha existência.

Ao Instituto de Biociências, seção de pós-graduação e às agências de fomento e amparo à pesquisa – CAPES (Processo 0708/2018), CNPq (Processo 401040/2016-0) e FAPESP (Processo 2019/00906-6 e Processo 2016/03993-9) - pelo suporte estrutural e financeiro.

Sumário

Resumo

O câncer de ovário apresenta elevada incidência em mulheres nos períodos de pós-menopausa e, devido ao seu diagnóstico tardio e baixo prognóstico, é a quinta causa mais comum de morte por câncer em mulheres. A doença responde inicialmente aos tratamentos convencionais, retardando o crescimento da massa tumoral, porém, com o tempo, muitas mulheres desenvolvem quimioresistência, frequentemente relacionada ao processo inflamatório, e a doença recorre. As imunoterapias têm sido propostas como uma alternativa complementar ao tratamento dos tumores de ovário, apesar de sua eficácia ainda não estar totalmente comprovada. O imunomodulador P-MAPA (agregado polimérico de fosfolinoleato-palmitoleato de magnésio e amônio proteico) é um biopolímero que tem apresentado efeitos significativos sobre componentes do sistema imunológico, sendo capaz de estimular os receptores celulares *toll-like* (TLR), particularmente TLR2 e TLR4, e também a produção de linfócitos T, citocinas como a IL-2 e IFN-γ, além de promover o aumento da atividade das células *natural killers* (NKs). Por sua vez, a interleucina (IL)-12 tem sido administrada em pacientes com tumores sólidos, incluindo os de ovário, na tentativa de estimular a resposta inflamatória polarizada T *helper* 1 (Th1), aumentando a produção de interferon-gama (IFN-γ). No entanto, o efeito direto desses dois agentes imunoterapêuticos nas células do câncer de ovário, importante constituinte do microambiente tumoral, permanece sem ser estudado. Desta forma, o objetivo deste trabalho foi analisar o efeito dos tratamentos com P-MAPA e IL-12, isolados ou em associação, na tumorigenicidade e processo inflamatório na linhagem de células SKOV-3 de carcinoma ovariano. Apesar de não promoverem a morte celular, os compostos P-MAPA e IL-12 diminuíram a atividade metabólica das células em aproximadamente 20% quando administrados isoladamente ou em associação. A combinação P-MAPA+IL-12 diminuiu os níveis de MyD88, IRF3 e NF-κB, possivelmente reduzindo a quimioresistência ligada ao processo inflamatório mediado por TLRs. Além de reduzir os níveis de TLR2, a terapia com P-MAPA estimulou a secreção de IL-3, IL-9, IL-10, CCL22 e CCL5. Além disso, o P-MAPA aumentou significativamente a sensibilidade das células SKOV-3 ao paclitaxel. Finalmente, a análise proteômica global demonstrou o efeito da combinação P-MAPA+IL-12 na regulação de importantes proteínas estruturais e envolvidas em processos metabólicos e energéticos. Entre elas, proteínas envolvidas em junção celular, adesão focal metabolismo de RNA e função ribossomal tiveram seus níveis aumentados após tratamento com a associação P-MAPA+IL-12. Por sua vez, proteínas relacionadas à sinalização celular, processos mitocondriais e energéticos e à via de sinalização Wnt apresentaram-se diminuídas. Desta forma, a imunoterapia com P-MAPA e/ou IL-12 representa uma alternativa terapêutica promissora no combate ao câncer de ovário, demonstrando efeito direto nas células tumorais, além do efeito imunomodulatório já conhecido nas células do sistema imune.

Palavras-chave: câncer de ovário, SKOV-3, P-MAPA, IL-12, imunoterapia, TLR, proteoma.

Capítulo 1

Introdução

Ovários

Os ovários são órgãos ovóides pares, localizados na cavidade pélvica feminina. Estão normalmente localizados próximos à fixação do ligamento largo do útero nas paredes laterais da pelve. Fazem contato com as tubas uterinas e o útero, conectados pelo ligamento largo do útero, que por sua vez é formado por três partes: mesométrio, mesossalpinge e mesovário. São as gônadas femininas, responsáveis pela produção dos gametas femininos (oócitos), além de possuírem função de glândula endócrina, produzindo hormônios como o estrógeno e a progesterona. Antes da primeira ovulação, o ovário apresenta-se liso e róseo, porém torna-se branco-acinzentado e rugoso devido à fibrose e distorção progressiva decorrentes dos repetidos processos ovulatórios (DANGELO & FATTINI, 2007). A superfície do ovário é coberta por um epitélio germinativo, de tecido epitelial pavimentoso ou cúbico simples, seguida por uma camada de tecido conjuntivo denso, a túnica albugínea. Abaixo da túnica albugínea encontra-se a região cortical, onde predominam os folículos ovarianos, que são o conjunto do ovócito e das células que o envolvem. A parte mais interna do ovário contém tecido conjuntivo frouxo e um rico leito vascular, sendo denominada região medular (JUNQUEIRA & CARNEIRO, 2013).

Câncer de ovário: incidência, fatores de risco, classificação e tratamento

O câncer de ovário é o quinto tipo de câncer mais letal entre todos aqueles que acometem as mulheres, sendo o mais letal entre os cânceres que acometem o sistema genital feminino (SIEGEL *et al.*, 2019) (Figura 1). Estima-se que, até o final de 2019, serão diagnosticados 22.530 novos casos de câncer de ovário e ocorrerão 13.980 óbitos em decorrência da doença nos Estados Unidos (SIEGEL *et al.*, 2019). No Brasil, para cada ano do biênio (2018-2019) são previstos 6.150 novos casos da doença, que causou óbito de aproximadamente 3.771 mulheres no ano de 2016, segundo o Instituto Nacional do Câncer (INCA, 2019). Os sintomas relacionados ao câncer de ovário são comumente inespecíficos e costumam ser ignorados, ou tratados de forma a eliminar desconfortos. Os sintomas mais freqüentes são aumento do volume abdominal, dor abdominopélvica persistente, dificuldade na alimentação e aumento da urgência ou freqüência urinária (LEDERMAN *et al.*, 2013). Associado à inespecificidade dos sintomas, a falta de métodos de diagnóstico precoce para esse tipo de câncer resultam em um alto índice de pacientes diagnosticadas com a doença em estágio avançado, fato que está associado à alta taxa de mortalidade relacionada ao câncer de ovário (JESSMON *et al.*, 2017). De fato, quando as

mulheres são diagnosticadas precocemente, cerca de 90% sobrevive por período maior que cinco anos pós-diagnóstico. No entanto, a taxa de sobrevida após 5 anos do diagnóstico é de 65% para tumores em estágio II, 34% para tumores em estágio III e de apenas 15% para pacientes com tumor em estágio IV do desenvolvimento (USACH *et al.*, 2015).

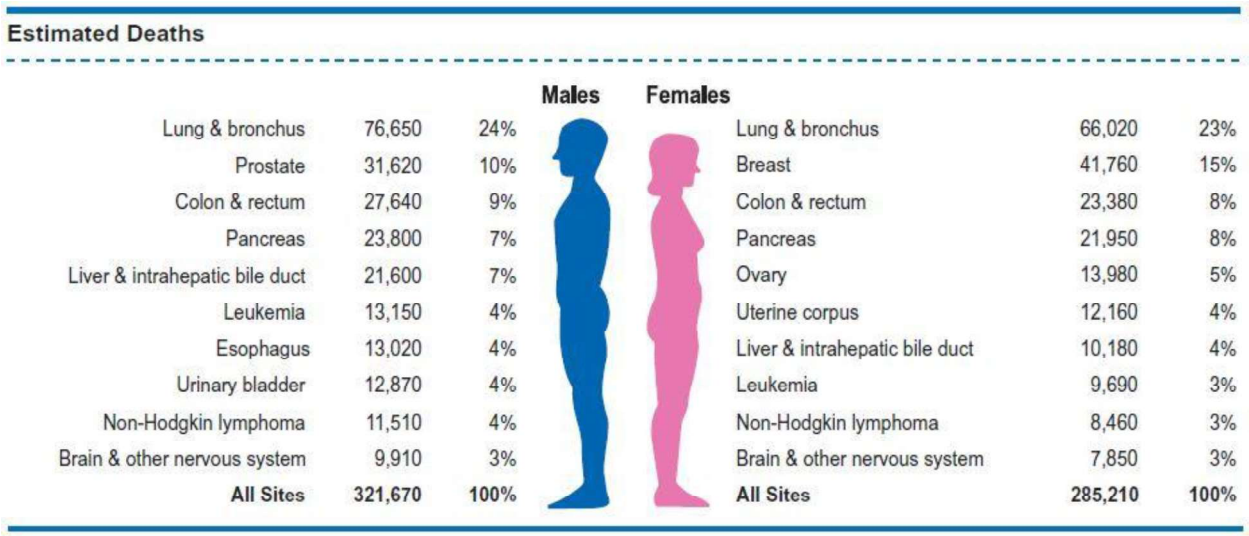

Figura 1. Estimativa dos dez tipos de câncer com maior número de mortes, por sexo, para o ano de 2019. O câncer de ovário figura como a quinta maior causa de morte em decorrência do câncer nas mulheres. Fonte: SIEGEL *et al.*, 2019.

O câncer de ovário é relativamente raro em mulheres com menos de 40 anos e, a partir dessa idade, o risco de desenvolvê-lo aumenta até atingir o pico de incidência por volta dos 70 anos de idade (WEBB *et al*., 2017). É bem estabelecido que mulheres com histórico familiar de câncer de ovário possuem maior risco de desenvolver a doença. O risco para aquelas que possuem pelo menos um parente de primeiro grau com diagnóstico dessa malignidade é aproximadamente três vezes maior comparado àquelas sem histórico familiar (STRATTON *et al.*, 1998). A presença de mutações no gene BRCA1 também parece favorecer o surgimento de tumores ovarianos, apresentando risco 40-50% maior em mulheres com idade próxima aos 70 anos, enquanto o risco associado a mutações do gene BRCA2 é de, aproximadamente, 10-20% (BOYD *et al.*, 2003). Outros conhecidos fatores de risco ao desenvolvimento do câncer de ovário são aqueles relacionados ao número de processos ovulatórios. Neste sentido, a menopausa tardia e a menarca precoce estão associadas à maior incidência da doença e o uso contínuo e combinado de contraceptivos orais parece funcionar como um fator protetor (WENTZENSEN *et al.*, 2016; WEBB *et al.*, 2017). Da mesma forma, a nuliparidade coloca as mulheres sob maior risco de desenvolvimento dessa patologia, enquanto aquelas com pelo menos uma gravidez bem sucedida possuem risco diminuído de forma proporcional ao número de filhos – probabilidade de 10-20% menor de ocorrência a cada filho nascido (WENTZENSEN *et al.*, 2016). Aliado a estas

evidências, a amamentação também diminui cerca de 20-25% o risco de surgimento do câncer de ovário, estando esse cada vez mais diminuído quanto maior o tempo de amamentação (LUAN *et al.*, 2013). Entre outros fatores, a terapia hormonal pós-menopausa, principalmente aquelas que usam exclusivamente estrógeno, e a presença de condições associadas a processos inflamatórios, como endometriose e síndrome do ovário policístico, estão correlacionados positivamente com a incidência de tumores ovarianos (WENTZENSEN *et al.*, 2016; WEBB *et al.*, 2017; LA VECCHIA *et al.*, 2017).

Segundo a classificação do Comitê de Oncologia Ginecológica da Federação Internacional de Ginecologia e Obstetrícia (FIGO), o câncer de ovário pode ser classificado em quatro estágios: estágio I, quando o tumor está confinado aos ovários; estágio II, quando o tumor acomete um ou ambos os ovários e apresenta extensão para a cavidade pélvica; estágio III, quando o tumor acomete um ou ambos os ovários, tem indícios cito ou histológicos de ter se disseminado para o peritônio abdominal e/ou promove metástase para os linfonodos retroperitoneais; estágio IV, quando o câncer apresenta metástases em órgãos mais distantes, além dos implantes peritoneais (DUSKA *et al.*, 2017; BEREK *et al.*, 2018). O câncer de ovário é, na verdade, um termo pouco específico usado para uma grande variedade de tumores que envolvem a gônada feminina. Pode ser classificado de três formas distintas: carcinoma epitelial, de células germinativas e de células estromais, dos quais o carcinoma epitelial é, de longe, o mais frequente e impactante (KROEGER *et al.*, 2017). Por muito tempo, as teorias mais aceitas para o surgimento e desenvolvimento desses tumores sugeriram que este se originava *de novo* ou devido às ovulações incessantes, que causam ciclos repetidos de lesão, inflamação e cicatrização. No entanto, a grande diversidade de aspectos clinicopatológicos e perfis moleculares dos diferentes tumores epiteliais que acometem o ovário levaram ao surgimento de um modelo dualístico de caracterização que acomodou a grande heterogeneidade de lesões, uma vez que tumores mais agressivos parecem se originar fora do órgão, principalmente nas tubas uterinas (KURMAN & SHIH, 2011). Desta forma, o grupo de tumores tipo I é composto por: carcinoma seroso de baixo grau, carcinoma endometrioide de baixo grau, carcinoma de células claras e carcinoma mucinoso, todos eles se desenvolvendo a partir de etapas bem definidas que se iniciam com uma lesão precursora, como tumores *borderline* ou endometriose (crescimento endometrial em regiões externas ao útero, como tubas uterinas e ovários). Tumores do tipo I caracterizam-se por apresentarem crescimento lento, desprovido de dor e bom prognóstico, além de normalmente estarem confinados no ovário. São relativamente estáveis geneticamente, apresentando uma sequência de mutações características que incluem *KRAS, BRAF, PTEN* e *ARID1A*, mas que raramente envolvem o gene *TP53* (SHIH & KURMAN, 2004; JONES *et al.*, 2010; WIEGAND *et al.*, 2010; KURMAN & SHIH, 2011). Por sua vez, os tumores epiteliais de

ovário do tipo II são compostos por: carcinoma seroso de alto grau, carcinoma endometrioide de alto grau, carcinosarcomas (tumores mesodérmicos) e carcinomas indiferenciados. Geralmente se apresentam em estágio avançado no diagnóstico (> 75% dos casos), apresentam rápido crescimento e alta malignidade. Esses tumores apresentam altíssima instabilidade genética e carregam mutações do gene *TP53* em mais de 95% dos casos, raramente possuindo alguma das mutações características dos tumores de tipo I (AHMED *et al.*, 2010).

Dos tumores de ovário diagnosticados, cerca de 80-90% são tumores epiteliais, a maioria deles em estágio avançado (II-IV) (JESSMON *et al.*, 2017). Dentre as alternativas de estudo da tumorigenicidade e das respostas a tratamentos, a cultura celular é uma das mais eficientes atualmente por apresentar alta reprodutibilidade dos experimentos e permitir maior autonomia e agilidade na condução dos procedimentos experimentais. A linhagem de células de câncer de ovário humano SKOV-3 (Figura 2) está entre as mais utilizadas mundialmente em pesquisas científicas sobre tumores epiteliais ovarianos. As células SKOV-3 são derivadas do fluido de ascite peritoneal de uma paciente caucasiana, de 64 anos, diagnosticada com câncer de ovário em 1973. Essa linhagem é resistente a uma variedade de substâncias, como fatores de necrose tumoral, adriamicina e cisplatina e apresenta alto potencial de proliferação e invasão. Sendo assim, as células SKOV-3 representam uma boa alternativa para o estudo do câncer de ovário, uma vez que representam o mais frequente dos tumores, possuindo tumorigenicidade compatível com lesões de estágio avançado.

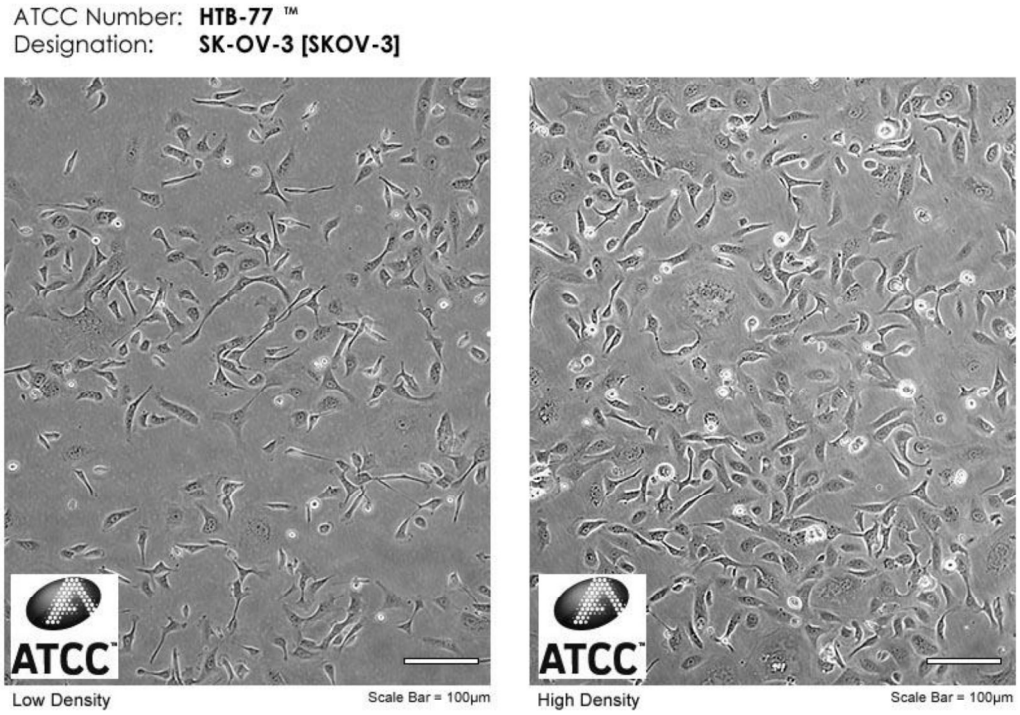

Figura 2. Células SKOV-3. Fonte: ATCC, 2018.

As atuais opções de tratamento para o câncer de ovário incluem quimioterapia, radioterapia, cirurgia de remoção e imunoterapia, dependendo do estágio tumoral e de exposição prévia a outras terapias. Pacientes diagnosticadas no estágio inicial da doença são frequentemente tratadas com cirurgia e administração de quimioterapia com derivados de platina (cisplatina ou carboplatina), enquanto nos estágios mais avançados da doença, o tratamento mais comum é a quimioterapia combinada, comumente com derivados da platina associados aos derivados do taxol (paclitaxel) (JESSMON *et al.*, 2017). De fato, o atual protocolo de tratamento para carcinomas epiteliais de alto grau foi estabelecido a mais de quinze anos atrás e consiste na administração de 75 mg/m² de cisplatina associada a 135 mg/m² de paclitaxel por 24 h a cada três semanas, repetidos até que se completem seis ciclos terapêuticos (MARKMAN, 2003), tendo sido recentemente proposto que a quimioterapia ocorra após cirurgia de citorredução (MATULONIS *et al*., 2016; LISIO *et al.*, 2019). Terapias alternativas para esses tumores têm sido testadas, mas nenhuma foi aplicada de forma consistente como uma segunda escolha para o combate da doença. Desta forma, apesar de cerca de 70% dos pacientes com carcinoma ovariano responderem inicialmente ao protocolo de tratamento padrão, estima-se que cerca de 80% deles apresentarão recorrência da doença em algum estágio do tratamento, adquirindo quimiorresistência aos principais derivados de platina e taxol (BAST *et al.*, 2009; MATULONIS *et al.*, 2016). Entre diversas vias pelas quais se supõe que os tumores de ovário adquiram resistência aos agentes terapêuticos, uma das mais evidentes atualmente tem sido a via de sinalização inflamatória dos receptores *toll-like* (TLRs).

Via de sinalização dos TLRs

A imunidade inata é a primeira resposta organizada pelo organismo a um desafio imunológico e envolve importantes células do sistema imune, como macrófagos, granulócitos, células dendríticas e células *natural killer* (NK). Ao serem desafiadas por um antígeno, essas células são capazes de organizar uma resposta para eliminá-lo através de uma série de mecanismos, como a fagocitose, geração de espécies reativas de oxigênio e outros sinais pró-inflamatórios (MUCCIOLI *et al.*, 2012). Os TLRs compõe uma família de receptores transmembrana do tipo I dotados de: um ectodomínio rico em leucina capaz de reconhecer ligantes, um domínio transmembrana, e um domínio TIR (*Toll-interleukin 1 receptor domain*) intracelular responsável pela transdução do sinal e ativação da cascata de sinalização (ROCK *et al.*, 1998; KAWAI & AKIRA, 2010) (Figura 3). São receptores especializados em reconhecimento de padrões moleculares associados a patógenos (PAMPs – *pathogen associated molecular patterns*), como lipídios, proteínas e lipoproteínas derivadas de microorganismos, e padrões moleculares associados ao dano celular (DAMPs – *damage-associated molecular*

patterns), como chaperonas e componentes da matriz extracelular, em sua grande maioria provenientes de tecidos em estágio de necrose (NEWTON & DIXIT, 2012; DAJON *et al.*, 2017).

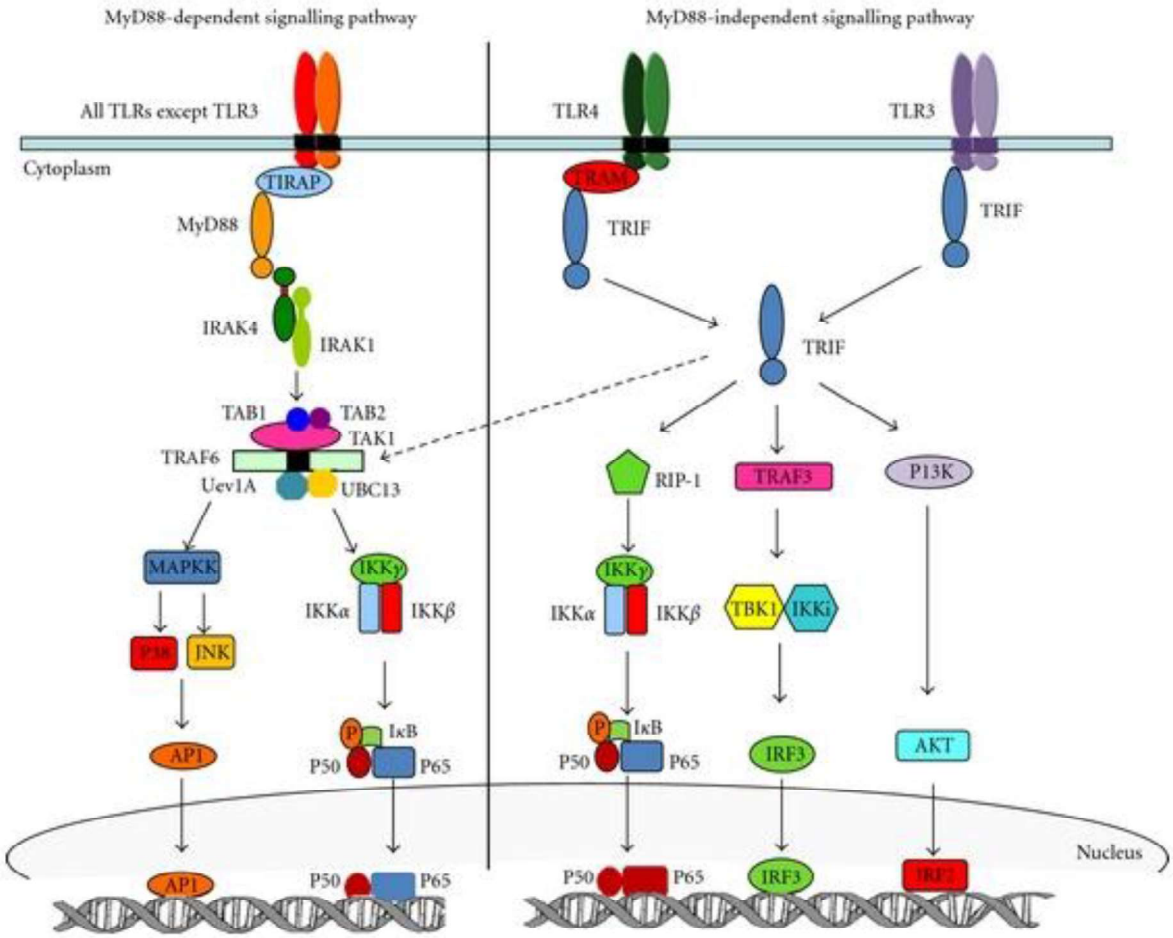

Figura 3. Via de sinalização canônica e não-canônica dos TLRs. Fonte: PATEL *et al.*, 2012.

Já foram descritos dez genes (TLR1 – TLR10) e três pseudogenes (TLR11, TLR12 e TLR13) codificadores desses receptores. Uma vez que reconhecem seus ligantes, a transdução do sinal se inicia com a dimerização e ativação dos domínios TIR, que formam uma espécie de plataforma de recrutamento de moléculas adaptadoras. Este processo leva à ativação de uma complexa cascata de sinalização que termina com a ativação de fatores transcricionais e, finalmente, ao aumento na produção de fatores pró-inflamatórios (MUCCIOLI *et al.*, 2012; DAJON *et al.*, 2017). As principais moléculas adaptadoras capazes de se associar ao domínio TIR dos TLRs são: MyD88 (*myeloid differentiation primary response gene 88*), TIRAP (*TIR domain-containing adapter protein*) ou Mal (*MyD88-adaptor like*), TRIF (*TIR domain-containing adaptor inducing interferon*), TRAM (*TRIF-related adaptor molecule*) e SARM (*armadillo-motif containing protein*) (BASITH *et al.*, 2011). Muitos estudos têm demonstrado que cada TLR possui vias individuais, que convergem para duas cascatas de sinalização, uma

dependendente de MyD88 (canônica) e outra dependente de TRIF (não-canônica) (TAKEDA & AKIRA, 2015). Os principais TLRs envolvidos na via de sinalização dependente de MyD88 são TLR2 e TLR4. Quando estimulados, esses receptores modificam seus domínios TIR com os quais as moléculas adaptadoras MyD88 estão associadas. O recrutamento destas leva à fosforilação e ativação de variados fatores intermediários, como IRAK-4, IRAK-1, TRAF6 e IKKs, que resultam na ativação dos importantes fatores de transcrição AP-1 e NF-κB (*nuclear factor-kappa B*) (AKIRA & TAKEDA, 2004). O NF-κB compreende uma família de fatores que regulam a transcrição de diversos genes inflamatórios e estimulam a produção de citocinas, quimiocinas e agentes antiapoptóticos e de resposta ao estresse, como fatores de crescimento e pró-angiogênicos (LI *et al.*, 2002). Além da via de sinalização canônica, a ativação de TLR4 também é capaz de desencadear a via dependente de TRIF, na qual esta molécula está associada ao domínio TIR do TLR4 e seu estímulo resulta no aumento dos níveis de IRF3 (*interferon regulatory factor 3*) (FITZGERALD *et al.*, 2003). Por sua vez, níveis aumentados de IRF3 levam ao aumento da produção de interferons (IFNs) e ativação da atividade citotóxica de linfócitos e células NK (MUCCIOLI *et al.*, 2012).

Além de sua característica expressão em células do sistema imune, os TLRs também são encontrados em outras células, inclusive células endoteliais e epiteliais, a fim de funcionar como um primeiro mecanismo de defesa em mucosas (MEDZHITOV *et al.*, 1997; HOPKINS & SRISKANDAN, 2005). Especificamente no ovário, são altamente expressos os subtipos TLR2, TLR3, TLR4 e TLR5, tanto no epitélio saudável, quanto naquele relacionado às neoplasias ovarianas (ZHOU *et al.*, 2009). Desta forma, apesar de seu importante papel na ativação da resposta imune e potencial função protetora nas mucosas, a expressão dos TLRs no microambiente tumoral tem sido amplamente discutida na literatura como um fator favorável ao desenvolvimento do câncer. Utilizando dos DAMPs provenientes, principalmente, de células necróticas como fator de estímulo endógeno, a hiperativação desses receptores em tumores de ovário mantém um microambiente pró-inflamatório, estando relacionado ao aumento das citocinas indutoras de inflamação crônica, supressão da resposta imune e quimiorresistência (SATO *et al.*, 2009; ZHOU *et al.*, 2009; GATA & LAURENTIU, 2017). De fato, o maior impacto causado pela ativação das vias de sinalização dos TLRs é o aumento da expressão de MyD88 e NF-κB, estando os níveis aumentados dessas duas moléculas diretamente relacionados com diminuição da expectativa de vida pós-diagnóstico, além da maior tumorigenicidade já discutida anteriormente (ZHU *et al.*, 2012; D'ADHEMAR *et al.*, 2014).

O paclitaxel é uma das primeiras escolhas para o tratamento do câncer de ovário, no entanto também é um agonista de TLR4 e seu efeito na ativação da via de sinalização TLR4/MyD88 tem sido sugerida como um importante fator na aquisição de resistência ao

tratamento (HUANG *et al.*, 2005; ZHU *et al.*, 2012). Estudos já demonstraram que células de tumores epiteliais do ovário que não expressam essa via de sinalização são mais responsivas a estímulos pró-apoptóticos e, consequentemente, são menos agressivos. De forma contrária, quando células negativas para MyD88 são transfectadas com a molécula adaptadora passam a apresentar resistência ao tratamento com paclitaxel (YANG *et al.*, 2010; CHEN *et al.*, 2012). No que se refere às linhagens celulares de câncer de ovário, as células SKOV-3, que possuem a via de sinalização do TLR2 e TLR4 ativas, são mais resistentes ao tratamento com paclitaxel quando comparadas às células A2780, que não expressam atividade dessa via de sinalização (ZHU *et al.*, 2012). Esses achados sugerem fortemente que são necessárias novas alternativas terapêuticas para o câncer de ovário, sendo uma promissora possibilidade o uso de compostos capazes de modular a via de sinalização dos TLRs, inclusive como terapias adjuvantes que restaurem a sensibilidade aos principais quimioterápicos.

Propriedades antitumorais do P-MAPA e IL-12

Avanços no uso de imunoterapias têm sido descritos para o tratamento de diversos tipos de câncer, entre eles o câncer de ovário. Uma diversidade de modalidades de tratamento têm sido exploradas, entre elas: o uso de imunomoduladores (e.g. CTLA-4, moduladores de PD-1 e PD-L1), terapias baseadas em anticorpos (e.g. bevacizumab, cetuximab) e vacinas contra o câncer (KRISHNAN *et al.*, 2017). O P-MAPA (agregado polimérico de fosfolinoleato-palmitoleato de magnésio e amônio proteico, Farmabrasilis®) é um biopolímero com propriedades imunomoduladoras, sendo uma molécula produzida através da fermentação do fungo *A. oryzae*. O P-MAPA tem sido utilizado experimentalmente em pesquisas envolvendo o câncer de bexiga, e vem apresentando bom prognóstico e baixa toxicidade (ausência de hepatotoxicidade e nefrototoxicidade). Seu principal mecanismo de ação é o aumento dos níveis da proteína p53, que possui atividade regulatória sobre os TLRs e está diretamente associada com o grau de agressividade do tumor (FÁVARO *et al*., 2012) (Figura 4).

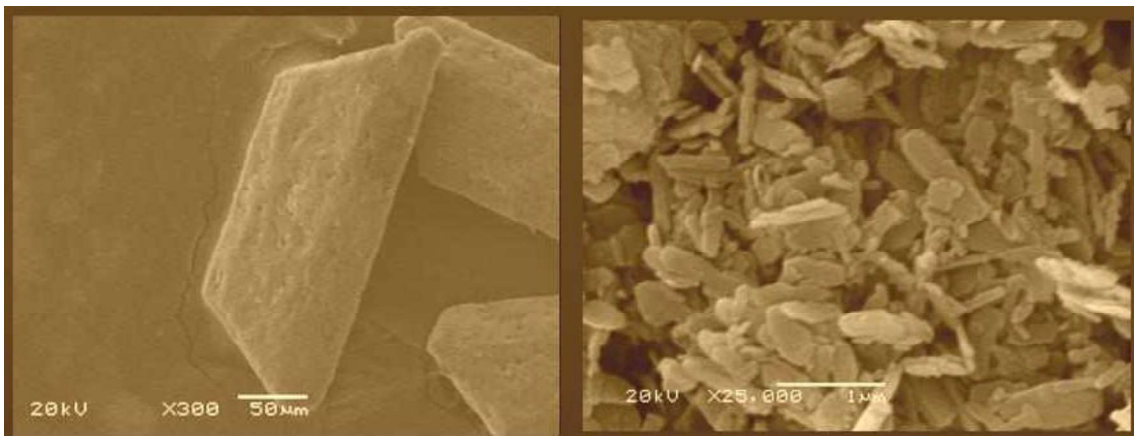

Figura 4. Micro e nanocristais de P-MAPA. Fonte: FARMABRASILIS, 2008.

O P-MAPA é um modificador de resposta biológica que apresenta efeitos significativos sobre componentes do sistema imunológico, sendo capaz de estimular os receptores TLR2 e TLR4, e aumentar a produção de linfócitos T, de citocinas como a IL-2 e o IFN-γ, além de promover o aumento da atividade das células *natural killers* (NKs), com concomitante produção e liberação de óxido nítrico pelos macrófagos (FARMABRASILIS, 2008). As citocinas tem a capacidade de regular as funções de proliferação, apoptose e diferenciação celular, sendo produzidas por vários tecidos e células, incluindo a célula tumoral. Em estudos clínicos com portadores de HIV, o P-MAPA levou ao aumento dos linfócitos T CD4+ e CD8+ e de granulócitos, trazendo-os de volta à normalidade. Resultados semelhantes foram encontrados em pesquisas experimentais, indicando que o P-MAPA possui capacidade de estimular o sistema imune (FARMABRASILIS, 2008). Estudos recentes *in vivo* e *in vitro* sugerem que o P-MAPA atua na modulação da resposta imune em tumores malignos, restaurando a imunocompetência celular (FÁVARO *et al*., 2012). Em modelo de câncer de ovário experimental, o tratamento com P-MAPA reduziu o volume tumoral, aumentou a taxa de sobrevida dos animais e potencializou a via mediada por TLR4 na presença de cisplatina (CHUFFA *et al.*, 2018). Recentemente, demonstrou-se que o P-MAPA é capaz de reduzir a migração e invasão de células SKOV-3 do câncer de ovário, além de diminuir os níveis de MyD88, IRF3 e NF-κB p65 nessas células. Quando associado com paclitaxel, o P-MAPA aumentou a sensibilidade das células de câncer de ovário ao tratamento, sugerindo que esse composto pode apresentar efeito contra a quimiorresistência associada à via de sinalização dos TLRs (LUPI *et al.*, 2019). Desta forma, o P-MAPA pode apresentar resultados promissores como estratégia terapêutica adicional aos tratamentos padrões contra o câncer de ovário, tornando-se relevante elucidar a sua ação direta nas células tumorais, já que apresenta baixa toxicidade e pode ser de grande valor para os casos de quimioresistência aos tratamentos convencionais.

A interleucina 12 (IL-12) (Figura 5) é uma citocina relacionada com a imunidade inata e adaptativa (TRINCHIERI, 1995). É produzida pelas células apresentadoras de antígenos (APCs), linfócitos B, células dendríticas e outras. A IL-12 atua sobre as células T e NK estimulando a atividade de linfócitos citotóxicos e induzindo proliferação e produção de citocinas, especialmente o IFN-γ (COLOMBO & TRINCHIERI, 2002). Além disso, a IL-12 é a citocina responsável pela diferenciação da resposta polarizada Th1, que por sua vez, também resulta na produção de IFN-γ. O IFN-γ aumenta a habilidade das APCs em produzir IL-12 (MA *et al.*, 1996) atuando como um potente feed-back positivo em várias respostas celulares. SMYTH *et al*. (2002) mostraram que altas doses dessa citocina levam à indução da imunidade tumoral mediada por células NKs, enquanto baixas doses não mostraram atividade anti-tumoral. Importantemente, diversos estudos experimentais têm apontado que a administração sistemática de IL-12 leva a

resposta imune antitumoral, principalmente através do aumento da produção de IFN-γ. Especificamente no câncer de ovário recorrente, o tratamento intravenoso com IL-12 mostrou ser uma estratégia funcional benéfica (HURTEAU *et al*., 2001). Nesse estudo, após os ensaios pré-dosagens para limitar a toxicidade, pacientes receberam 250 ng/kg de IL-12 em dose única, seguido por um intervalo de duas semanas, com ciclos subsequentes de administração durante cinco dias consecutivos, seguido de intervalo de 16 dias, até alcançar a regressão do tumor.

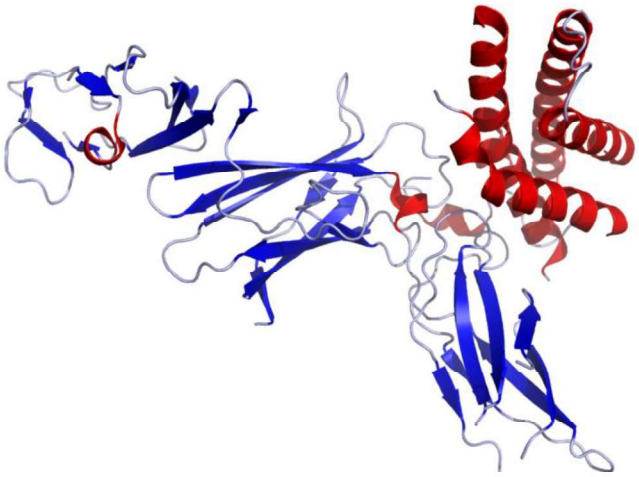

Figura 5. Estrutura quaternária da IL-12. Fonte: domínio público (*Protein data bank, PDB:1F45*)

As células T NK têm seu papel bem estabelecido na imunidade tumoral (SMYTH *et al.* 2002), apesar de estudos adicionais serem necessários para sua aplicabilidade terapêutica. A terapia antitumoral mediada por IL-12 também está relacionada com ativação dessas células T NK em camundongos (CUI *et al*. 1997), e seu uso como agente imunoterapêutico parece potencializar a rejeição tumoral, conforme já descrito em modelos experimentais de tumores como melanoma, timoma e sarcoma (KAWANO *et al*. 1997, SMYTH *et al*. 2002). Em modelo de câncer de ovário murino, o tratamento com IL-12 (0.33 mcg/dia, via i.p., durante 20 dias) resultou em redução no crescimento tumoral com aumento no número de células NK agrupadas em seu interior (SILVER *et al.* 1999). Diante desse cenário, a IL-12, associada ou não com P-MAPA, também pode representar uma importante alternativa como agente adjuvante no combate a diversos tipos de câncer, inclusive o câncer de ovário.

Hipótese e relevância do tema

Considerando que mecanismos ainda desconhecidos que participam do desenvolvimento e progressão do câncer de ovário possam estar diretamente associados à inflamação e ao sistema imune, e tendo a propósito as terapias adjuvantes como ferramentas úteis no entendimento dos aspectos moleculares que controlam a carcinogênese do ovário, o presente estudo visa explorar *in vitro* os caminhos que predispõe ao processo inflamatório mediado por TLR2 e TLR4. É bem sabido que os quimioterápicos, como os derivados da platina e o taxol, desempenham atividades fundamentais no controle do crescimento tumoral, porém, de forma súbita, muitas mulheres desenvolvem quimioresistência ao tratamento e a progressão tumoral avança descompensadamente. Esse mecanismo de quimioresistência está ligado diretamente à modulação do processo inflamatório e pode levar a paciente a óbito. Portanto, o presente estudo visa ressaltar duas questões: 1) Será que o imunomodulador P-MAPA exerce ação sobre mediadores inflamatórios e o sistema imune associado ao câncer de ovário? 2) Neste contexto, poderia o P-MAPA potencializar a resposta da IL-12 sobre a via mediada por TLR no câncer de ovário?

O uso de imunoterapias adjuvantes tem-se mostrado eficiente na redução dos efeitos deletérios em vários tipos de câncer. A terapia com P-MAPA possui importante ação moduladora sobre alguns mediadores do processo inflamatório em tumores sólidos, podendo favorecer o prognóstico da doença, auxiliar no bem estar do paciente e, principalmente, no entendimento dos mecanismos que geram quimioresistência aos tratamentos. Ademais, a melhor compreensão desses efeitos poderá trazer novas perspectivas para o entendimento dessa patologia. Desse modo, a avaliação do câncer de ovário, sob o ponto de vista inflamatório, e o papel dos compostos P-MAPA e IL-12 como estratégia terapêutica na atenuação desse processo vislumbram potenciais abordagens que podem auxiliar no desenvolvimento de novas ferramentas de combate a essa doença.

Objetivo geral

Avaliar o efeito dos tratamentos com o imunomodulador P-MAPA e IL-12 isoladas, assim como a associação de P-MAPA e IL-12, sobre o processo inflamatório e agressividade de células de carcinoma ovariano humano (SKOV-3).

Objetivos específicos

1. Avaliar os efeitos dos tratamentos nas linhagens de células SKOV-3 frente a diferentes doses e períodos de incubação;
2. Avaliar a viabilidade celular, citotoxicidade, migração/invasão celular e efeitos na parada do ciclo e morte celular frente aos tratamentos específicos;
3. Imunolocalizar por fluorescência os receptores TLR2 e TLR4 e quantificar, por *western blot,* os receptores TLR2 e TLR4, os fatores MyD88, TRIF, IRF3 e NF-kB envolvidos no processo inflamatório;
4. Avaliar, através da estratégia proteômica global por eletrospray (LCMS/MS), as diferentes proteínas produzidas pelas células SKOV-3 após os tratamentos;
5. Quantificar os mediadores do processo inflamatório (pró e anti-inflamatórios, entre outros) no sobrenadante da cultura e no extrato celular através de ensaio *multiplex*.

Capítulo 2

molecules

MDPI

Article

P-MAPA and Interleukin-12 Reduce Cell Migration/Invasion and Attenuate the Toll-Like Receptor-Mediated Inflammatory Response in Ovarian Cancer SKOV-3 Cells: A Preliminary Study

Luiz Antonio Lupi [1], Flávia Karina Delella [2], Maira Smaniotto Cucielo [1], Graziela Gorete Romagnoli [3], Ramon Kaneno [3], Iseu da Silva Nunes [4], Raquel Fantin Domeniconi [1], Marcelo Martinez [5], Francisco Eduardo Martinez [1], Wagner José Fávaro [6] and Luiz Gustavo de Almeida Chuffa [1,*]

1 Department of Anatomy, UNESP-São Paulo State University, Institute of Biosciences, Botucatu, 18618-689 São Paulo, Brazil; luiz.lupi@unesp.br (L.A.L.); maira.cucielo@gmail.com (M.S.C.); raquel.domeniconi@unesp.br (R.F.D.); fe.martinez@unesp.br (F.E.M.)
2 Department of Morphology, UNESP-São Paulo State University, Institute of Biosciences, Botucatu, 18618-689 São Paulo, Brazil; flavia.delella@unesp.br
3 Department of Microbiology and Immunology, UNESP-São Paulo State University, Institute of Biosciences, Botucatu, 18618-689 São Paulo, Brazil; graziela.romagnoli@unesp.br (G.G.R.); rskaneno@yahoo.com.br (R.K.)
4 Farmabrasilis R&D Division, Campinas, 13279-020 SP, Brazil; iseununes@gmail.com
5 Department of Morphology and Pathology, Federal University of São Carlos, 13565-905 São Paulo, Brazil; martinez@ufscar.br
6 Department of Structural and Functional Biology, UNICAMP-University of Campinas, Campinas, 13083-970 São Paulo, Brazil; favarowj@unicamp.br
* Correspondence: guchuffa@yahoo.com.br; Tel.: +55-(14)-3880-0027

Academic Editor: Qiao-Hong Chen
Received: 16 October 2019; Accepted: 9 December 2019; Published: 18 December 2019

Abstract: Immunotherapies have emerged as promising complementary treatments for ovarian cancer (OC), but its effective and direct role on OC cells is unclear. This study examined the combinatory effects of the protein aggregate magnesium–ammonium phospholinoleate–palmitoleate anhydride, known as P-MAPA, and the human recombinant interleukin-12 (hrIL-12) on cell migration/invasion, apoptosis, toll-like receptor (TLR)-mediated inflammation, and cytokine/chemokine profile in human OC cell line SKOV-3. P-MAPA and IL-12 showed cancer cell toxicity under low doses after 48 h. Although apoptosis/necrosis and the cell cycle were unchanged by the treatments, P-MAPA enhanced the sensitivity to paclitaxel (PTX) and P-MAPA associated with IL-12 significantly reduced the migratory potential and invasion capacity of SKOV-3 cells. P-MAPA therapy reduced TLR2 immunostaining and the myeloid differentiation factor 88 (MyD88), but not the TLR4 levels. Moreover, the combination of P-MAPA with IL-12 attenuated the levels of MyD88, interferon regulatory factor 3 (IRF3) and nuclear factor kappa B (NF-kB p65). The IL-12 levels were increased and P-MAPA stimulated the secretion of cytokines IL-3, IL-9, IL-10, and chemokines MDC/CCL22 and, regulated on activation, normal T cells expressed and secreted (RANTES)/CCL5. Conversely, combination therapy reduced the levels of IL-3, IL-9, IL-10, MDC/CCL22, and RANTES/CCL5. Collectively, P-MAPA and IL-12 reduce cell dynamics and effectively target the TLR-related downstream molecules, eliciting a protective effect against chemoresistance. P-MAPA also stimulates the secretion of anti-inflammatory molecules, possibly having an immune response in the OC microenvironment.

Keywords: ovarian cancer; P-MAPA; IL-12; TLR signaling; inflammation; chemoresistance

1. Introduction

Ovarian cancer (OC) is the fifth largest cause of cancer-related death in the United States and is the most lethal of all gynecological malignancies [1]. OC originates from the ovarian surface epithelium, fallopian tube (fimbriae region) or endometriosis-related tissue, and often exhibits a late diagnosis due to the lack of clear signs or symptoms in the early stages of development [2–5]. Unfortunately, there is no screening method for achieving the best curative result, and traditional chemotherapy and surgery are limited for patients with advanced OC [6]. After cisplatin and paclitaxel (PTX) resistance, several patients become susceptible to developing recurrent OC and metastasis [7]. Therefore, new therapeutic options that overcome chemoresistance and enhance drug sensitivity are promising for the treatment of OC.

Immunotherapies have demonstrated great efficiency by activating host immune responses into the OC microenvironment [8]; however, what is happening with the cancer cells as a direct result of immunostimulation requires further investigation. We recently reported the effect of the immunomodulatory agent termed protein aggregate magnesium-ammonium phospholinoleate-palmitoleate anhydride (P-MAPA), a natural biopolymer extracted from the *Aspergillus oryzae*, which exhibits a number of antitumor responses in different experimental models of cancer [9–11]. In association with cisplatin, P-MAPA showed a greater survival rate and a reduced OC volume in addition to the increased expression of proteins involved in toll-like receptor (TLR)-mediated inflammatory response (canonical and non-canonical pathways) in OC-bearing animals [11]. Recent studies also supported the immunological mechanism of action of P-MAPA through the activation of TLR2 and TLR4 signaling in both cancer and infections, in addition to regulating the activity of T cells (especially CD4+T and CD8+T cells) and natural killer (NK) cells [9,10]. Importantly, P-MAPA did not show toxicity in preclinical in vitro (V-79 Chinese hamster cell line) and in vivo models (Swiss mice, Wistar rats, and monkeys) nor in human clinical trial phase I [9]; its effects in cancer treatment have been tested in non-muscle invasive urinary bladder cancer [9,10] and in OC [11]. The directive role of P-MAPA on human OC cells, considering its feasibility, sensibility, resistance, and toxicity, has not been explored yet.

TLRs are transmembrane molecules that signal via myeloid differentiation factor 88 (MyD88) or TLR-associated activator of interferon (TRIF) to induce cell proliferation, chemoresistance, and cytokine/chemokine production [12]. Most importantly, TLRs can trigger a different response depending on the cell type (e.g., cancer cell or immune cell), and particularly, TLR4 has been reported to be a precursor of the immune escape of OC cells [13,14]. The crosstalk between the immunoadjuvant and the OC cells targeting the TLR signaling and related cytokine secretion has never been proposed as to their impact and specific response.

Interleukin-12 (IL-12) is a cytokine related to innate and adaptive immunity, being mainly produced by the antigen-presenting cells (APCs), such as B lymphocytes, dendritic cells (DCs), and others [15,16]. It acts on T and NK cells stimulating a cytotoxic CD8+ response and inducing cytokine production, especially interferon-γ (IFN-γ) [15,17]; IL-12 is involved in the differentiation of naïve T cells into a polarized T helper 1 (Th1) immune response. Patients with recurrent OC who underwent IL-12 treatment, in a well-established dosage regimen, showed significant tumor regression [18]; the major challenge involving the treatment with IL-12 is related to the adverse effects due to its high diffusion and toxicity (e.g., lymphopenia and irreversible elevation of transaminases at 600 ng/kg and neutropenia, fatigue, and headache at 300 ng/kg) [19], and a more precise and direct administration may limit their undesirable effects. Notably, a phase II study involving intraperitoneal infusions of recombinant IL-12 in patients with residual disease ≤1 cm showed to be well-tolerated after fist-line therapy for OC-related peritoneal carcinomatosis [19]. Recently, Cohen et al. [16] studied the relationship between membrane-bound IL-12 in tumor cells and the potential to disrupt protumorigenic signaling and tumor outgrowth within peritoneal cavities; IL-12 significantly led to a tumor refractory state, thereby delaying the onset of metastatic disease.

Because P-MAPA is thought to increase IFN-γ levels, which may potentiate the Thelper (Th1)-mediated immune response, and adjuvant therapies with IL-12 have long been proposed as beneficial for patients with OC, this study investigates the effects of P-MAPA and IL-12, alone or in combination, on cancer cell activities with focus to the TLR-mediated inflammatory process and cytokines/chemokines profiling in human SKOV-3 cell line.

2. Results

2.1. P-MAPA and IL-12 Reduce Cell Viability and Induce Apoptosis in the Presence of PTX in SKOV-3 Cells

An MTT assay was carried out using three biological and technical replicates to unravel the most suitable dose and period of treatment. Based on previous results, the SKOV-3 cells were challenged with P-MAPA at doses of 25 μg/mL, 50 μg/mL, and 100 μg/mL, and rhIL-12 at doses of 0.5 ng/mL, 1 ng/mL, and 2 ng/mL for 24 h, 48 h, and 72 h. Then, we tested three different cell concentrations to achieve the better treatment response (1×10^3 cells, 1×10^4 cells, and 5×10^4 cells; Supplementary Figure S1). The SKOV-3 cell viability was efficiently reduced after the low-dose P-MAPA treatment (25 μg/mL for 48 h; viability was reduced by ~27%), and then started to increase after 72 h exposure (Figure 1A). Treatment with rhIL-12 also showed reduction in cell viability at an intermediate dose of 1 ng/mL mainly after 48-h exposure (Figure 1B; viability reduction by ~25% after 48 h). Combinatory therapy with P-MAPA and IL-12 also reduced the cell viability by about 33% (Figure 1C), and the treatment doses were set at 25 μg/mL of P-MAPA and 1 ng/mL of IL-12. Annexin V- fluorescein isothiocyanate (FITC)/Propidium iodide (PI) staining was used to effectively determine the apoptosis/necrosis rate induced by P-MAPA and rhIL-12 immunotherapies. In this study, we set early apoptosis (Annexin V-FITC+/PI−) as apoptosis and late apoptosis (Annexin V+/PI+) and necrosis (Annexin V−/PI+) as necrosis. The apoptosis index was not influenced by P-MAPA, IL-12, or P-MAPA+IL-12 (Figure 1D,E), which pointed out that these agents are unable to induce cell death at this concentration. We also observed that P-MAPA and IL-12 did not alter the cell cycle significantly (Figure 1F,G). These data indicate that these immunotherapeutic agents do not have a direct and high toxic effect to the cell, which is, in fact, expected from immunotherapies. Because the treatments did not promote cell death or cell proliferation, the reduction of cell viability might have been a result of decreased cell metabolism, because the MTT test indirectly reflects the mitochondrial activity.

To better understand whether P-MAPA and IL-12 therapies potentially increase the effect of standard chemotherapy, they were tested in association with PTX (Figure 2A,B). After 48 h, P-MAPA decreased cell viability in association with different doses of PTX compared with cells treated with PTX only (~30% reduction with 5 μM PTX; ~30% reduction with 2.5 μM PTX; ~24% reduction with 1.25 μM PTX and ~34% reduction with 0.625 μM PTX). Because IL-12 had no effect on cell viability when associated with PTX, the decreased cell viability observed after combining P-MAPA with IL-12 in association with doses of PTX is probably due to the P-MAPA effect (~19% reduction with 5 μM PTX, ~30% reduction with 2.5 μM PTX, ~30% reduction with 1.25 μM PTX, and ~38% reduction with 0.625 μM PTX). To confirm these effects on SKOV-3 cell death, an Annexin V-FITC/PI assay was performed using the lowest dose of PTX (0.625 μM). Concordantly, with the MTT results, P-MAPA and P-MAPA+IL-12 increased cell death in association with PTX at dose of 0.625 μM. The apoptosis/necrosis ratio of PTX was 0.64 and became higher when associated with P-MAPA (1.18) or P-MAPA+IL-12 (0.88), thus enhancing the P-MAPA effect as apoptotic inductor. Finally, PTX significantly increased the number of cells in G0/G1 and decreased cells in G2/M phase of the cell cycle, thus inducing cell cycle arrest. In this case, the addition of P-MAPA and IL-12 did not potentiate the PTX effects in cell cycle (Figure 2D,E).

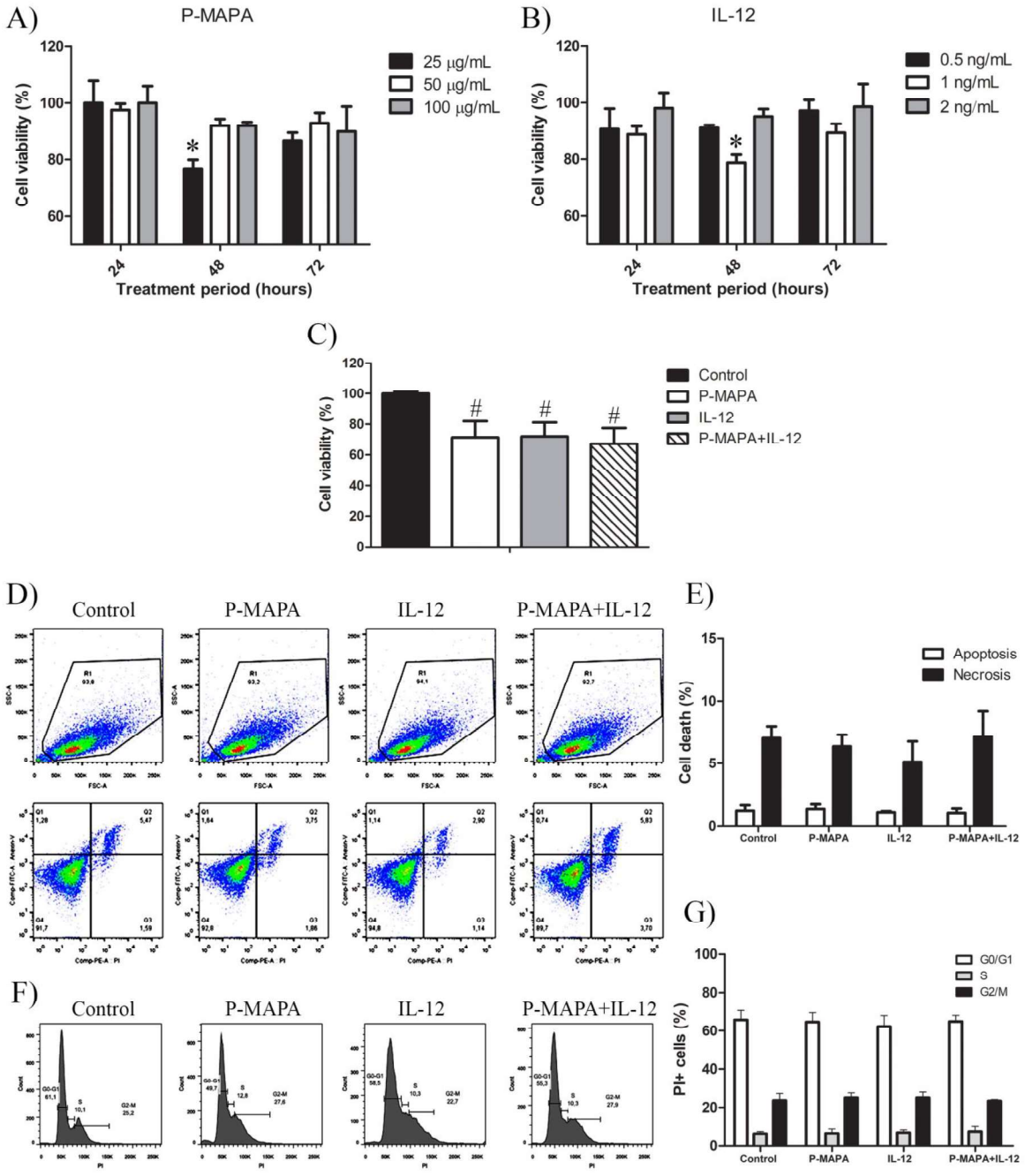

Figure 1. Protein aggregate magnesium–ammonium phospholinoleate–palmitoleate anhydride (P-MAPA) and interleukin-12 (IL-12) suppress cell viability without changing the apoptosis rate and cell cycle. SKOV-3 cells were treated with various concentrations of P-MAPA (**A**) and IL-12 (**B**) for 24, 48, and 72 h, and the cytotoxicity (expressed as percentage) was assayed by MTT; (**C**) Cell viability (%) after standardization of treatments (25 µg P-MAPA and 1 ng IL-12) after 48 h exposure; 1×10^3 SKOV-3 cells showed the best reproducibility. (**D**) Representative apoptotic index in SKOV-3 cells treated with P-MAPA and IL-12 for 48 h detected by annexin V/PI flow cytometry. (**E**) Percentage of cells in apoptosis and necrosis. (**F**) Representative cell cycle analysis in SKOV-3 cells treated with P-MAPA and IL-12 for 48 h detected by PI and RNAase flow cytometry. (**G**) Percentage of PI+ cells in G0/G1, S, and G2/M phases. The samples were assayed in three technical and biological replicates. Results are expressed as the mean ± SD and described as column chart. * $p < 0.05$ vs. different doses at 48 h; # $p < 0.05$ vs. control group.

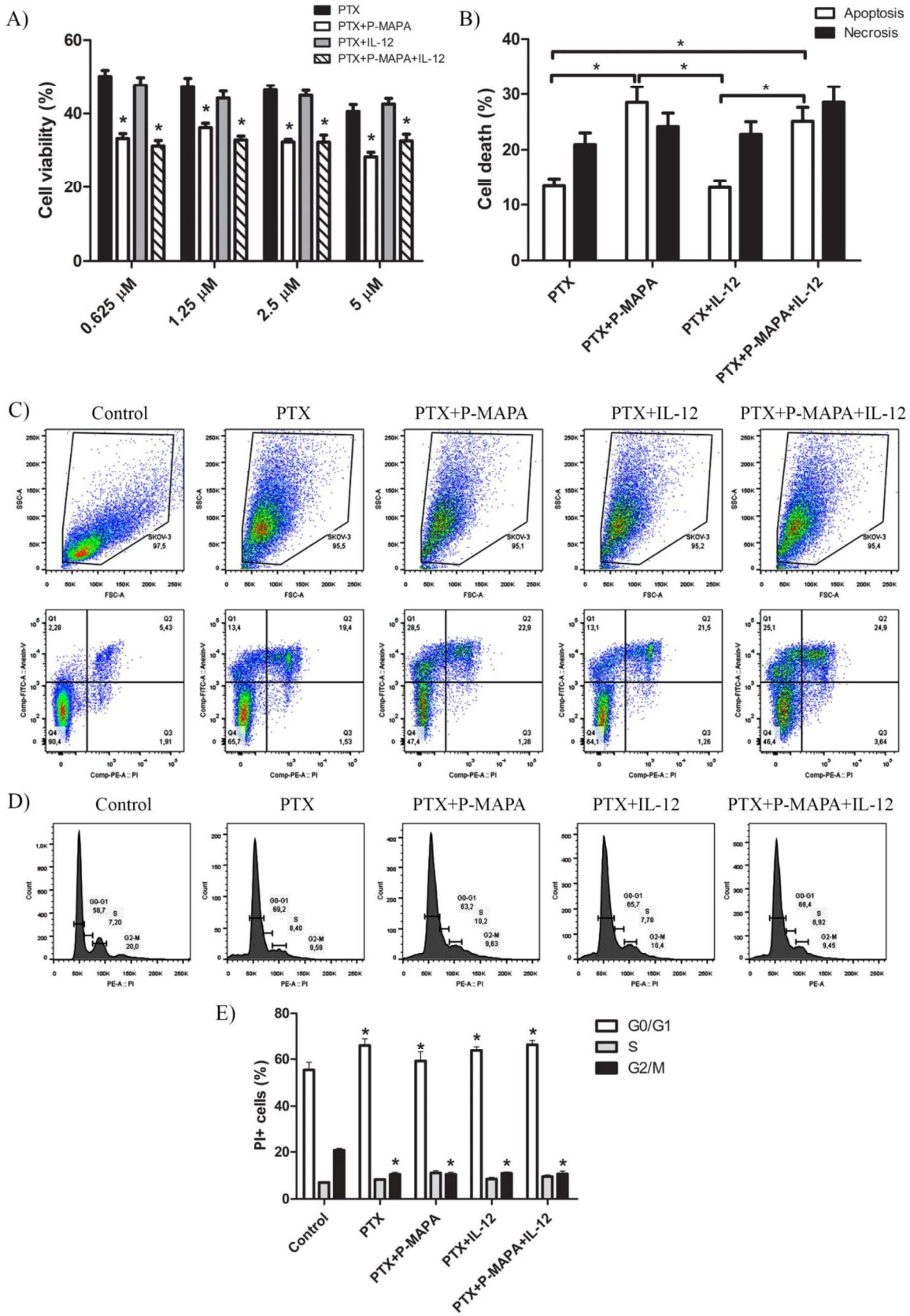
A)
PTX
PTX+P-MAPA
PTX+IL-12
PTX+P-MAPA+IL-12
Cell viability (%)
0.625 μM
1.25 μM
2.5 μM
5 μM
B)
Apoptosis
Necrosis
Cell death (%)
PTX
PTX+P-MAPA
PTX+IL-12
PTX+P-MAPA+IL-12
C)
Control
PTX
PTX+P-MAPA
PTX+IL-12
PTX+P-MAPA+IL-12
SSC-A
FSC-A
SKOV-3
97,5
95,5
95,1
95,2
95,4
Comp-FITC-A :: Anexin-V
Comp-PE-A :: PI
Q1 2,28
Q2 5,43
Q4 90,4
Q3 1,91
Q1 13,4
Q2 19,4
Q4 65,7
Q3 1,53
Q1 28,5
Q2 22,9
Q4 47,4
Q3 1,26
Q1 13,1
Q2 21,5
Q4 64,1
Q3 1,26
Q1 25,1
Q2 24,9
Q4 46,4
Q3 3,64
D)
Control
PTX
PTX+P-MAPA
PTX+IL-12
PTX+P-MAPA+IL-12
Count
PE-A :: PI
G0-G1 58,7
S 7,20
G2-M 20,0
G0-G1 69,2
S 8,40
G2-M 9,59
G0-G1 83,2
S 10,2
G2-M 9,63
G0-G1 65,7
S 7,78
G2-M 10,4
G0-G1 88,4
S 8,92
G2-M 9,45
E)
G0/G1
S
G2/M
PI+ cells (%)
Control
PTX
PTX+P-MAPA
PTX+IL-12
PTX+P-MAPA+IL-12

Figure 2. P-MAPA and P-MAPA+IL-12 reduce cell viability and apoptosis/necrosis rate in the presence of PTX. (**A**) Cell viability was assessed by an MTT assay; SKOV-3 cells were treated with various concentrations of PTX alone or in association with P-MAPA and IL-12 for 48 h. * $p < 0.05$ vs. PTX and PTX+IL-12 groups. (**B**) Percentage of cells in apoptosis and necrosis after exposure to 0.625 μM PTX plus P-MAPA, IL-12, or P-MAPA+IL-12. * $p < 0.05$. (**C**) Representative apoptotic index in SKOV-3 cells detected by Annexin V/PI flow cytometry. (**D**) Representative cell cycle analysis in SKOV-3 cells treated with PTX, P-MAPA and IL-12 for 48 h detected by PI and RNase flow cytometry. (**E**) Percentage of PI+ cells in the G0/G1, S, and G2/M phases. The samples were assayed in three technical and biological replicates.* $p < 0.05$ vs. control group. Results are expressed as the mean ± SD.

2.2. Combination of P-MAPA with IL-12 Is Essential to Reduce Cell Migration Whereas P-MAPA Alone Decreased The Invasive Potential of SKOV-3 Cells

To investigate the inhibitory effect of P-MAPA and IL-12 as a single or combinatory treatment on SKOV-3 cells, a wound-healing assay was performed in different periods. Although the treatment with IL-12 showed a reduced migration rate (~ 17%) after 36 h and 48 h exposure, cells treated with P-MAPA migrated significantly less (~ 13%) only at 48 h exposure (Figure 3A,B). Combination of P-MAPA and IL-12 reduced the migratory potential of cells after 36 h and 48 h treatment (>20%), being the most efficient after 36 h (Figure 3A,B); this overall analysis suggests that IL-12 was more effective than P-MAPA in delaying wound closure. SKOV-3 cells that were treated with 0.9% saline solution (control group) had an accelerated growth and migration rate when compared with all the treatments. Because the wound-healing assay might be biased by cell proliferation, transwell migration and invasion assays were performed and effectively showed that P-MAPA reduced cell migration when administered alone or in association with IL-12 (Figure 4A). When Geltrex® was added to the chambers, the number of invasive cells was reduced after P-MAPA treatment in comparison to IL-12 treatment or its association (Figure 4B).

2.3. Immunotherapy with P-MAPA and IL-12 Significantly Reduced the TLR-Mediated Downstream Molecules Involved in the Inflammatory Process of SKOV-3 Cells

One of the most important factors responsible for the acquisition of malignant phenotypes of OC cells is associated with chemoresistance to treatments and uncovering new agents that downregulate the inflammatory pathway(s) may be of significant interest. To evaluate whether P-MAPA or IL-12 play a role on OC-related inflammation, TLR2- and TLR4-mediated pathways were evaluated through canonical and non-canonical signaling. Although the expressions of TLR2 and TLR4 did not vary significantly, the downstream target molecules were affected by the treatments (Figure 5A,B). P-MAPA and IL-12 alone or in combination led to a profound reduction in the MyD88 levels (0.53-, 0.48-, and 0.61-fold reduction, respectively vs. the control group; Figure 5A,B). We also evaluated the NF-kB p65 expression in the extracts of SKOV-3 cells, and notably, IL-12 alone or combined with P-MAPA induced a significant reduction in the p65 levels (0.66- and 0.63-fold reduction, respectively vs. control group; Figure 5A,B). To explore the non-canonical pathway, the TRIF and IRF3 levels were measured. Although the TRIF levels were unchanged after the treatments ($p > 0.05$), P-MAPA, IL-12, and the combination of P-MAPA with IL-12 induced a significant decrease in the IRF3 levels (0.70-, 0.43-, and 0.71-fold reduction, respectively vs. the control group; Figure 5A,B). These findings provide evidence that P-MAPA and IL-12 potentially act on MyD88-dependent and MyD88-independent pathways, which also encourages the possibility that these immunomodulatory agents could even increase the chemosensitivity of other therapeutics.

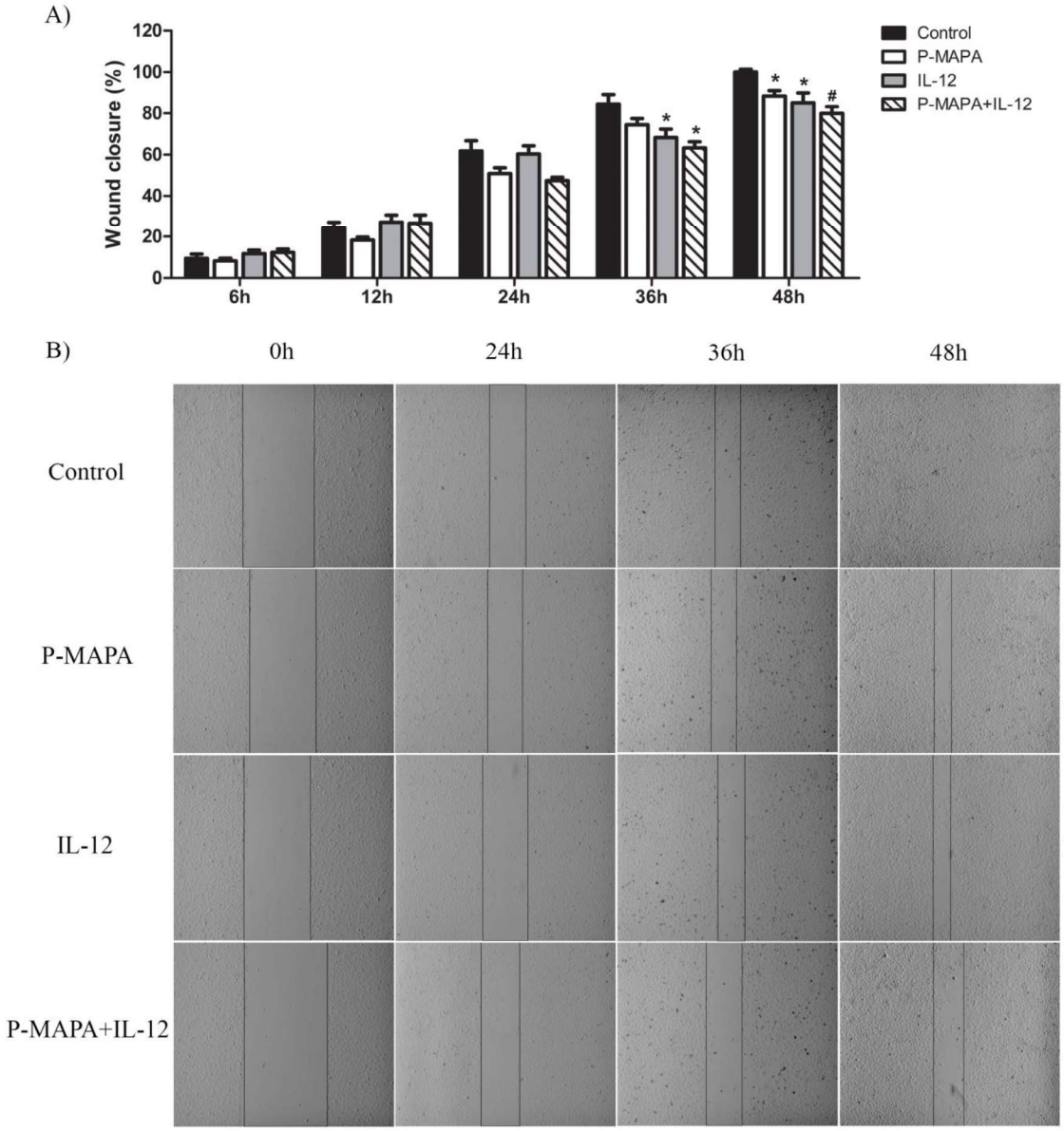

Figure 3. Migratory potential of SKOV-3 cells determined by wound-healing assay. (**A**) Percentage of wound closure after 0, 6, 12, 24, 36, and 48 h. * $p < 0.05$, # $p < 0.01$ vs. control group. (**B**) Photographs of each wound-healing analysis at 0, 24, 36, and 48 h which were representative for specific closing area; vertical black bars were used to show the incision edges (10× magnification). The samples were assayed in three technical and biological replicates.

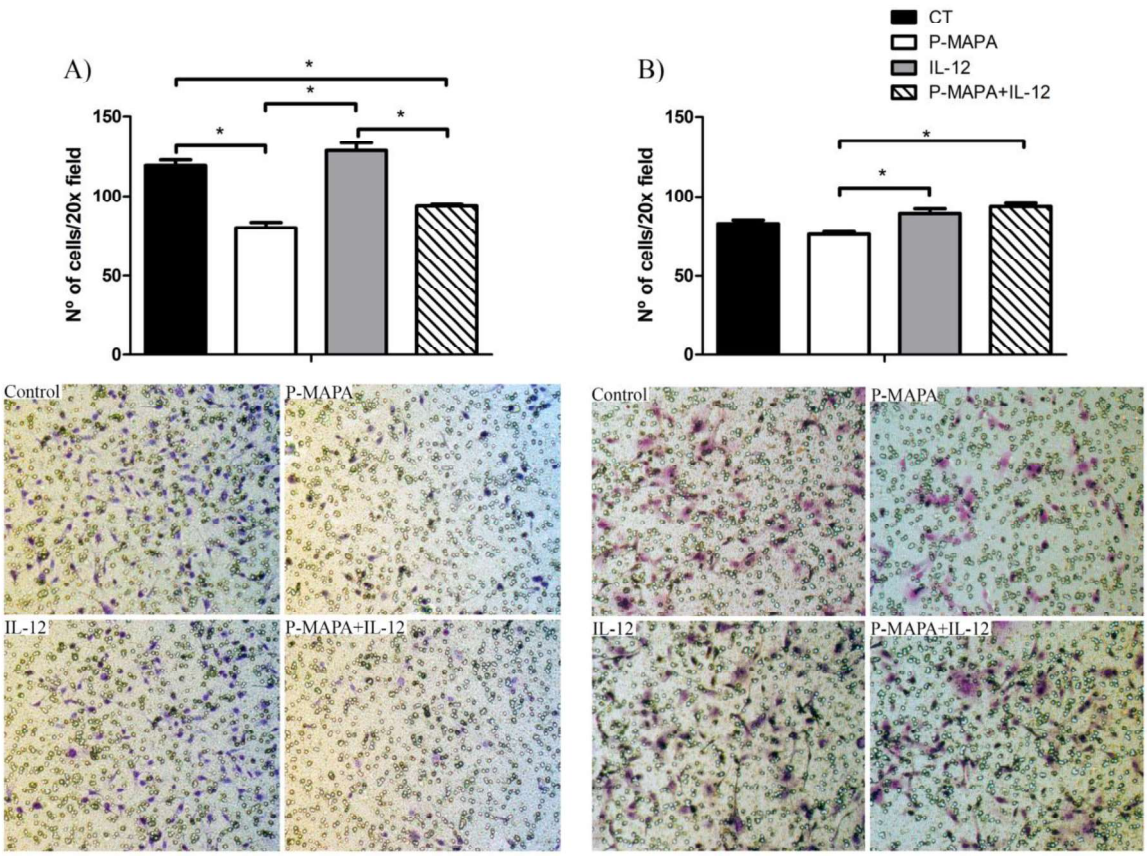

Figure 4. Effects of P-MAPA and IL-12 alone or in combination on the migration and invasion capacity of SKOV-3 cells. (**A**) Cell migration was measured by the amount of cells located in the lower part of the insert. (**B**) Cell invasion was determined by the amount of cells located in the lower part of the insert previously covered by Geltrex®. Representative images of the assay were obtained at 20× magnification. The samples were assayed in three technical and biological replicates. Results are expressed as the mean ± SD; * $p < 0.05$; CT, control group.

To further investigate and elucidate the location and the relative expression levels of the TLR2 and TLR4 receptors, an immunofluorescence assay was performed on SKOV-3 cells. As evidenced by the cellular fluorescence level, the P-MAPA treatment significantly decreased the expression level of cytoplasmic and nuclear TLR2 (48% fluorescence reduced vs. the control group; Figure 5C). On the contrary, IL-12 and the combination of P-MAPA and IL-12 promoted the highest TLR2 immunofluorescence intensity (135% and 151% fluorescence level, respectively vs. P-MAPA; Figure 5C), which suggests that IL-12 is responsible for restoring TLR2 activation after P-MAPA therapy in SKOV-3 cells. Lastly, the relative immunofluorescence of the TLR4 was unchanged after the treatments (Figure 5D).

2.4. P-MAPA Stimulates the Secretion of Pro- and Anti-Inflammatory Molecules, Whereas Its Association with IL-12 Induced the Synthesis of Inflammatory Cytokines in SKOV-3 Cells

To determine which cytokines/chemokines are secreted by the SKOV-3 cells and how P-MAPA and IL-12 act to regulate its production, a wide range of these molecules were evaluated in both supernatants (Figure 6A) and cellular extracts (Figure 6B). As expected, the IL-12 levels were higher in the cells treated with IL-12 and P-MAPA+IL-12 (244% and 243% fold-increased, respectively vs. the control group, and 154% and 155% fold-increased, respectively vs. the P-MAPA group; Figure 6A); IL-12 was slightly elevated with P-MAPA, even at low concentrations.

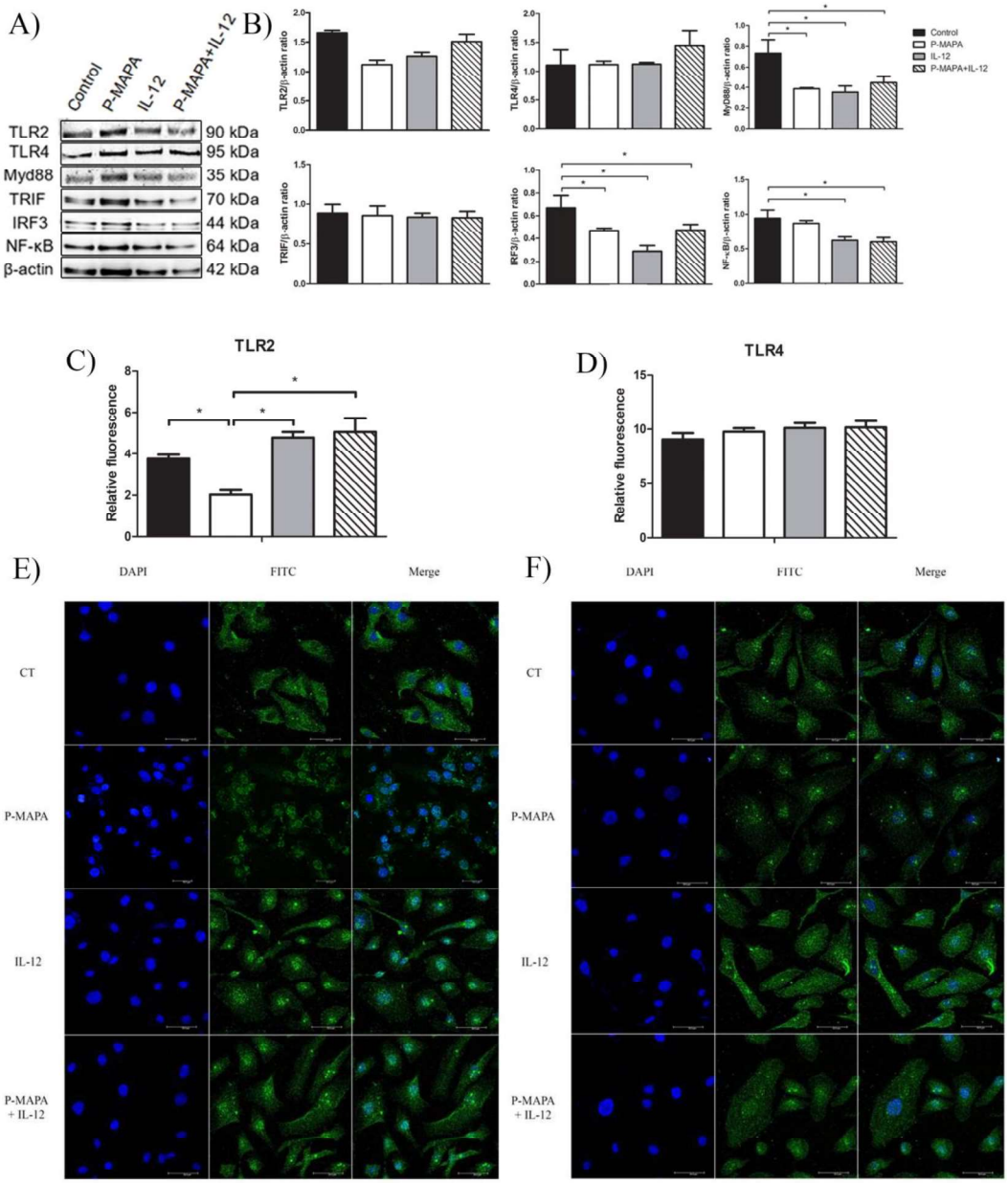

Figure 5. TLR2- and TLR4-mediated signaling pathways are involved with inflammatory process and chemoresistance in human OC. (**A**) Representative protein profiles of TLR2, TLR4, MyD88, TRIF, IRF3, and NF-kB; fractions containing 50 μg protein were pooled from 5 samples per group. (**B**) Individual blots were used for densitometric analysis of the TLR2 and TLR4 levels and related downstream molecules (MyD88, TRIF, IRF3, and NF-kB) after normalization to the β-actin. Data are expressed as the mean ± SD. * $p < 0.05$ vs. control group. Relative fluorescence intensity of TLR2 (**C**) and TLR4 (**D**) receptors. The values are expressed as the mean ± SD. The samples were assayed in three technical and biological replicates. * $p < 0.05$. Confocal imaging of TLR2 (**E**) and TLR4 (**F**) immunostaining using fluorescein isothiocyanate (FITC)-conjugated antibodies anti-TLR2 and anti-TLR4 was obtained in SKOV-3 cells (Alexafluor®488, bar = 50 μm). DAPI was used for nuclear staining and merged images were performed using Image J software. Negative controls were used. CT, control; DAPI, 4′,6-diamidino-2-phenylindole; FITC, fluorescein isothiocyanate.

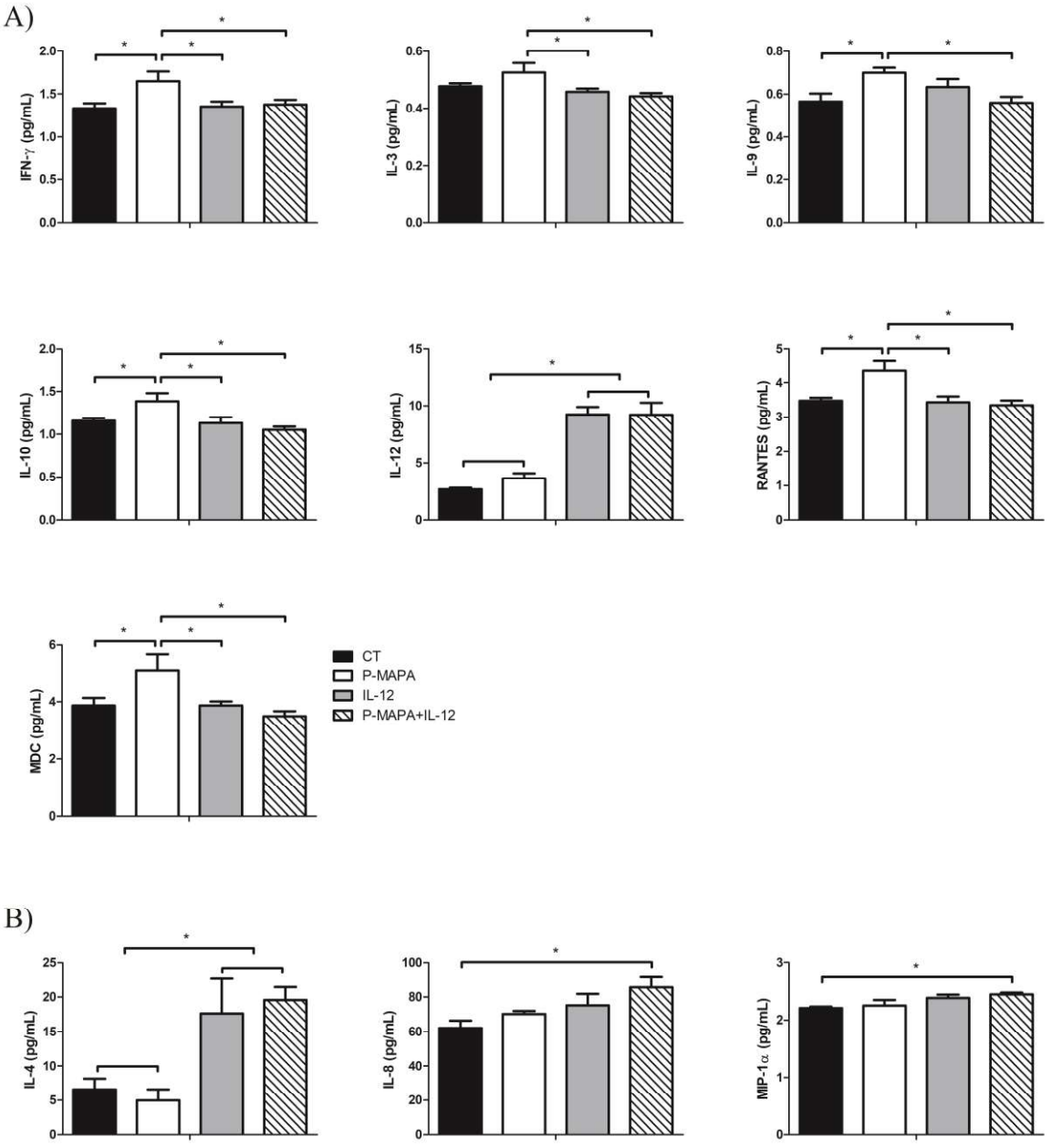

Figure 6. Multiplex analysis of cytokines and chemokines produced by SKOV-3 cells in response to P-MAPA and IL-12 treatments. (**A**) Concentrations of IFN-γ, IL-3, IL-9, IL-10, IL-12, RANTES, and MDC were altered in the supernatants of cell culture. (**B**) Levels of IL-4, IL-8, and MIP-1α were altered in SKOV-3 cell extracts. All data are expressed as the mean ± SD. * $p < 0.05$ as compared with the corresponding group; One-way ANOVA complemented by the Tukey test. The samples were assayed in three technical and biological replicates. CT, control; IFN-γ, interferon gamma; RANTES, regulated on activation, normal T cell expressed and secreted; MDC, macrophage-derived chemokine; MIP-1α, macrophage inflammatory protein 1-alpha.

Comparing the treatments, P-MAPA significantly stimulated the secretion of IFN-γ (24% vs. the control, IL-12 and P-MAPA+IL-12 groups; Figure 6A), which is probably related to the activation of the Th1 response. P-MAPA also stimulated IL-10 (21% vs. control, 23% vs. IL-12 and 32% vs. P-MAPA+IL-12 groups), MDC/CCL22 (31% vs. control and IL-12 groups, and 45% vs. P-MAPA+IL-12), and, regulated on activation, normal T cells expressed and secreted (RANTES)/CCL5 (25% vs. the control, 27% vs. the IL-12, and 30% vs. the P-MAPA+IL-12 groups). Furthermore, P-MAPA increased IL-3 and treatment with IL-12 or P-MAPA+IL-12 promoted a reduction in its levels (13% and 17% reduction, respectively vs. P-MAPA; Figure 6A). Treatment with P-MAPA also increased the IL-9 levels (25% increased vs. the control and P-MAPA+IL-12 groups; Figure 6A). A part of these results suggests the secretion of molecules involved in the Th2 response (e.g., IL-10, CCL22), but their regulatory signaling combined with other molecules released by immune cells into the OC microenvironment could not be proved to have a favorable or unfavorable effect. The IL-4 levels were internally elevated in SKOV-3 cells (Figure 6B) after therapies with IL-12 alone or combined with P-MAPA (169% and 254% increased vs. the control group and 198% and 293% increased vs. the P-MAPA group, respectively). Interestingly, the association of P-MAPA with IL-12 induced the highest production of intracellular IL-8 (37% vs. the control group) and MIP-1α (11% vs. control group; Figure 6B). In brief, cytokines that were not significantly influenced by P-MAPA and IL-12 included IL-1β, IL-2, IL-6, IL-7, IL-13, IL-15, IL-17, IP-10, MCP-1, and MIP-1β (Supplementary Tables S1 and S2).

3. Discussion

We reported that lower doses of P-MAPA efficiently reduce cell invasion, whereas P-MAPA in combination with IL-12 reduces cell migration in addition to attenuating the TLR-mediated inflammatory response in human SKOV-3 cells (Figure 7). Although these compounds have individually showed important effects in reducing OC volume and mass while enhancing overall survival and immunostimulation in animals and humans [11,16], this study is the first to describe a therapeutic rationale against human OC, thus revealing the mechanisms underlying cancer cell-related inflammatory aspects rather than those of immune cells.

P-MAPA and IL-12 elicited a decrease in cell metabolism, but no effect on cell apoptosis/necrosis and cell cycle was observed. Although an MTT assay is largely used as the viability/toxicity assay, it could be biased by decreased metabolism activity. This utilizes mitochondrial machinery to convert a colorless tetrazolium salt solution into purple formazan crystals [20]. Once we had pursued a treatment dose with low cell toxicity but considerable modulatory potential, we believed that either P-MAPA or IL-12 may be changing OC cell metabolism to a reduced activity (metabolomics could be of significant value to find the targets more precisely). The impact of this reduction was indeed confirmed by the migration and invasion assays. P-MAPA was able to reduce the migration and invasion capacity, and the delayed wound closure in IL-12-treated cells may be likely due to its decreased metabolic activity. Given that lower doses of P-MAPA and IL-12 are recommended to be well-tolerated, OC cell apoptosis could be prevented by the low-level toxicity of chemicals; conversely, these concentrations are safely used to activate immune responses and modulate cell metabolism. When associated with PTX, P-MAPA was able to increase cell death and apoptosis/necrosis ratio without potentiating the PTX effects on cell cycle. In accordance with a previous study in which approximately 50% of SKOV-3

cells died after 48 h exposure to 5 μM of PTX [21], we observed that P-MAPA not only was effective to increase cell death in the presence of PTX but also to maintain cell toxicity even after considerably lower levels of PTX. This increase in cell death might be a result of apoptosis induction, since the apoptosis/necrosis ratio was significantly higher in animals treated with the combination of P-MAPA and PTX. Because apoptosis lead to the release of the damage-associated molecular pattern (DAMP), this higher ratio may facilitate immunogenic cell death (ICD) [22].

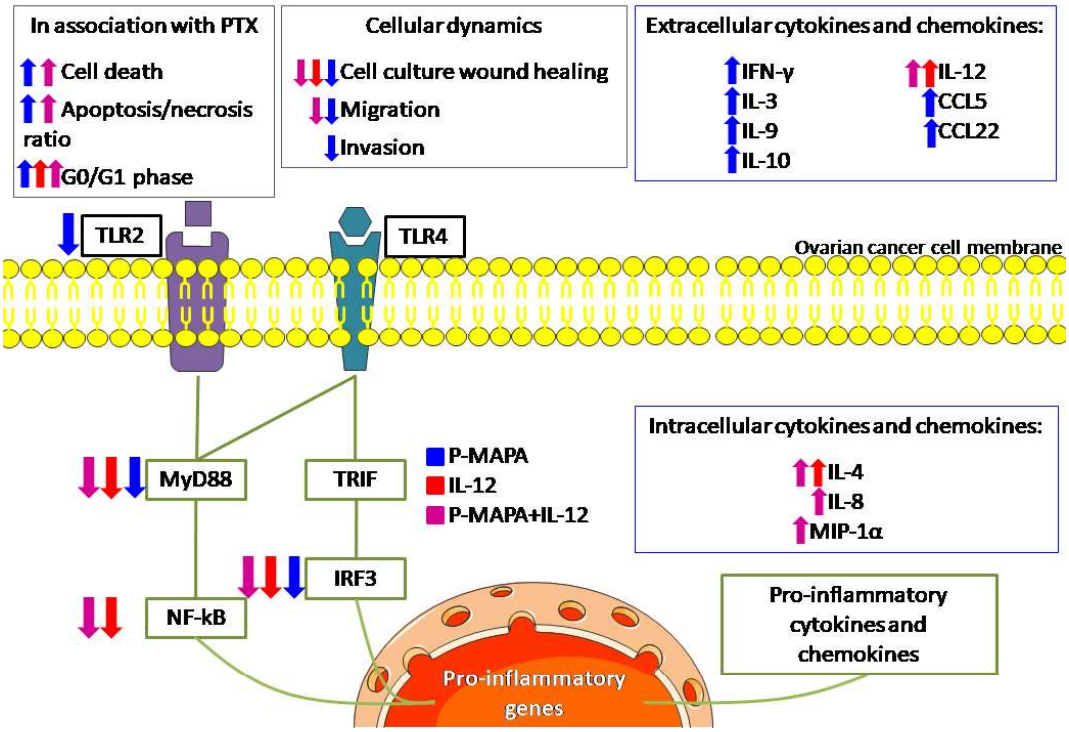

Figure 7. Schematic view of the effects of P-MAPA and IL-12 on human SKOV-3 cells. The effect of each treatment is shown by its representative color. Up and down arrows indicate whether the treatment increased or decreased, respectively, such as cellular function or molecule at these levels. The treatments reduced the downstream molecules (MyD88, NF-kB, and IRF3, with the exception of P-MAPA in reducing NF-kB) of both canonical and non-canonical toll-like receptor (TLR) signaling pathways, and only P-MAPA significantly downregulated the TLR2 levels. The intracellular cytokine/chemokine levels were increased after treatment with IL-12 (IL-4) or P-MAPA+IL-12 (IL-4, IL-8 and MIP-1α); P-MAPA was more effective in increasing the secretion of the following cytokines/chemokines: IFN-γ, IL-3, IL-9, IL-10, RANTES/CCL5, MDC/CCL22). As expected, IL-12 was used to treat SKOV-3 cells and appeared increased after IL-12 and P-MAPA+IL-12 treatments. Although IL-12 only reduced the SKOV-3 cells' wound closure, P-MAPA efficiently regulated the cellular dynamics by reducing the wound closure, cell migration and invasion. The combination of P-MAPA with IL-12 decreased the period of wound closure and cell migration rate. MyD88, myeloid differentiation primary response 88; NF-kB, nuclear factor kappa B; TRIF, TIR-domain-containing adapter-inducing interferon-β; IRF-3, interferon regulatory factor 3; TLR2, toll-like receptor 2; TLR4, toll-like receptor 4; P-MAPA, protein aggregate magnesium-ammonium phospholinoleate-palmitoleate anhydride; IL, interleukin; MIP-1α, macrophage inflammatory protein 1α; IFN-γ, interferon gamma; RANTES, regulated on activation, normal T cell expressed and secreted; MDC, macrophage-derived chemokine; CCL, C-C motif chemokine ligand.

The pro-inflammatory actions of TLR signaling in cancer cells and immune cells may severely affect tumor progression [23], and, particularly, the immunosuppressive OC microenvironment needs to be continuously immunostimulated [23,24]. Although TLR4 was unchanged by the treatments, P-MAPA induces a reduction in the TLR2 levels together with downstream molecules in SKOV-3 cells. Additionally, we found TLR2 nuclear expression in SKOV-3 cells treated with P-MAPA. Although we are not the first to observe nuclear staining of TLR2 and TLR4 [25], the effect of the switch of cytoplasmic to nuclear expression in SKOV-3 cells remains unclear. Based on our results, this nuclear expression seems not to have any negative effect favoring cancer development. Although the TLR2-induced MyD88-dependent pathway is related to an increase in IL-12 secretion [26], the immunoregulatory mechanisms whereby IL-12 restores TLR2 to levels close to control remain to be elucidated. In immune cells, P-MAPA has reportedly been described as a TLR4 agonist [9–11], thereby enhancing the synthesis of cytokines and activating a Th1-polarized response. Our data evidenced the protective effect of P-MAPA in attenuating TLR2-mediated signaling in OC cells. The activation of TLR, especially via MyD88, is associated with increased tumor growth, chemoresistance, and the early recurrence of ovarian epithelial tumors [7,27]. In addition, OC expressing high levels of MyD88 presents a higher proliferative index and increased production of pro-inflammatory cytokines and chemokines [7,28,29]. Importantly, the association of P-MAPA and IL-12 decreased the levels of MyD88 in SKOV-3 cells compared with their respective control; because P-MAPA and P-MAPA + IL-12 also significantly decreased the migratory and invasive potential of the cells, it can be suggested that the MyD88-dependent signaling pathway may be one of the mechanisms by which SKOV-3 cells promote migration and invasion. It has also been reported that increased expression of MyD88 is related to a decreased sensitivity to chemotherapy (e.g., PTX) in the MyD88-negative OC A2780 cell line [30]; moreover, the activation of MyD88 and NF-kB in MyD88-positive SKOV-3 cells promoted cell proliferation and tumor growth, likely due to the increased secretion of pro-inflammatory cytokines, thus rendering the cells PTX resistant [13]. In this line, the downregulation of MyD88 and NF-kB may be a possible mechanism by which P-MAPA improves the chemosensitivity of PTX in SKOV-3 cells.

The activation of TLR4/MyD88/NF-kB signaling by ligands is strongly related to an inflammatory microenvironment, thereby contributing to a more aggressive OC phenotype and poorer clinical outcomes in women [31]. In SKOV-3 cells, silencing the membrane-associated RING-CH (MARCH), an ubiquitin ligase that downregulates MHC class II expression, resulted in reduced cell migration and invasion in addition to inhibition of NF-kB signaling [32], thus reinforcing that NF-kB may play a role in the regulation of numerous cellular dynamics. Taken together, the combination of P-MAPA and IL-12 was efficient to induce the downregulation of both MyD88 and NF-kB, which can be of great value to enhance the overall survival of patients while attenuating OC progression and metastasis.

TRIF activation is responsible for triggering the TLR non-canonical pathway, thus activating several transcriptional factors, such as NF-kB, IRF3 and AP-1, and resulting in cytokines and type I IFN production [33,34]. Although few studies have explored the role of TRIF/IRF3 in OC cells, they seem to be critical for therapy [35]. Recently, Chuffa et al. [23] reported the downregulation of TRIF and IRF3 in OC-induced rats, whereby the immunomodulatory agent dramatically reduced the volume and mass of ovarian tumors. Importantly, P-MAPA and IL-12, either alone or in association, significantly downregulated IRF3 levels, evidencing the potential of immunotherapies to act by both canonical and non-canonical TLR pathways.

Immunostimulatory and immunosuppressive molecules can contribute to either inhibiting or enhancing anti-tumor immune activity of such a response by immunotherapy. We screened a number of molecules displaying important effects in OC, but most of them displayed no changes in SKOV-3 cells after P-MAPA and IL-12 treatments. Treatment of SKOV-3 with rhIL-12 showed its availability in both IL-12 and P-MAPA+IL-12 groups, thus proving that the agent was present in the supernatants; whether IL-12 therapy was still capable of stimulating more IL-12 production by the cells is uncertain. IL-3 levels are stimulated by P-MAPA therapy, and this increase might be protective for patients during OC chemotherapy; administration of rhIL-3 to patients with platelet count < 75,000/mm^3 is effective to

fight thrombocytopenia and neutropenia after chemotherapy [36]. Moreover, IL-3 is able to intensify the dose of carboplatin for primary advanced OC [37]. P-MAPA also enhanced IL-9 secretion by SKOV-3 cells, and this effect seems to have a dual impact on the immune system. IL-9 was initially recognized as a T-cell growth factor with oncogenic potential. However, Th9 cell-secreted IL-9 has been revisited for the immunity of some tumors [38]. IL-9 activates innate immune cells like mast cells, contributing to tumor growth prevention [38], and in addition to Th9 cell-derived IL-3, induction of adaptive anti-cancer responses that favor DCs survival has been reported in various cancers [39].

Regulatory T (Treg) cells can infiltrate into solid OC or ascitic fluid, contributing to an immunosuppressive microenvironment by secreting IL-10 and TGFB-1 while reducing the IFN-γ levels [40]. Because these cytokines participate either in stimulating or inhibiting the activities of other immune cells, P-MAPA seems to work as a double-edge sword regarding the SKOV-3 cells. Although mechanistically unclear, P-MAPA contributes partially to reducing the immunosuppression, likely due to the increased levels of IFN-γ rather than IL-10. In fact, high IFN-γ secretion meets our proposal by enhancing OC-cell immunogenicity through the recruitment of CD8+T and natural killer (NK) cells, in addition to increasing the anti-tumor activity of macrophages; we recently found that P-MAPA reduces Treg cells and stimulates CD8+T effector cells in OC-bearing animals (unpublished data). Recently, the expression of programmed death-ligand 1 (PD-L1) on tumor cells represents an important pathway by which malignant cells evade the immune system. In SKOV-3 cells, PD-L1 was variably found in the surface and cytoplasm [41], and its expression was correlated with high levels of TNF-α, IL-10, and IL-6 released from tumor-associated macrophages (TAMs). Because P-MAPA and IL-12 attenuated the downstream mediators of the TLR signaling, the altered expression of some cytokines may be independent of TLR-mediated inflammatory response.

A complex network represented by chemokines and its receptors, growth factors, inflammatory products, and other molecules (e.g., NF-kB), is responsible for tumor progression or rejection. Chemokines signal not only for tumor cells but may control tumor development through activation of specific receptors expressed in a variety of cells, thereby regulating the traffic of infiltrating macrophages, lymphocytes, DCs, and neutrophils [42]. The secretion of CCL5, which binds to the CCR4 receptor, is strongly associated with the presence of tumor-infiltrating CD8+T cells; the upregulation of its receptor in activated vaccine-primed T cells improved tumor homing in OC [43]. In SKOV-3 cells, the levels of CCL22/MDC and CCL5/RANTES were higher after P-MAPA therapy. Although these chemokines appear to be associated with a poor prognosis when released by immune cells, the functional meaning of their production by OC cells as to their significance in the OC microenvironment remains to be investigated. CCL22 is secreted by DCs and macrophages and acts on target cells by interacting with the CCR4 receptor located in the cell surface [44]. CCL22 is correlated to the chemoattraction of Treg cells in advanced stages of OC, and its expression was increased in response to IFN-γ signaling [45]. This finding partially corroborates our results in which both CCL22 and IFN-γ were higher in SKOV-3 cells after P-MAPA therapy; in contrast, P-MAPA does not promote elevation in the number of Treg cells (data not shown). A previous study by Giuntoli et al. [46] showed that ascites specimens originating from patients with malignant OC were accomplished by elevated levels of IL-6, IL-8, IL-10, IL-15, IP-10, MCP-1, MIP-1β, and VEGF, in contrast to significantly reduced levels of IL-2, IL-5, IL-7, IL-17, and CCL5/RANTES. Although controversial, IL-8 production by human OC cells plays a role in controlling tumor growth [47], and MIP-1α is involved in the recruitment of Th1 and cytotoxic effector T cells [48]. We found a higher secretion IL-8 and MIP-1α after combinatory treatment of P-MAPA and IL-12. Partially supporting our results, IL-8 levels have already been reported to be augmented in OC, even after the downregulation of NF-kB [49]; however, the alternative mechanism involved with this production remains unclear. Additionally, we observed increased levels of RANTES after P-MAPA treatment. RANTES is responsible for recruiting T cells, macrophages, eosinophils, and basophils into the inflammatory sites. In addition to IL-2 and IFN-γ, RANTES is thought to induce the activation and proliferation of NK cells while enhancing the anti-tumor response in animal models [46]. In addition to the overexpression of VEGF and MCP-1, a reduction in RANTES levels is associated with activating

pathways for tumor growth. Normally, OCs produce large amounts of RANTES, and this production is correlated with the infiltration of TAMs, CD8+T cells, and tumor progression [50,51]; these chemokines are further related to the acquisition of polarized immune responses (Th1 versus Th2). Although some negative effects are associated with the efficacy of chemotherapy related to RANTES, therapy with P-MAPA may be helpful against tumor expansion.

4. Materials and Methods

4.1. Cell Line and Cell Culture

The human OC cell line SKOV-3 was purchased from the American Type Culture Collection (ATCC, Rockville, MD, USA). The SKOV-3 cells were routinely incubated in RPMI 1640 (Life Technologies, Grand Island, NY, USA) supplemented with 10% Fetal Bovine Serum (FBS) and 1% anti-anti solution (100 mg/mL penicillin G, and 100 μg/mL streptomycin (Merck, Darmstadt, Germany). The culture medium was changed every 2 to 3 days. All cells were maintained at 37 °C in a humidified atmosphere of 5% CO_2.

4.2. Treatments with P-MAPA and IL-12

To evaluate the in vitro effect of the treatments, different doses of P-MAPA (25 μg/mL, 50 μg/mL, and 100 μg/mL) were tested in accordance with Favaro et al. [9]. Initially, 5 mg P-MAPA was diluted in 1 mL of saline solution to achieve the desired stock solution of 5 mg/mL, which were then diluted in the cell culture medium to obtain the testing doses. For the treatment with recombinant (rh)IL-12, concentrations of 0.5 ng/mL, 1 ng/mL, and 2 ng/mL were diluted in the culture medium based on the previous report by Su et al. [52]. For the combination of P-MAPA and IL-12, the most effective dose and incubation period were determined after performing an MTT assay. The saline solution was used as a solvent vehicle control and prepared in the same volume and dilution for both treatments. All experiments were performed at 0, 24, 48, and 72 h time exposure and assayed in three technical and biological replicates.

4.3. Cell Cytotoxicity (MTT Assay)

The SKOV-3 cells were seeded in a 96-well plate at a density of 1×10^3 cells/well. The cellular activity and/or toxicity were evaluated in different concentrations of P-MAPA and IL-12 and periods (0, 24, and 48 h) to define the best treatment protocol. For this experiment, the choice of dose and period of treatment was the combination of high cellular viability with low toxicity and efficient signaling regulation. Thereafter, different doses of PTX were associated with P-MAPA and IL-12 to verify the sensitivity effects. An MTT solution (5 mg/mL) was added to the wells for 4 h, and the crystals were diluted with DMSO under agitation. The concentration was determined by an Epoch microplate reader (BioTek Instruments, Highland Park, PO, USA) at 540 nm, being the reference curve fixed at 650 nm. The percentage of crystal formation was calculated by fixing the control group crystal formation as 100%.

4.4. Apoptosis Rate by Annexin V-FITC/PI Staining

During the apoptosis process, cells normally externalize the phospholipid phosphatidylserine (PS), which binds with high affinity to Annexin V in the presence of calcium. Herein, we used the Annexin V assay with the BD Pharmingen™ Annexin V-FITC Apoptosis Detection Kit (ApoAlert Annexin V, Clontech, CA, USA). The SKOV-3 cells (1×10^5 cells) were placed in a 6-well plate and left for 6 h to attach. The cells were then treated with 25 μg/mL of P-MAPA, 1 ng/mL of rhIL-12 or their association for 48 h. In addition, P-MAPA and IL-12 were added to the lowest dose of PTX (0.625 μM) to confirm chemosensitivity. After the treatment period, cells were trypsinized and centrifuged (Centrifuge 5804 R, Eppendorf, Hamburg, Germany)) for 10 min at 1200 rpm for culture medium removal. The cell pellet was washed twice with phosphate-buffered saline (PBS) and centrifuged at 10,000 rpm for 30 s, followed by resuspension with 100 μL Annexin V binding buffer and incubation with Annexin V and propidium iodide (PI) for 15 min in the dark at room temperature. After the incubation, the prepared cells were then analyzed by flow cytometry in a FACSCantoTMII with FACSDiva (BD Biosciences, Clontech, CA, USA) software. The flow cytometric results were analyzed by the FlowJo software (vX.10.6 version, Tree Stars Inc., Ashland, OR, USA).

4.5. Cell Cycle Determination by PI Staining

The cell cycle stages (G0/G1, S, and G2/M) were performed by flow cytometry analysis through the DNA content measurement of nuclei stained with PI dye. After all the treatments, the SKOV-3 cells (1×10^5) were trypsinized, washed with PBS, and centrifuged for 5 min at 1500 rpm. After the cells were fixed in 70% cold ethanol at 4 °C for 1 h, they were incubated with PI staining solution of 50 μg/mL PI and 10 mg/mL RNase A for 1 h at room temperature in a dark room. Flow cytometry was performed in a FACSCantoTMII with FACSDiva (BD Biosciences, Clontech, CA, USA) software to analyze DNA content. The relative ratios of cells in the G0/G1, S, and G2/M phases were calculated using FlowJo software (vX.10.6 version, Tree Stars Inc.).

4.6. Wound-Healing Assay

The wound-healing method was performed to verify the effects of P-MAPA and rhIL-12 alone or in combination on cell migration capacity. Briefly, 3×10^5 SKOV-3 cells were placed in 6-well plates with a serum-free culture medium for cell starvation. When the cells reached high confluence, a wound was created through the confluent cell monolayer using an angled tip at 45°, and the SKOV-3 cells were then immediately treated with the pre-determined doses of P-MAPA, rhIL-12, or both, diluted in 2 mL of complete RPMI 1640 medium. Images were obtained at 0 h, 6 h, 12 h, 24 h, 36 h, and 48 h until the wound closure. Migration area (%) was measured using Image-J software. All experiments were analyzed in biological and technical triplicate.

4.7. Cell Migration Using Transwell Insert

To evaluate the migratory potential of the cells, 1×10^4 SKOV-3 cells were seeded in triplicates into the upper chambers of 24-well ThinCert™ cell culture inserts (GBO, Americana, SP, Brazil) with PVDF filters (8.0 μm pore size) containing the corresponding treatment diluted in serum free RPMI 1640 medium. In the lower chamber, RPMI supplemented with 10% FBS was added as a chemotactic factor. After the plates were incubated at 37 °C and 5% CO_2 for 24 h, the cells in the upper chamber were gently removed with a cotton swab. The cells that had migrated to the lower surface of the insert through the 8.0 μm pore were fixed in methanol for 8 min and stained with hematoxylin for 45 s. The migrated cells were photographed with 20× objectives under an inverted microscope (ZeissAxiovert®, Germany). Four non-overlapped images were randomly analyzed for each well and the migrated cells were counted using Image J software.

4.8. Invasion Assay

The invasion assay was performed using a 24-well ThinCert™ cell culture insert (GBO, Americana, SP, Brazil) with PVDF filters (8.0 μm pore size). Briefly, 24-well plates were previously coated with Geltrex® (ThermoFisher, Waltham, MA, USA), which mimics the biological basement membrane matrix, and 1×10^4 cells were placed in the upper chamber with a serum-free culture medium containing the treatments. After 24 h, the invasive potential was determined by the amount of cells capable of crossing the barrier when chemotactically attracted by the RPMI 1640 medium supplemented with 10% FBS in the lower chamber. The protocol of cell fixing and staining was the same described for cell migration. Finally, four non-overlapped images were randomly analyzed per well and the invasive cells were counted using Image J software.

4.9. Immunofluorescence Assay

After the SKOV-3 cells were seeded in coverslips and treated with P-MAPA, rhIL-12, or their association for 48 h, they were fixed in methanol for 8 min at room temperature and then washed in sterile ice-cold PBS. To avoid nonspecific bindings, a blocking solution containing 3% (*v*/*v*) bovine serum albumin (BSA) was added for 1 h. Then, cells were incubated overnight with rabbit polyclonal anti-TLR2 and anti-TLR4 antibodies diluted 1:200 (Abcam, Cambridge, MA) for 4 h, followed by post incubation with secondary polyclonal anti-IgG conjugated to FITC (1:200 dilution in 1% BSA, Santa Cruz Biotechnology, Inc., CA) for 1 h. After the reactions, 4,6-diamidino-2-phenylindole (DAPI; Sigma, St Louis, MO) was used for nuclei staining. Positive staining was analyzed using a confocal fluorescence microscope Zeiss Axiophot II (Carl Zeiss, Oberköchen, Germany) at different magnification (excitation filter 590 nm, emission filter 650 nm) and for DAPI staining (excitation filter 365 nm, emission filter 485 nm). The relative fluorescence in FITC images was calculated using Image J software.

4.10. Western Blot Analysis

After the treatments, five replicates of each experiment were used. After being washed with cold PBS, 1×10^6 SKOV-3 cells were added to radioimmunoprecipitation assay buffer (RIPA) lysis buffer containing protease inhibitors and rapidly frozen for 24 h. Under constant agitation for 30 min at 4 °C, the cells were resuspended and transferred to 1.5 mL tubes and centrifuged for 20 min at 12,000 rpm. Protein quantification was performed using a Bradford assay, and the same amount of protein (40 μg) was solubilized in 1.5×Laemmli buffer and then used for 4–20% SDS-PAGE (Bio-Rad Laboratories, Hercules, CA, USA). After electrophoresis was carried out on tris-glycine running buffer system (120 V for 2 h), the proteins were electro-transferred (350 mA) to nitrocellulose membranes, and then blocked with 3% BSA in tris-buffered saline plus tween 20 (TBS-T) solution for 1 h. Afterward, the proteins were incubated with respective primary antibodies (1:500; Abcam, Cambridge, UK) at 4 °C overnight: anti-TLR2, anti-TLR4, anti-MyD88, anti-NF-kB p65, anti-TRIF, anti-IRF3. Subsequently, the membranes were washed three times and then incubated for 90 min with specific secondary antibodies (Sigma-Aldrich, St. Louis, MO, USA) diluted 1:20,000 in 1% BSA. After sequential washes, positive reactions were performed using ECL kit (Thermo Fisher Scientific, MA). All of the blots were calculated using individual samples obtained from three replicates/group and were represented as the mean optical density (band intensity/housekeeping protein). β-actin was used as the endogenous control.

4.11. Cytokine and Chemokine Assay

Levels of different cytokines and chemokines were determined in both supernatants and cell homogenates using a MilliPlex® Map Kit (EMD Millipore, Darmstadt, Germany) with a standard 20-plex detection kit according to the manufacturer's protocols. The human cytokine/chemokine Panel I kit (cat. no. HCYTOMAG-60K) included the following analytes: interferon-gamma (IFN-γ), interleukin (IL)-1β, IL-2, IL-3, IL-4, IL-6, IL-7, IL-8, IL-9, IL- 10, IL-12, IL-13, IL-15, IL-17, IP-10, macrophage-derived chemokine (MDC/CCL22), monocyte chemotactic protein-1 (MCP-1), macrophage inflammatory protein-1 (MIP)-1α, MIP-1β, and regulated upon activation normal T cell expressed and secreted (RANTES/CCL5). The concentrations were ranged between 0 and the lowest detectable level in each assay before log transformation. The analyses combined fluorescent cytometry and ELISA technology, so that each magnetic bead was added to a specific anti-cytokine to achieve a specific binding. For this experiment, the levels of analytes varied from 0.4 to 3500 pg/mL and the intra-assay CV was < 10%, inter-assay CV < 15%. No cross-reactivity was observed among cytokines and other molecules. The fluorescence intensity was measured using the MAGPIX system (Luminex Corporation, Austin, TX, USA).

4.12. Statistical Analysis

All data were evaluated using the analysis of variance (ANOVA) and presented as the mean ± standard deviation (SD). Significant results were then compared by Tukey or Newman-Keuls *post hoc* tests, and statistical significance was set at $p < 0.05$ for all analyses. Data were analyzed and constructed using GraphPad Prism 5.0 scientific graphing software (GraphPad Software, San Diego, CA, USA).

5. Conclusions

In summary, we demonstrated that P-MAPA in association with IL-12, both considered potent immunomodulatory agents, exhibited anti-cancer activities on human SKOV-3 cells. Although P-MAPA combined with IL-12 promotes a reduction in cell viability and cell migration, P-MAPA alone reduces the invasion capacity and enhances apoptosis in the presence of PTX. Similarly to either P-MAPA or IL-12 alone, the combinatory therapy induced the downregulation of TLR-downstream molecules involved with inflammation, which may result in protection against chemoresistance; these effects seem to be associated with TLR2 suppression rather than TLR4 signaling. P-MAPA alone stimulated the secretion of pro- and anti-inflammatory mediators, and its association with IL-12 increased the production of IL-4, -8, and MIP-1α by the SKOV-3 cells; this may promote changes in the immune responsiveness of the OC microenvironment. In addition to the effect on OC-infiltrated immune cells, these immunotherapies might provide a sustained opportunity for a novel combined strategy against malignant OC cells.

Supplementary Materials: The following are available online. Figure S1: MTT assay was tested with different cell densities to find the most appropriate strategy for cell counting. SKOV-3 cells at density of 1×10^3 were representative to determine cell viability; Table S1: Multiplex assay of the cytokines and chemokines (pg/mL) in the supernatant of cell culture; Table S2: Multiplex assay of the cytokines and chemokines (pg/mL) in the SKOV-3 cells.

Author Contributions: L.A.L., L.G.d.A.C., F.K.D.: conceived the hypothesis of the study, collected and analyzed the data, and drafted the manuscript. W.J.F., F.E.M., M.M., G.G.R., R.K., M.S.C., R.F.D., I.d.S.N.: participated in its design, intellectual conception of the study, and in the acquisition of data. All authors have read and agreed to the published version of the manuscript.

Funding: We would like to give a special thanks to Farmabrasilis-Brazil, FAPESP (*Fundação de Amparo à Pesquisa do Estado de São Paulo*, grant numbers: 2019/00906-6 and 2016/03993-9), CAPES (grant number: 0708/2018), and CNPq (grant number: 401040/2016-0) by providing financial support.

Acknowledgments: We are grateful to HélioKushima and Valeria Sandrim from Department of Pharmacology, IBB/UNESP, Botucatu, SP, Brazil, for excellent technical assistance and support.

Conflicts of Interest: The authors declare no conflict of interest.

Abbreviations

BSA	Bovine serum albumin
CEEA	Ethical Committee of the Institute of Bioscience/UNESP
CEMIB	Multidisciplinary Center for Biological Investigation
DAB	Diaminobenzidine
DAPI	6-diamidino-2-phenylindole
DCs	Dendritic cells
FITC	Fluorescein Isothiocyanate
HRP-conjugated	Horseradish peroxidase-conjugated
H	Hematoxylin
IFN	Interferon
IFN-γ	Interferon gamma
IL-6	Interleukin 6
IL-8	Interleukin 8
IRF3	Interferon regulatory factor 3
MyD88	Myeloid differentiation factor 88
NF-kB p65	Nuclear factor kappa B subunit p65
NK	natural killer cells
OC	ovarian cancer
PBS	phosphate-buffered saline
P-MAPA	Protein aggregate magnesium-ammonium phospholinoleate-palmitoleate anhydride
PTX	paclitaxel
RIPA	Radioimmunoprecipitation assay buffer
SDS-PAGE	Sodium dodecyl sulphate-polyacrylamide gel electrophoresis
TBS-T	Tris-Buffered Saline plus Tween 20
CD4 + T	CD4-positive T cells
CD8 + T	CD8-positive T cells
Th1	T helper 1
TLR (s)	Toll-like receptor (s)
TLR2	Toll-like receptor 2
TLR4	Toll-like receptor 4
TRIF	TIR domain-containing adaptor inducing interferon-beta

References

1. Siegel, R.L.; Miller, K.D.; Jemal, A. Cancer statistics, 2018. *CA Cancer J. Clin.* **2018**, *68*, 7–30. [CrossRef] [PubMed]
2. Fallows, S.; Price, J.; Atkinson, R.J.; Johnston, P.G.; Hickey, I.; Russell, S.E. P53 mutation does not affect prognosis in ovarian epithelial malignancies. *J. Pathol.* **2001**, *194*, 68–75. [CrossRef] [PubMed]
3. Cannistra, S.A. Cancer of the ovary. *N. Engl. J. Med.* **2004**, *351*, 2519–2565. [CrossRef] [PubMed]
4. Chuffa, L.G.; Fioruci-Fontanelli, B.A.; Mendes, L.O.; Fávaro, W.J.; Pinheiro, P.F.; Martinez, M.; Martinez, F.E. Characterization of chemically induced ovarian carcinomas in an ethanol-preferring rat model: Influence of long-term melatonin treatment. *PLoS ONE* **2013**, *8*, e81676. [CrossRef] [PubMed]
5. Chuffa, L.G.; Lupi-Júnior, L.A.; Costa, A.B.; Amorim, J.P.; Seiva, F.R. The role of sex hormones and steroid receptors on female reproductive cancers. *Steroids* **2017**, *118*, 93–108. [CrossRef]
6. Ebell, M.H.; Culp, M.B.; Radke, T.J. A systematic review of symptoms for the diagnosis of ovarian cancer. *Am. J. Prev. Med.* **2016**, *50*, 384–394. [CrossRef]
7. Kelly, M.G.; Alvero, A.B.; Chen, R.; Silasi, D.A.; Abrahams, V.M.; Chan, S.; Visintin, I.; Rutherford, T.; Mor, G. TLR-4 signaling promotes tumor growth and paclitaxel chemoresistance in ovarian cancer. *Cancer Res.* **2006**, *66*, 3859–3868. [CrossRef]
8. Bronte, G.; Cicero, G.; Sortino, G.; Pernice, G.; Catarella, M.T.; D'Alia, P.; Cusenza, S.; Lo Dico, S.; Bronte, E.; Sprini, D.; et al. Immunotherapy for recurrent ovarian cancer: A further piece of the puzzle or a striking strategy? *Expert Opin. Biol. Ther.* **2014**, *14*, 103–114. [CrossRef]
9. Fávaro, W.J.; Nunes, O.S.; Seiva, F.R.; Nunes, I.S.; Woolhiser, L.K.; Durán, N.; Lenaerts, A.J. Effects of P-MAPA immunomodulator on Toll-like receptors and p53: Potential therapeutic strategies for infectious diseases and cancer. *Infect. Agent. Cancer* **2012**, *7*, 1–15.
10. Garcia, P.V.; Seiva, F.R.; Carniato, A.P.; de Mello Júnior, W.; Duran, N.; Macedo, A.M.; de Oliveira, A.G.; Romih, R.; de Oliveira, A.G.; Romih, R.; et al. Increased toll-like receptors and p53 levels regulate apoptosis and angiogenesis in non-muscle invasive bladder cancer: Mechanism of action of P-MAPA biological response modifier. *BMC Cancer* **2016**, *16*, 422. [CrossRef]
11. de Almeida Chuffa, L.G.; de Moura Ferreira, G.; Lupi, L.A.; da Silva Nunes, I.; Fávaro, W.J. P-MAPA immunotherapy potentiates the effect of cisplatin on serous ovarian carcinoma through targeting TLR4 signaling. *J. Ovarian Res.* **2018**, *11*, 8. [CrossRef]
12. Chen, R.; Alvero, A.B.; Silasi, D.A.; Steffensen, K.D.; Mor, G. Cancers take their Toll–the function and regulation of Toll-like receptors in cancer cells. *Oncogene* **2008**, *27*, 225–233. [CrossRef]
13. Szajnik, M.; Szczepanski, M.J.; Czystowska, M.; Elishaev, E.; Mandapathil, M.; Nowak-Markwitz, E.; Spaczynski, M.; Whiteside, T.L. TLR4 signaling induced by lipopolysaccharide or paclitaxel regulates tumor survival and chemoresistance in ovarian cancer. *Oncogene* **2009**, *28*, 4353–4363. [CrossRef] [PubMed]
14. Wang, A.C.; Su, Q.B.; Wu, F.X.; Zhang, X.L.; Liu, P.S. Role of TLR4 for paclitaxel chemotherapy in human epithelial ovarian cancer cells. *Eur. J. Clin. Investig.* **2009**, *39*, 157–164. [CrossRef] [PubMed]
15. Trinchieri, G. Interleukin-12 and the regulation of innate resistance and adaptive immunity. *Nat. Rev. Immunol.* **2003**, *3*, 133–146. [CrossRef] [PubMed]
16. Cohen, C.A.; Shea, A.A.; Heffron, C.L.; Schmelz, E.M.; Roberts, P.C. Interleukin-12 Immunomodulation Delays the Onset of Lethal Peritoneal Disease of Ovarian Cancer. *J. Interferon Cytokine Res.* **2016**, *36*, 62–73. [CrossRef] [PubMed]
17. Colombo, M.P.; Trinchieri, G. Interleukin-12 in anti-tumor immunity and immunotherapy. *Cytokine Growth Factor Rev.* **2002**, *13*, 155–168. [CrossRef]

18. Hurteau, J.A.; Blessing, J.A.; DeCesare, S.L.; Creasman, W.T. Evaluation of recombinanthuman interleukin-12 in patients with recurrent or refractory ovarian cancer: Agynecologic oncology group study. *Gynecol. Oncol.* **2001**, *82*, 7–10. [CrossRef]
19. Lenzi, R.; Edwards, R.; June, C.; Seiden, M.V.; Garcia, M.E.; Rosenblum, M.; Freedman, R.S. Phase II study of intraperitoneal recombinant interleukin-12 (rhIL-12) in patients with peritoneal carcinomatosis (residual disease <1 cm) associated with ovarian cancer or primary peritoneal carcinoma. *J. Transl. Med.* **2007**, *5*, 66.
20. Präbst, K.; Engelhardt, H.; Ringgeler, S.; Hübner, H. Cell Viability Assays: Methods and Protocols. *Methods Mol. Biol.* **2017**, *1601*, 117.
21. Ahn, H.J.; Kim, Y.S.; Kim, J.U.; Han, S.M.; Shin, J.W.; Yang, H.O. Mechanism of taxol-inducedapoptosis in human SKOV3 ovarian carcinoma cells. *J. Cell Biochem.* **2004**, *91*, 1043–1052. [CrossRef]
22. Wang, Y.J.; Fletcher, R.; Yu, J.; Zhang, L. Immunogenic effects of chemotherapy-induced tumor cell death. *Genes Dis.* **2018**, *5*, 194–203. [CrossRef]
23. Chuffa, L.G.; Fioruci-Fontanelli, B.A.; Mendes, L.O.; Ferreira Seiva, F.R.; Martinez, M.; Fávaro, W.J.; Domeniconi, R.F.; Pinheiro, P.F.; Delazari Dos Santos, L.; Martinez, F.E. Melatonin attenuates the TLR4-mediated inflammatory response through MyD88- and TRIF-dependent signaling pathways in an in vivo model of ovarian cancer. *BMC Cancer* **2015**, *15*, 34. [CrossRef]
24. Lavoue, V.; Thedrez, A.; Leveque, J.; Foucher, F.; Henno, S.; Jauffret, V.; Belaud-Rotureau, M.A.; Catros, V.; Cabillic, F. Immunity of human epithelial ovarian carcinoma: The paradigm of immunesuppression in cancer. *J. Transl. Med.* **2013**, *11*, 1–12. [CrossRef]
25. Jouhi, L.; Koljonen, V.; Böhling, T.; Haglund, C.; Hagström, J. The expression of toll-like receptors 2, 4, 5, 7 and 9 in Merkel cell carcinoma. *Anticancer Res.* **2015**, *35*, 1843–1849.
26. Zhu, G.; Gui, Z. Effect of silkworm peptide on inducting M1 type polarization andTh1 activation via TLR2-induced MyD88-dependent pathway. *Food Sci. Nutr.* **2019**, *7*, 1251–1260. [CrossRef] [PubMed]
27. d'Adhemar, C.J.; Spillane, C.D.; Gallagher, M.F.; Bates, M.; Costello, K.M.; Barry-O'Crowley, J.; Haley, K.; Kernan, N.; Murphy, C.; Smyth, P.C.; et al. The MyD88+ phenotype is an adverse prognostic factor in epithelial ovarian cancer. *PLoS ONE* **2014**, *9*, e100816. [CrossRef]
28. Kim, K.H.; Jo, M.S.; Suh, D.S.; Yoon, M.S.; Shin, D.H.; Lee, J.H.; Choi, K.U. Expression and significance of the TLR4/MyD88 signaling pathway in ovarian epithelial cancers. *World J. Surg. Oncol.* **2012**, *10*, 193. [CrossRef] [PubMed]
29. Gaikwad, S.M.; Thakur, B.; Sakpal, A.; Singh, R.K.; Ray, P. Differential activation of NF-κB signaling is associated with platinum and taxane resistance in MyD88deficient epithelial ovarian cancer cells. *Int. J. Biochem. Cell Biol.* **2015**, *61*, 90–102. [CrossRef] [PubMed]
30. Zhan, Y.; Xiang, F.; Wu, R.; Xu, J.; Ni, Z.; Jiang, J.; Kang, X. MiRNA-149 modulates chemosensitivity of ovarian cancer A2780 cells to paclitaxel by targeting MyD88. *J. Ovarian Res.* **2015**, *8*, 48. [CrossRef] [PubMed]
31. Li, Z.; Block, M.S.; Vierkant, R.A.; Fogarty, Z.C.; Winham, S.J.; Visscher, D.W.; Kalli, K.R.; Wang, C.; Goode, E.L. The inflammatory microenvironment in epithelial ovarian cancer: A role for TLR4 and MyD88 and related proteins. *Tumour Biol.* **2016**, *37*, 13279–13286. [CrossRef] [PubMed]
32. Meng, Y.; Hu, J.; Chen, Y.; Yu, T.; Hu, L. Silencing MARCH1 suppresses proliferation, migration and invasion of ovarian cancer SKOV3 cells via downregulation of NF-κB and Wnt/β-catenin pathways. *Oncol. Rep.* **2016**, *36*, 2463–2470. [CrossRef] [PubMed]
33. Yamamoto, M.; Sato, S.; Hemmi, H.; Hoshino, K.; Kaisho, T.; Sanjo, H.; Takeuchi, O.; Sugiyama, M.; Okabe, M.; Takeda, K.; et al. Role of adaptor TRIF in the MyD88-independent toll-like receptor signaling pathway. *Science* **2003**, *301*, 640–643. [CrossRef] [PubMed]

34. Ullah, M.O.; Sweet, M.J.; Mansell, A.; Kellie, S.; Kobe, B. TRIF-dependent TLR signaling, its functions in host defense and inflammation, and its potential as a therapeutic target. *J. Leukoc. Biol.* **2016**, *100*, 27–45. [CrossRef] [PubMed]
35. Muccioli, M.; Sprague, L.; Nandigam, H.; Pate, M.; Benencia, F. Toll-like receptors as novel therapeutic targets for ovarian cancer. *ISRN Oncol.* **2012**, *2012*, 642141. [CrossRef] [PubMed]
36. Yamamoto, K.; Yajima, A.; Terashima, Y.; Nozawa, S.; Taketani, Y.; Yakushiji, M.; Noda, K. Phase II clinical study on the effects of recombinant human interleukin-3 onthrombocytopenia after chemotherapy for advanced ovarian cancer. SDZ ILE 964[IL-3] Study Group. *J. Immunother.* **1999**, *22*, 539–545. [CrossRef]
37. Veldhuis, G.J.; Willemse, P.H.; van Gameren, M.M.; Aalders, J.G.; Mulder, N.H.; Mull, B.; Biesma, B.; deVries, E.G. Recombinant human interleukin-3 to dose-intensify carboplatin and cyclophosphamide chemotherapy in epithelial ovarian cancer: A phase I trial. *J. Clin. Oncol.* **1995**, *13*, 733–740. [CrossRef]
38. Rivera-Vargas, T.; Humblin, E.; Végran, F.; Ghiringhelli, F.; Apetoh, L. Th9 cells inanti-tumor immunity. *Semin. Immunopathol.* **2017**, *39*, 39–46. [CrossRef]
39. Park, J.; Li, H.; Zhang, M.; Lu, Y.; Hong, B.; Zheng, Y.; He, J.; Yang, J.; Qian, J.; Yi, Q. Murine Th9 cells promote the survival of myeloid dendritic cells in cancerimmunotherapy. *Cancer Immunol. Immunother.* **2014**, *63*, 835–845. [CrossRef]
40. Singh, M.; Loftus, T.; Webb, E.; Benencia, F. Minireview: Regulatory T Cells and Ovarian Cancer. *Immunol. Investig.* **2016**, *45*, 712–720. [CrossRef]
41. Qu, Q.X.; Xie, F.; Huang, Q.; Zhang, X.G. Membranous and cytoplasmic expression ofPD-L1 in ovarian cancer cells. *Cell. Physiol. Biochem.* **2017**, *43*, 1893–1906. [CrossRef] [PubMed]
42. Barbieri, F.; Bajetto, A.; Florio, T. Role of chemokine network in the development and progression of ovarian cancer: A potential novel pharmacological target. *J. Oncol.* **2010**, *2010*, 426956. [CrossRef] [PubMed]
43. Zsiros, E.; Duttagupta, P.; Dangaj, D.; Li, H.; Frank, R.; Garrabrant, T.; Hagemann, I.S.; Levine, B.L.; June, C.H.; Zhang, L.; et al. The ovarian cancer chemokine landscape isconducive to homing of vaccine-primed and CD3/CD28-costimulated T cells prepared for adoptive therapy. *Clin. Cancer Res.* **2015**, *21*, 2840–2850. [CrossRef]
44. Vulcano, M.; Albanesi, C.; Stoppacciaro, A.; Bagnati, R.; D'Amico, G.; Struyf, S.; Transidico, P.; Bonecchi, R.; Del Prete, A.; Allavena, P.; et al. Dendritic cells as a major source of macrophage-derived chemokine/CCL22 in vitro and in vivo. *Eur. J. Immunol.* **2001**, *31*, 812–822. [CrossRef]
45. Fialová, A.; Partlová, S.; Sojka, L.; Hromádková, H.; Brtnický, T.; Fučíková, J.; Kocián, P.; Rob, L.; Bartůňková, J.; Spíšek, R. Dynamics of T-cell infiltration during thecourse of ovarian cancer: The gradual shift from a Th17 effector cell response toa predominant infiltration by regulatory T-cells. *Int. J. Cancer* **2013**, *132*, 1070–1079.
46. Giuntoli, R.L., 2nd; Webb, T.J.; Zoso, A.; Rogers, O.; Diaz-Montes, T.P.; Bristow, R.E.; Oelke, M. Ovarian cancer-associated ascites demonstrates altered immune environment: Implications for antitumor immunity. *Anticancer Res.* **2009**, *29*, 2875–2884.
47. Lee, L.F.; Hellendall, R.P.; Wang, Y.; Haskill, J.S.; Mukaida, N.; Matsushima, K.; Ting, J.P. IL-8 reduced tumorigenicity of human ovarian cancer in vivo due to neutrophil infiltration. *J. Immunol.* **2000**, *164*, 2769–2775. [CrossRef]
48. Colvin, E.K. Tumor-associated macrophages contribute to tumor progression in ovarian cancer. *Front. Oncol.* **2014**, *4*, 137. [CrossRef]
49. Tino, A.B.; Chitcholtan, K.; Sykes, P.H.; Garrill, A. Resveratrol and acetyl-resveratrol modulate activity of VEGF and IL-8 in ovarian cancer cell aggregates via attenuation of the NF-κB protein. *J. Ovarian Res.* **2016**, *9*, 84. [CrossRef]
50. Milliken, D.; Scotton, C.; Raju, S.; Balkwill, F.; Wilson, J. Analysis of chemokinesand chemokine receptor expression in ovarian cancer ascites. *Clin. Cancer Res.* **2002**, *8*, 1108–1114.

51. Soria, G.; Ben-Baruch, A. The inflammatory chemokines CCL2 and CCL5 in breastcancer. *Cancer Lett.* **2008**, *267*, 271–285. [CrossRef] [PubMed]
52. Su, W.; Ito, T.; Oyama, T.; Kitagawa, T.; Yamori, T.; Fujiwara, H.; Matsuda, H. The direct effect of IL-12 on tumor cells: IL-12 acts directly on tumor cells to activate NF-kB and enhance IFN-g-mediated STAT1 phosphorylation. *Biochem. Biophys. Res. Commun.* **2001**, *280*, 503–5121. [CrossRef] [PubMed]

Sample Availability: Samples of the compounds are not available from the authors.

Supplementary material

Supplementary Figure. MTT assay was tested with different cell densities to find the most appropriate strategy for cell counting. SKOV-3 cells at density of 1 x 10^3 were representative to determine cell viability.

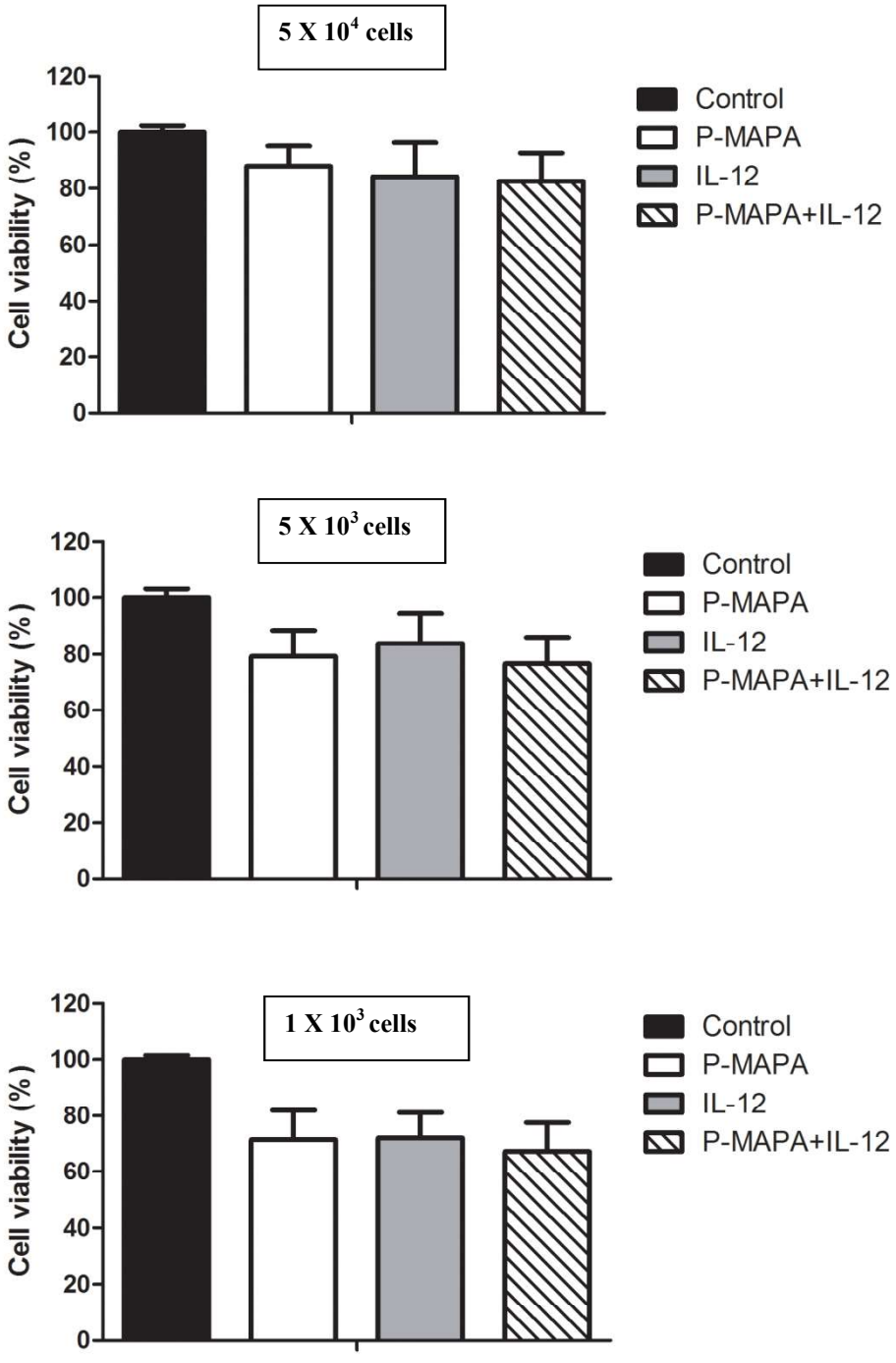

Table 1. Multiplex assay of the cytokines and chemokines (pg/mL) in the supernatant of cell culture.

Supernatant samples

Analytes	Groups				
	p	Control	P-MAPA	IL-12	P-MAPA+IL-12
IL-1β	0.57	0.95±0.03	1.00±0.04	0.99±0.08	0.90±0.05
IL-2	0.93	1.25±0.11	1.27±0.08	1.20±0.02	1.24±0.07
IL-4	***0.09***	11.12±1.43	15.42±3.20	11.34±1.01	8.16±1.23
IL-6	0.25	711.96±21.78	742.56±9.77	713.43±21.70	773.01±34.77
IL-7	***0.07***	7.63±0.63	10.38±1.20	8.02±0.51	8.02±0.51
IL-8	0.93	2425.17±212.67	2564.33±270.22	2476.67±230.15	2613.50±134.71
IL-13	0.42	5.56±0.80	7.57±1.74	5.13±0.82	5.35±0.90
IL-15	0.10	7.21±0.29	7.10±0.23	6.67±0.18	7.71±0.37
IL-17	0.29	1.13±0.028	1.22±0.04	1.16±0.03	1.16±0.04
IP-10	0.59	31.85±0.61	32.03±0.99	33.15±0.73	32.72±0.61
MCP-1	0.21	5.19±0.76	4.23±0.47	3.88±0.17	3.94±0.22
MIP-1α	0.34	2.36±0.06	2.46±0.08	2.33±0.04	2.33±0.03
MIP-1β	***0.06***	2.84±0.10	3.31±0.25	2.85±0.14	2.72±0.05

No significant values are presented for these analytes. The results are means ± SD of 3 biological replicates. *One-Way ANOVA.*

Table 2. Multiplex assay of the cytokines and chemokines (pg/mL) in the SKOV-3 cells.

Cell samples

Analytes	Groups				
	p	Control	P-MAPA	IL-12	P-MAPA+IL-12
IFN-γ	0.43	1.793±0.095	2.178±0.297	2.185±0.166	2.250±0.221
IL-1β	0.23	1.047±0.052	1.268±0.091	1.303±0.086	1.285±0.131
IL-2	0.52	1.183±0.073	1.278±0.110	1.320±0.091	1.430±0.165
IL-3	0.17	0.507±0.009	0.552±0.039	0.585±0.031	0.615±0.043
IL-6	0.86	99.333±7.386	106.290±7.668	102.955±5.242	110.415±14.494
IL-7	0.89	55.663±1.698	57.483±2.478	54.293±2.034	55.865±4.411
IL-9	0.88	72.683±10.873	78.472±13.781	75.458±5.267	67.703±5.772
IL-10	0.20	0.973±0.031	1.135±0.140	1.130±0.046	1.250±0.077
IL-12	0.22	3.113±0.200	4.165±0.583	4.308±0.439	4.662±0.678
IL-13	0.98	38.013±1.177	38.987±2.108	37.520±3.027	37.835±3.933
IL-15	0.29	54.893±3.757	63.215±5.637	67.510±6.760	76.310±11.575
IL-17	0.48	1.633±0.051	1.728±0.098	1.703±0.052	1.823±0.113
IP-10	0.48	34.030±0.349	34.105±1.365	33.590±1.477	37.765±3.623
MCP-1	0.75	2.927±0.033	3.035±0.347	3.183±0.263	3.288±0.244
MDC	0.13	2.993±0.098	3.665±0.425	4.053±0.363	3.885±0.246
MIP-1β	***0.08***	11.680±0.208	13.063±2.580	10.293±1.858	6.545±1.069
RANTES	0.21	8.597±0.724	9.580±1.646	9.800±1.087	6.590±0.700

No significant values are presented for these analytes. The results are means ± SD of 3 biological replicates. *One-Way ANOVA.*

Capítulo 3

ACS OMEGA

Cite This: ACS Omega 2019, 4, 21761−21777

Article

http://pubs.acs.org/journal/acsodf

P-MAPA and IL-12 Differentially Regulate Proteins Associated with Ovarian Cancer Progression: A Proteomic Study

Luiz Antonio Lupi Júnior,[†] Maira Smaniotto Cucielo,[†] Raquel Fantin Domeniconi,[†] Lucilene Delazari dos Santos,[‡] Henrique Spaulonci Silveira,[†] Iseu da Silva Nunes,[§] Marcelo Martinez,[⊥] Francisco Eduardo Martinez,[†] Wagner José Fávaro,[∥] and Luiz Gustavo de Almeida Chuffa*[,†]

[†]Department of Anatomy, Institute of Biosciences and [‡]Center for the Study of Venoms and Venomous Animals (CEVAP), UNESP—Universidade Estadual Paulista, Botucatu, São Paulo 18618-689, Brazil

[§]Farmabrasilis R&D Division, Campinas, São Paulo 18610-307, Brazil

[∥]Department of Structural and Functional Biology, UNICAMP—University of Campinas, Campinas, São Paulo 13083-970, Brazil

[⊥]Department of Morphology and Pathology, Federal University of São Carlos, São Carlos, São Paulo 13565-905, Brazil

ABSTRACT: To investigate the potential role of immunotherapies in the cellular and molecular mechanisms associated with ovarian cancer (OC), we applied a comparative proteomic toll using protein identification combined with mass spectrometry. Herein, the effects of the protein aggregate magnesium-ammonium phospholinoleate-palmitoleate anhydride, known as P-MAPA, and the human recombinant interleukin-12 (hrIL-12) were tested alone or in combination in human SKOV-3 cells. The doses and period were defined based on a previous study, which showed that 25 μg/mL P-MAPA and 1 ng/mL IL-12 are sufficient to reduce cell metabolism after 48 h. Indeed, among 2,881 proteins modulated by the treatments, 532 of them were strictly concordant and common. P-MAPA therapy upregulated proteins involved in tight junction, focal adhesion, ribosome constitution, GTP hydrolysis, semaphorin interactions, and expression of SLIT and ROBO, whereas it downregulated ERBB4 signaling, toll-like receptor signaling, regulation of NOTCH 4, and the ubiquitin proteasome pathway. In addition, IL-12 therapy led to upregulation of leukocyte migration, tight junction, and cell signaling, while cell communication, cell metabolism, and Wnt signaling were significantly downregulated in OC cells. A clear majority of proteins that were overexpressed by the combination of P-MAPA with IL-12 are involved in tight junction, focal adhesion, DNA methylation, metabolism of RNA, and ribosomal function; only a small number of downregulated proteins were involved in cell signaling, energy and mitochondrial processes, cell oxidation and senescence, and Wnt signaling. These findings suggest that P-MAPA and IL-12 efficiently regulated important proteins associated with OC progression; these altered proteins may represent potential targets for OC treatment in addition to its immunoadjuvant effects.

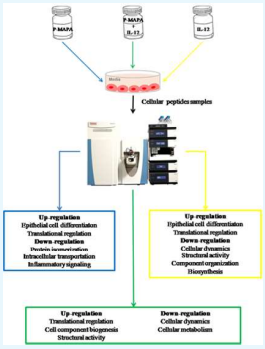

1. INTRODUCTION

Ovarian cancer (OC) represents the most lethal of gynecological malignancies being often diagnosed at a late stage.[1,2] The majority of patients experience difficulties over the course of treatment, with a 5 years survival rate of 35% when diagnosed late.[3] Because no evident symptom is present at an early-stage OC, the disease can rapidly progress to an incurable form.[4−11] Importantly, patients are generally responsive to the treatments; however, through several mechanisms, they develop resistance to chemotherapy and OC grows wildly.[12] New promising strategies to overcome chemoresistance and increase chemosensitivity have been developed for OC treatment, including immunotherapies.

We evaluated the effect of two immunotherapeutic agents from the proteomic standpoint. The immunomodulatory agent termed protein aggregate magnesium-ammonium phospholinoleate-palmitoleate anhydride (P-MAPA) is a natural biopolymer extracted from the *Aspergillus oryzae*. Experimentally, P-MAPA exhibits a number of antitumor responses in different in vivo models of cancer,[11,13,14] and specifically in OC, P-MAPA potentiated the effects of cisplatin, thereby enhancing TLR signaling in immune cells and attenuating tumor growth.[11] Another tested agent was interleukin-12 (IL-12), a cytokine secreted by antigen-presenting cells (APCs), which is involved in the differentiation of naïve T cells into a polarized Th1 immune response.[15,16] Treatment with IL-12 promotes tumor regression and reduces the potential of tumor outgrowth in patients with recurrent OC;[16,17] although IL-12 therapy results in an OC refractory state, the major challenge is related to its high cellular toxicity.[18] Although these immunotherapies have demonstrated to be quite effective in the treatment of OC with regard to the tumor microenvironment, their exact role on OC cells in terms of protein synthesis and secretion is far from being understood; certainly, there must be other particular functions in addition to those related to the immune system.

Received: August 6, 2019
Accepted: November 27, 2019
Published: December 11, 2019

DOI: 10.1021/acsomega.9b02512
ACS Omega 2019, 4, 21761−21777

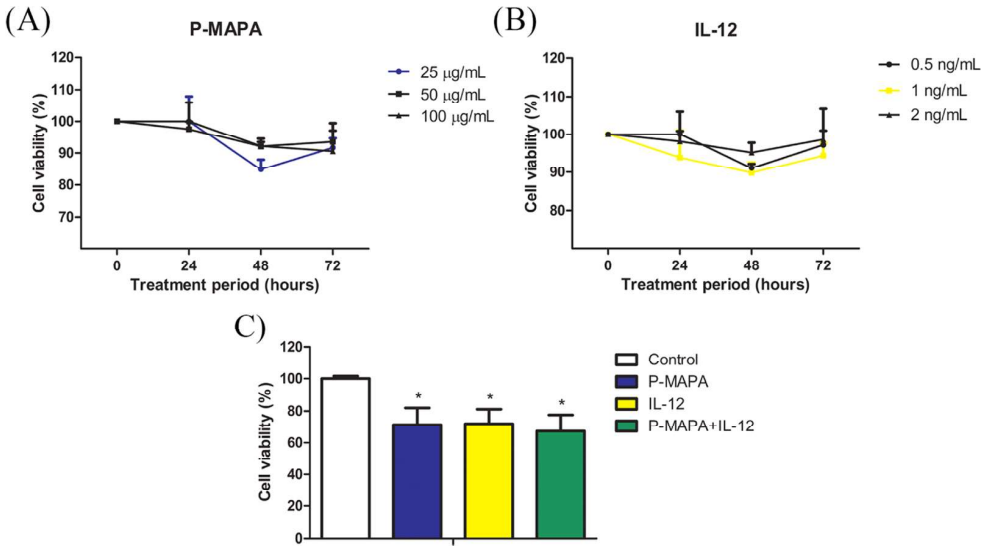

Figure 1. Defining the treatments with P-MAPA and IL-12. (A) Cell viability (%) after exposure to three different doses of P-MAPA (25, 50, and 100 μg/mL) in four different periods (0, 24, 48, and 72 h). (B) Cell viability (%) after exposure to three different doses of IL-12 (0.5, 1, and 2 ng/mL) in four different periods (0, 24, 48, and 72 h). Colored line of the selected dose is highlighted. (C) Cell viability (%) was assessed by MTT (1×10^3 cells) after exposure to standardized doses of treatments (25 μg/mL P-MAPA, 1 ng/mL IL-12, or both) at 48 h. The results are expressed as the mean ± standard deviation (SD). *$p < 0.05$ vs control.

Identifying successfully signaling pathways that coordinate tumor cell metabolism, protein−protein interactions, secretion of molecules and factors, and activity of specific enzymes is needed to discover new chemical agents and further modify the OC aggressiveness. Thus, proteomic analysis using mass spectrometry (MS) may provide a wide body of information considering proper candidates for OC development and treatment.[10,19−21] Large or small molecules are definitely recognized to be involved in intra- or intercellular processes, in which one molecule can possibly be sharing different signaling mechanisms in the same tumor cell.

Although there are important studies reporting the use of mass spectrometry in the diagnosis of cancers, including the monitoring strategies for OC,[10,22,23] none has shown the concurrent role of immunotherapies in predicting clinical outcomes from the "omics" standpoint. To further strengthen this issue, we studied the effects of immunotherapeutic agents, P-MAPA and IL-12, directly on human ovarian cancer SKOV-3 cells through proteomic profiling.

2. RESULTS AND DISCUSSION

2.1. Influence of Low-Dose Administration of P-MAPA and IL-12 in SKOV-3 Cells' Viability. The global behavior of OC cells in response to different conditions of treatment is crucial for designing future strategies. We previously reported an immunostimulatory effect of P-MAPA in an in vivo OC model,[11] while IL-12 is a well-known inductor of polarized Th1 immune response.[15,16] Despite the consistent effects on the tumor microenvironment, the direct effect of these compounds in cancer cells is uncertain, and understanding how they act in OC in a safe dose regimen may be greatly beneficial for patients. Although several proteomic approaches in animal models with OC have recently been tested, little is known about the effects of P-MAPA and IL-12 on this disease. The effects of P-MAPA and IL-12 were first tested using three different doses and four exposure times (Figure 1A). After an 3-(4,5-dimethylthiazol-2-yl)-2,5-diphenyltetrazolium bromide (MTT) assay, cell viability was reduced by P-MAPA at a dose of 25 μg/mL (~ 25% reduction), by IL-12 at a dose of 1 ng/mL (~ 25% reduction), and by the association of P-MAPA with IL-12 (~ 30% reduction) after 48 h (Figure 1B) (see details in Experimental Section, Section 4.3). We then performed a global proteomic analysis in OC cells treated with P-MAPA, IL-12, and P-MAPA associated with IL-12, reporting an extensive catalogue of differentially expressed proteins that are affected by these immunotherapies. The majority of proteins described herein are involved in key cellular processes and signaling pathways, such as metabolic processes; catalytic functions; structural activity; protein, DNA, and RNA binding; and transcription/translation regulatory activity. The variety of biological functions impacted by these agents makes them interesting candidates as potential alternatives to OC treatment.

2.2. Label-Free Proteomic Analysis of SKOV-3 Cells Treated with P-MAPA and IL-12. Samples were fractionated with reverse-phase columns to separate protein mixtures, and label-free analysis was performed on peptides by their charges and hydrophobicity. This analysis identified a total of 896 proteins among control, P-MAPA, IL-12, and P-MAPA + IL-12 groups. We reported a total of 636 molecules in the control, 719 in the P-MAPA group, 709 in the IL-12 group, and 740 proteins in the P-MAPA + IL-12 group, while 532 were commonly found in all tested groups (Figure 2). General intersections showing the proteins that are present in one or more groups were represented and varied with the treatment. Figure 3 shows the interaction between up- and downregulated proteins with the highest confidence (0.900) after P-MAPA therapy compared with the control. We found a total of 770 proteins in these groups, while 585 were coexpressed. In the P-MAPA group, there were 50 downregulated and 21 upregulated proteins (Table 1) compared with the control, considering the differential expression by at least ±1.5-fold change. The great majority of upregulated molecules are proteins related to protein localization to the membrane,

DOI: 10.1021/acsomega.9b02512
ACS Omega 2019, 4, 21761−21777

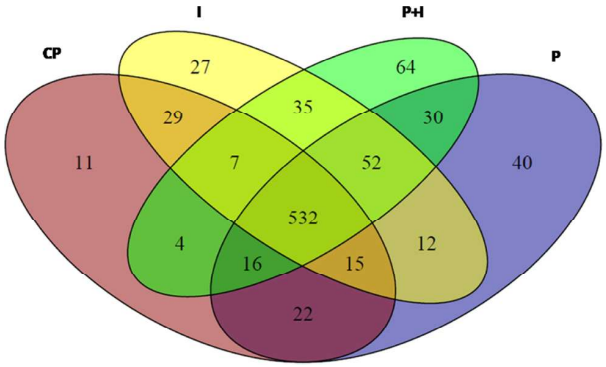

Figure 2. Cartoon displaying the intersection of proteins between the experimental groups; 532 proteins coexisted among the control, P-MAPA, IL-12, and P-MAPA + IL-12 groups. CP, control; I, IL-12; P, P-MAPA; P + I, P-MAPA + IL-12.

epithelial cell differentiation, SRP-dependent cotranslational protein targeting the membrane, and translational initiation. Otherwise, the downregulated proteins are involved in protein peptidyl-prolyl isomerization, intracellular transport, error-free and -prone translesion synthesis, and the TRIF-dependent toll-like receptor signaling pathway.

Figure 4 shows the up- and downregulated protein networks with clusters of strong confidence (highest confidence: 0.900) between the proteins produced by the SKOV-3 cells after IL-12 treatment versus the control group. A total of 762 proteins were identified, and 583 of them were coexpressed in the two groups. Based on differential expression by at least a factor of ±1.5 in the IL-12 group relative to the corresponding control group, we reported 85 downregulated proteins (Table 2), which are involved in different biological processes and molecular function: cytoskeleton organization, cellular component organization or biogenesis, structural molecule activity, protein-containing complex binding, and actin filament binding. Conversely, from the 30 upregulated proteins, we found some of them involved in a number of cellular events, such as intracellular transport, chromosome and organelle organization, chromatin silencing, structural molecule activity, and protein heterodimerization.

The combinatory treatment of P-MAPA and IL-12 versus the control group showed the up- and downregulated protein network with a very strong confidence relationship (0.900) (Figure 5). We found a total of 817 proteins, with 559 of them being differentially expressed by at least a factor of ±1.5 in the P-MAPA + IL-12 group relative to the corresponding untreated group. Among the 31 upregulated proteins, most of them were involved in different biological processes and molecular functions including canonical glycolysis, doxorubicin and daunorubicin metabolic processes, trans-1,2-dihydrobenzene-1,2-diol dehydrogenase activity, ketosteroid monooxygenase activity, androsterone dehydrogenase activity, phenanthrene 9,10-monooxygenase activity, and aldo-keto reductase (NADP) activity (Table 3). We found 76 downregulated proteins, with proteins involved in translational initiation, SRP-dependent cotranslational protein targeting the membrane, nuclear-transcribed mRNA catabolic process, nonsense-mediated decay, mRNA catabolic process, cellular component biogenesis, nucleosomal DNA binding, structural molecule activity, protein-containing complex binding, cytoskeletal protein binding, and structural constituent of ribosome.

2.3. P-MAPA and IL-12 Differentially Alter Cellular Function-Related Proteins in SKOV-3 Cells. To provide another view of which categories the differentially expressed proteins belong to, gene ontology (GO) annotation was carried out. We used PANTHER classification to demonstrate the molecular function, cellular component, biological processes, and protein class whereby specific treatment was able to alter. The result was a large and complex molecule network for each treatment. The main protein functions that differentially varied after treatments with P-MAPA, IL-12, and P-MAPA + IL-12 are summarized in Figures 6−8, respectively. The proteins differentially regulated by P-MAPA, IL-12, and P-MAPA + IL-12 treatments were the most closely related to molecular functions such as binding, catalytic activity, and structural molecule activity. With regard to biological processes, the majority of these proteins were involved in a metabolic process, biological regulation, and cellular component organization or biogenesis, being represented mostly by chaperones, cytoskeletal proteins, enzyme modulators, and hydrolases. Importantly, modulation of key processes that allow cancer cells to have a metabolic advantage and increased capacity to regulate cell binding with other tissues might be an important feature of all treatments.

We observed increased expressions of hybrid ubiquitin-ribosomal protein L40 (RPL40) and ubiquitin-ribosomal protein s27a (RPS27a) after the treatment with P-MAPA (2.9-fold increase), IL-12 (1.94-fold increase), and P-MAPA + IL-12 (2.6-fold increase). It has long been documented that ubiquitin targets proteins for proteasome degradation or nondegradation signaling.[24] Anticancer drugs, such as 5-fluorouracil, trichostatin A, and paclitaxel, often lead to overexpression of ubiquitin, which causes increased susceptibility to apoptotic cell death in a number of tumor cell lines.[25] In this process, the aggregation of ubiquitylated proteins in the nucleus is an important event, and this transport can be facilitated by ubiquitin binding to either RPS27a or RPL40.[25] In colorectal cancer cells, upregulation of the *UBA52* gene, which encodes the ubiquitin-RPL40 hybrid protein, is related to cell-cycle arrest and apoptosis induction via activation of the RPL40-MDM2-p53 pathway, resulting in increased expression of the tumor-suppressor p53.[26] Additionally, all treatments were able to upregulate polyubiquitin-B and -C, in which the chains are highly related with caspase-8 activation mediated by tumor necrosis factor receptor-associated factor 2 (TRAF2) and, consequently, sensibilization of TNF-related apoptosis-inducing ligand (TRAIL)-induced apoptosis.[27] Since chemoresistance and tumor aggressiveness are common challenges in the treatment of OC, the combined use of traditional chemotherapeutics and adjuvant components capable of modulating ubiquitination and promoting cell death might improve the therapy efficacy.

Among proteins that were downregulated by P-MAPA, IL-12, and P-MAPA + IL-12 treatments were myosin-9 (1.9-, 2.03-, and 2.5-fold decrease vs the control group, respectively), T-complex protein 1 (2.08-, 2.24-, and 3.08-fold decrease), and prohibitin-2 (2.24-, 2.07-, and 2.34-fold decrease). Myosin-9 is a heavy chain of myosin IIA and is involved in cytokinesis, maintenance of cell shape, and cell motility.[28] It has been suggested as a possible target for anti-invasive treatment in the breast cancer cell line MCF-7[29] and in gastric cancer.[30] Its overexpression has been related to both decreased overall survival and disease-free survival in esophageal squamous cell carcinoma (ESCC)[30] and also in lung adenocarcinoma.[31] T-

DOI: 10.1021/acsomega.9b02512
ACS Omega 2019, 4, 21761−21777

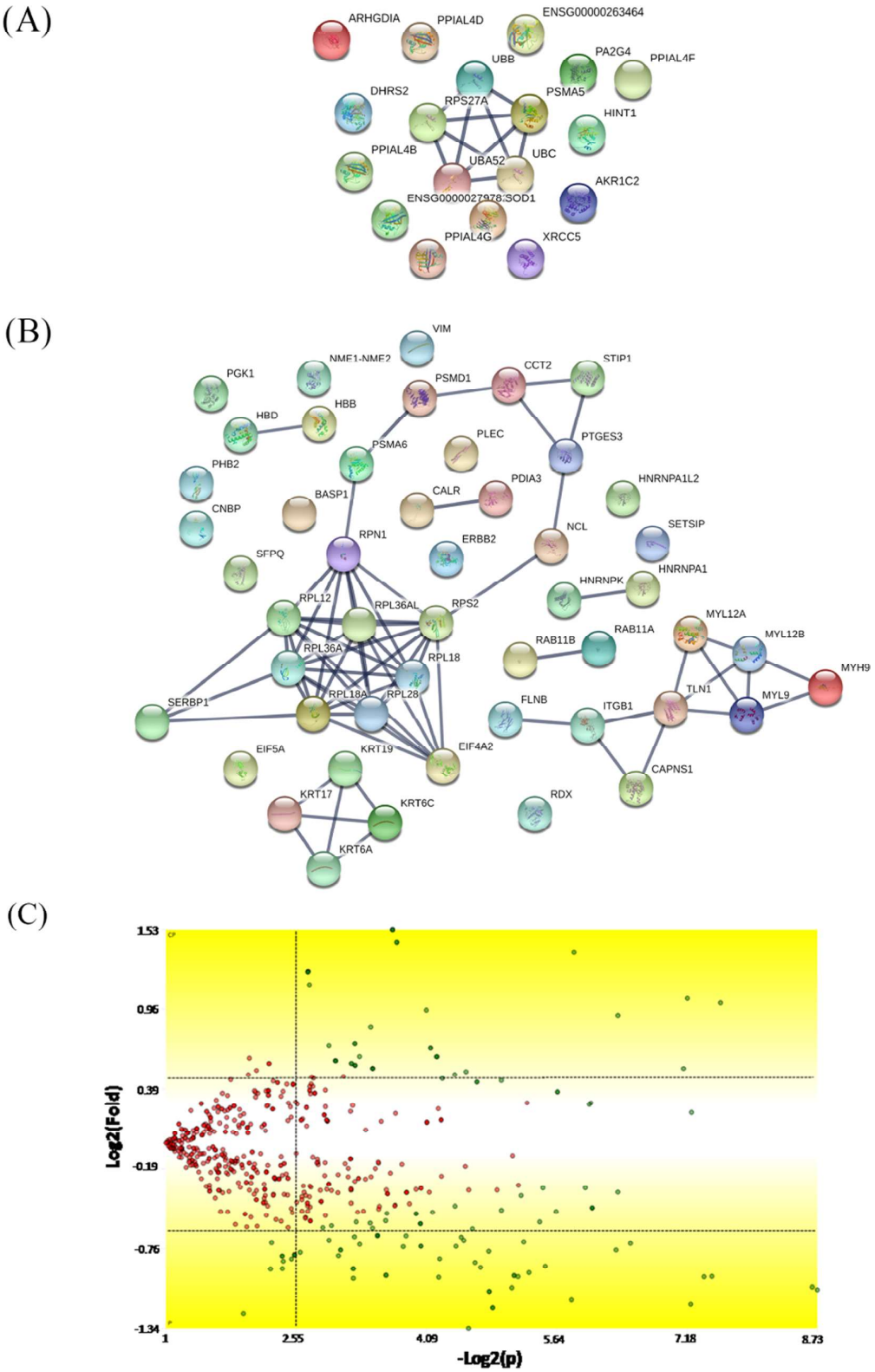

Figure 3. Mapping of the protein association network in P-MAPA-treated SKOV-3 cells. Source of the protein−protein interaction is based on cellular processing and its related molecular systems. Thicker lines show the highest confidence score (0.900) for upregulated (A) and downregulated (B) molecules of a functional association in response to P-MAPA therapy in SKOV-3 cells. (C) Volcano plot indicates large magnitude fold-changes (*y*-axis) and statistical significance (*p*-value, *x*-axis); this plot indicates log 2 fold change vs −log 2 false discovery rate (FDR)-corrected *p*-value. Differentially expressed proteins are shown in the upper and lower right areas. See legends in Table 1.

DOI: 10.1021/acsomega.9b02512
ACS Omega 2019, 4, 21761−21777

Table 1. Differentially Expressed Proteins in the P-MAPA Group versus the Control Group

protein ID	description	% coverage	protein score	fold change
P62979	ubiquitin-40S ribosomal protein S27a	21.8	15.5	2.90
P62987	ubiquitin-60S ribosomal protein L40	26.6	15.5	2.90
P0CG47	polyubiquitin-B	14.9	15.5	2.90
P28066	proteasome subunit α type-5	12.0	8.5	2.58
P0CG48	polyubiquitin-C	14.9	15.5	2.35
P49773	histidine triad nucleotide-binding protein 1	7.1	2.9	2.34
Q13268	SDR family member 2, mitochondrial	3.6	4.6	2.05
Q9UQ80	proliferation-associated protein 2G4	5.1	5.6	1.89
B2RPK0	putative high mobility group protein B1-like 1	10.9	7.6	1.78
P52895	aldo-keto reductase family 1 member C2	10.2	8.8	1.62
Q6DRA6	putative histone H2B type 2-D	10.4	12.9	1.60
Q6DN03	putative histone H2B type 2-C	8.8	12.9	1.60
P52565	Rho GDP-dissociation inhibitor 1	8.3	7.3	1.54
P13010	X-ray repair cross-complementing protein 5	3.1	4.4	1.54
P00441	superoxide dismutase [Cu−Zn]	10.4	3.0	1.52
P0DN37	peptidyl-prolyl cis−trans isomerase A-like 4G	7.9	4.4	1.51
A0A0B4J2A2	peptidyl-prolyl cis−trans isomerase A-like 4C	7.9	4.4	1.51
A0A075B759	peptidyl-prolyl cis−trans isomerase A-like 4E	7.9	4.4	1.51
F5H284	peptidyl-prolyl cis−trans isomerase A-like 4D	7.9	4.4	1.51
P0DN26	peptidyl-prolyl cis−trans isomerase A-like 4F	7.9	4.4	1.51
Q9Y536	peptidyl-prolyl cis−trans isomerase A-like 4A	7.9	4.4	1.51
P63241	eukaryotic translation initiation factor 5A-1	18.2	6.6	−1.50
P46779	60S ribosomal protein L28	25.6	10.1	−1.51
P00558	phosphoglycerate kinase 1	18.2	24.0	−1.51
P80723	brain acid soluble protein 1	37.9	19.0	−1.53
P15880	40S ribosomal protein S2	13.7	15.3	−1.53
P83881	60S ribosomal protein L36a	8.5	3.8	−1.59
Q969Q0	60S ribosomal protein L36a-like	8.5	3.8	−1.59
O14950	myosin regulatory light chain 12B	11.6	4.6	−1.59
P24844	myosin regulatory light polypeptide 9	11.6	4.6	−1.59
P19105	myosin regulatory light chain 12A	11.7	4.6	−1.59
P27797	calreticulin	20.4	39.1	−1.60
P04626	receptor tyrosine-protein kinase erbB-2	4.3	9.4	−1.63
Q99460	26S proteasome non-ATPase regulatory subunit 1	1.0	3.1	−1.63
P31948	stress-induced-phosphoprotein 1	10.3	15.8	−1.64
P08670	vimentin	24.5	46.7	−1.64
O75369	filamin-B	6.8	41.9	−1.65
P30101	protein disulfide-isomerase A3	19.2	36.4	−1.66
Q9Y490	Talin-1	6.9	49.0	−1.67
P61978	heterogeneous nuclear ribonucleoprotein K	23.5	44.7	−1.67
P30050	60S ribosomal protein L12	24.2	18.5	−1.68
P08727	keratin, type I cytoskeletal 19	33.5	51.3	−1.71
P0DME0	protein SETSIP	4.3	7.9	−1.72
Q15149	plectin	3.5	37.4	−1.72
P02042	hemoglobin subunit delta	12.9	8.9	−1.75
P68871	hemoglobin subunit β	12.9	8.9	−1.75
Q04695	keratin, type I cytoskeletal 17	21.5	54.7	−1.76
P35241	radixin	10.6	23.9	−1.78
P02538	keratin, type II cytoskeletal 6A	21.6	41.7	−1.80
P60900	proteasome subunit α type-6	9.4	11.1	−1.82
P22392	nucleoside diphosphate kinase B	36.2	25.8	−1.85
Q8NC51	plasminogen activator inhibitor 1 RNA-binding protein	12.5	17.6	−1.86
Q02543	60S ribosomal protein L18a	11.9	6.0	−1.87
Q32P51	heterogeneous nuclear ribonucleoprotein A1-like 2	10.0	10.3	−1.87
P48668	keratin, type II cytoskeletal 6C	21.6	44.2	−1.87
P35579	myosin-9	9.7	49.0	−1.91
P62633	cellular nucleic acid-binding protein	11.9	5.8	−1.94
P62491	ras-related protein Rab-11A	14.8	6.7	−1.94
Q15907	ras-related protein Rab-11B	14.7	6.7	−1.94
P04632	calpain small subunit 1	9.3	5.3	−1.95
Q14240	eukaryotic initiation factor 4A-II	9.1	13.9	−1.95

DOI: 10.1021/acsomega.9b02512
ACS Omega 2019, 4, 21761−21777

Table 1. continued

protein ID	description	% coverage	protein score	fold change
P05556	integrin β-1	7.6	15.6	−1.96
P04843	dolichyl-diphosphooligosaccharide-protein glycosyltransferase subunit 1	4.5	6.7	−1.97
O60361	putative nucleoside diphosphate kinase	31.4	18.4	−2.05
P23246	splicing factor, proline- and glutamine-rich	5.9	12.4	−2.06
P78371	T-complex protein 1 subunit β	11.0	15.6	−2.08
P09651	heterogeneous nuclear ribonucleoprotein A1	15.9	18.9	−2.10
P19338	nucleolin	6.2	13.9	−2.19
Q99623	prohibitin-2	4.0	5.0	−2.24
Q15185	prostaglandin E synthase 3	14.4	7.2	−2.28
Q07020	60S ribosomal protein L18	11.7	8.2	−2.52

complex 1 protein is involved in a number of biological processes, particularly in cytoskeletal organization and cell-cycle progression,[32] and many studies found these proteins to be strictly related to tumor progression.[33,34] Particularly, in ESCC, a T-complex protein 1 subunit expression increased cell migration and invasion via regulation of α-actin and β-tubulin, and its silencing has been suggested as a possible treatment alternative.[35] Notably, prohibitins have been shown to be involved in cancer cell growth and survival, resistance to chemotherapy, immune response, and metastasis through a number of mechanisms, including p53-related transcriptional regulation, TGF-β signaling pathway modulation, and Ras/ERK pathway activation.[36,37] In ovarian epithelial tumors, prohibitin-2 is thought to induce cancer cell growth and increase the susceptibility of malignant transformation,[38] while prohibitin-1 promotes survival of cancer cells, acting as an antiapoptotic factor.[39] Furthermore, cytoplasmic expression of prohibitin-2 is involved in hormone-related growth of breast cancer cells because it upregulates the estrogen-signaling pathway.[40] Prohibitin-1 and prohibitin-2 are overexpressed in colorectal cancer, and serum concentration of these proteins, also elevated in colorectal cancer patients, was suggested as a potential biomarker for this disease.[41] Prohibitin-2 clustering with glucose-related protein 75 (GPR75)/mortalin is related to increased cell proliferation and tumorigenesis in metastatic cells.[42] To determine whether P-MAPA and IL-12 are capable of slowing down the tumor cell motility (as they were already proved to reduce migratory/proliferation capacity of cells), novel approaches based on timing and tumor features (subtype, grading, and staging) should be taken into consideration during OC treatment.

Among proteins that were simultaneously and significantly altered after treatments with IL-12 or the association P-MAPA + IL-12, we observed upregulation of cofilin-2 (2.41- and 2.46-fold increase vs the control group, respectively). Cofilin-2, which is known as the actin depolymerization factor, is a member of the cofilins family, being crucial modulators of actin dynamics.[43] The role of human cofilin-2 (protein and gene) is controversial in cancer. Important data suggest that cofilin-2 is downregulated in pancreatic tumor tissues[44] and that the ability of actin depolymerization by cofilin is associated with mitochondrial damage, cytochrome c release, and apoptosis induction in cancer cells.[45] Additionally, cofilin-2 translocation to mitochondria and interaction with Drp1 constitute key events for mitochondrial fission and apoptosis induced by erucin in breast cancer cells.[46] On the other hand, studies have suggested that cofilin-2 expression may play a role in malignant progression, modulating cancer cell proliferation, invasion, and metastasis.[47−49] Since we previously reported a reduction in cell viability after exposure to all treatments, we believe that increased cofilin-2 levels might hamper the ovarian tumor growth by disrupting the cell metabolism, thus inducing cell death and diminishing metabolic activity.

The most positive effects of treatments with IL-12 and P-MAPA + IL-12 seem to be associated with downregulated proteins: 6-phosphogluconate dehydrogenase (6PGD) (2.51- and 2.35-fold decrease vs the control group, respectively), Hsc70-interacting protein (2.44- and 2.38-fold decrease), plectin (2.04- and 2.61-fold decrease), and myosin light chains (2.66- and 2.34-fold decrease). 6PGD is an enzyme of the oxidative pentose phosphate pathway, which is involved in anabolic biosynthesis, glycolysis, and redox homeostasis in cancer cells, thus providing metabolic advantages to cellular survival and proliferation.[50,51] The activity of this enzyme is upregulated in a number of cancers and has been implicated in chemoresistance of ovarian and other tumors.[52] Inhibition of 6PGD selectively targeted breast cancer cells, sparing normal breast cells[53] and increasing the efficacy of chemotherapy in cervical cancer through AMPK-independent inhibition of RhoA and Rac1 activities.[54] In addition, suppression of 6PGD sensitized cisplatin-resistant ovarian cancer cells to cisplatin treatment via the AMPK-dependent pathway, thus restoring its therapeutic efficacy.[52] In the highly aggressive anaplastic thyroid carcinoma, 6PGD inhibition is associated with resensitization to doxorubicin treatment by decreasing levels of NADPH, NADH, and enzymatic activity of sirtuin-1.[55] Briefly, the disruption of cancer cell metabolism provided by downregulation of 6PGD might be a highly positive effect of treatment with IL-12 and association of P-MAPA and IL-12, including chemosensitivity restoration.

Modulating the tumor ability for signaling and interacting with normal cells is an important aim of alternative therapy. In this context, treatment of OC cells with IL-12 and P-MAPA + IL-12 significantly reduced the levels of the carboxyl terminus Hsc70-interacting protein (CHIP). Notably, CHIP seems to have dual functions in cancer, with some studies reporting its role as a tumor suppressor and others as an oncogene.[56] Decreased CHIP expression in ER-positive breast cancer and pancreatic cancer tissues is related with poor prognostic and short survival of patients.[56,57] Additionally, CHIP levels are inversely correlated with tumor malignancy in gastric cancer.[58] Conversely, CHIP promotes the downregulation of Profilin-1 in breast cancer cells, thus possibly playing a role in cell migration and metastasis.[59] A number of studies have been implicating CHIP in the modulation of the apoptosis-inducing factor (AIF), tumor-suppressor p53, and interferon regulatory factor 1 (IRF-1).[60−62] In esophageal squamous cell carcinoma, high CHIP expression is correlated with increased number of

DOI: 10.1021/acsomega.9b02512
ACS Omega 2019, 4, 21761−21777

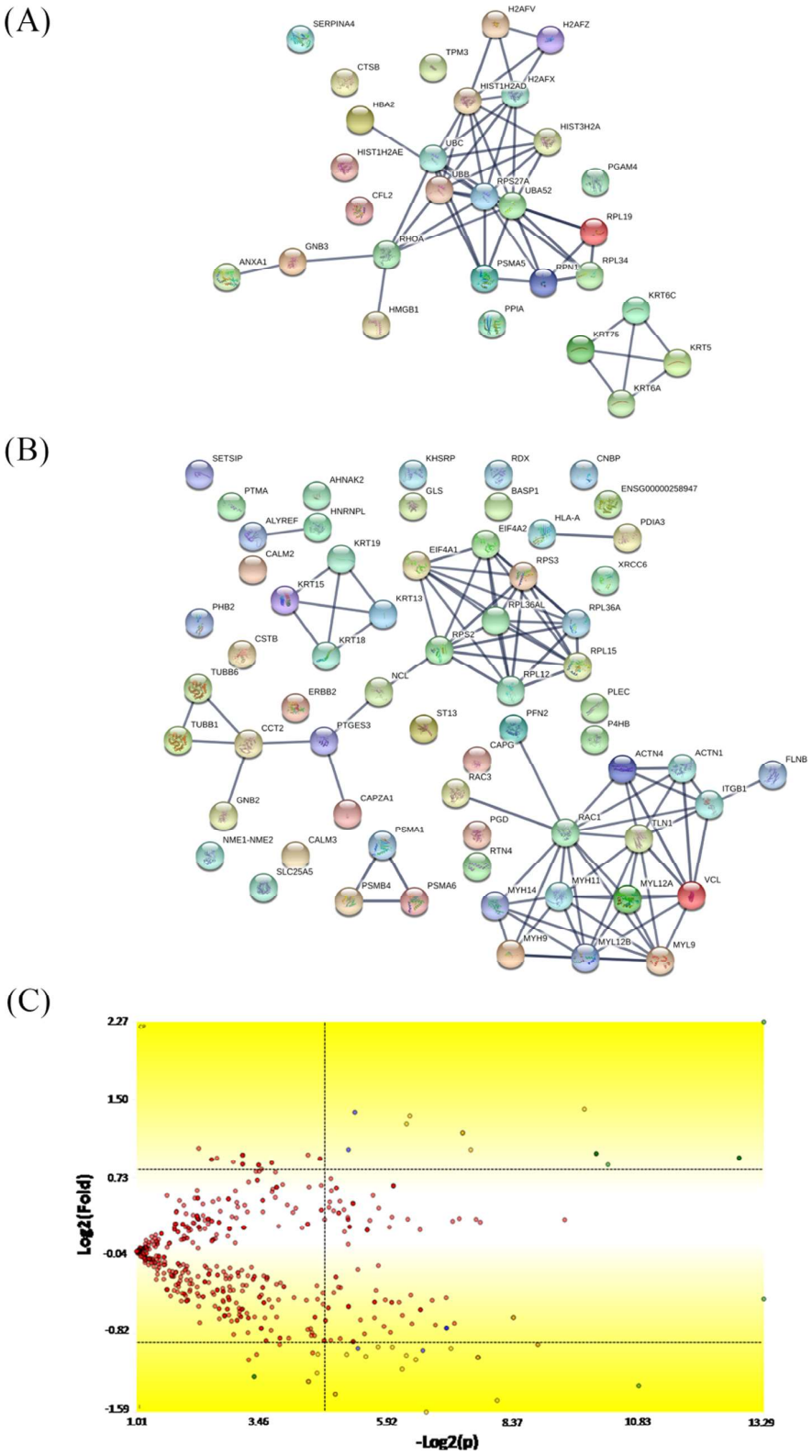

Figure 4. Mapping of the protein association network in IL-12-treated SKOV-3 cells. Source of the protein−protein interaction is based on cellular processing and its related molecular systems. Thicker lines show the highest confidence score (0.900) for upregulated (A) and downregulated (B) molecules of a functional association in response to IL-12 therapy in SKOV-3 cells. (C) Volcano plot indicates large magnitude fold-changes (*y*-axis) and statistical significance (*p*-value, *x*-axis); this plot indicates log 2 fold change vs −log 2 FDR-corrected *p*-value. Differentially expressed proteins are shown in the upper and lower right areas. See legends in Table 2.

DOI: 10.1021/acsomega.9b02512
ACS Omega 2019, 4, 21761−21777

Table 2. Differentially Expressed Proteins in the IL-12 Group versus the Control Group

protein ID	description	% coverage	protein score	fold change
O95678	keratin, type II cytoskeletal 75	4.9	9.2	4.84
Q9Y281	cofilin-2	16.9	7.7	2.41
P07858	cathepsin B	6.2	4.7	2.03
Q8N0Y7	probable phosphoglycerate mutase 4	3.9	3.9	2.01
P62979	ubiquitin-40S ribosomal protein S27a	21.8	15.5	1.94
P62987	ubiquitin-60S ribosomal protein L40	26.6	15.5	1.94
P0CG48	polyubiquitin-C	5.0	15.5	1.94
P0CG47	polyubiquitin-B	14.9	15.5	1.94
P49207	60S ribosomal protein L34	15.4	7.8	1.94
P16520	guanine nucleotide-binding protein G(I)/G(S)/G(T) subunit β-3	2.9	3.7	1.91
P84098	60S ribosomal protein L19	4.6	3.0	1.90
P02538	keratin, type II cytoskeletal 6A	6.6	15.8	1.89
P69905	hemoglobin subunit α	15.5	6.1	1.88
P29622	kallistatin	1.9	5.7	1.84
P13647	keratin, type II cytoskeletal 5	7.8	21.7	1.81
P48668	keratin, type II cytoskeletal 6C	6.6	15.8	1.72
P28066	proteasome subunit α type-5	12.0	8.5	1.65
B2RPK0	putative high mobility group protein B1-like 1	10.9	7.6	1.61
P62937	peptidyl-prolyl cis−trans isomerase A	18.8	18.9	1.58
P0C0S5	histone H2A.Z	12.5	17.8	1.57
Q71UI9	histone H2A.V	12.5	17.8	1.57
Q7L7L0	histone H2A type 3	12.5	17.8	1.57
P20671	histone H2A type 1-D	12.5	17.8	1.57
P04908	histone H2A type 1-B/E	12.5	17.8	1.57
P16104	histone H2AX	12.5	17.8	1.57
P06753	tropomyosin α-3 chain	10.9	15.6	1.57
P61586	transforming protein RhoA	10.9	7.8	1.55
P04083	annexin A1	17.3	32.9	1.52
P04843	dolichyl-diphosphooligosaccharide-protein glycosyltransferase subunit 1	1.7	3.8	1.52
P09429	high mobility group protein B1	17.2	16.2	1.51
O94925	glutaminase kidney isoform, mitochondrial	7.9	19.7	−1.51
P04080	cystatin-B	39.8	8.6	−1.53
P04439	HLA class I histocompatibility antigen, A-3 α chain	9.0	8.5	−1.55
P16188	HLA class I histocompatibility antigen, A-30 α chain	9.0	8.5	−1.55
P13746	HLA class I histocompatibility antigen, A-11 α chain	9.0	8.5	−1.55
P30512	HLA class I histocompatibility antigen, A-29 α chain	9.0	8.5	−1.55
P16189	HLA class I histocompatibility antigen, A-31 α chain	9.0	8.5	−1.55
P30453	HLA class I histocompatibility antigen, A-34 α chain	9.0	8.5	−1.55
P30459	HLA class I histocompatibility antigen, A-74 α chain	9.0	8.5	−1.55
P10316	HLA class I histocompatibility antigen, A-69 α chain	9.0	8.5	−1.55
P05534	HLA class I histocompatibility antigen, A-24 α chain	9.0	8.5	−1.55
Q09160	HLA class I histocompatibility antigen, A-80 α chain	9.0	8.5	−1.55
P30450	HLA class I histocompatibility antigen, A-26 α chain	9.0	8.5	−1.55
P10314	HLA class I histocompatibility antigen, A-32 α chain	9.0	8.5	−1.55
P16190	HLA class I histocompatibility antigen, A-33 α chain	9.0	8.5	−1.55
P01891	HLA class I histocompatibility antigen, A-68 α chain	9.0	8.5	−1.55
P30456	HLA class I histocompatibility antigen, A-43 α chain	9.0	8.5	−1.55
P30447	HLA class I histocompatibility antigen, A-23 α chain	9.0	8.5	−1.55
P01892	HLA class I histocompatibility antigen, A-2 α chain	9.0	8.5	−1.55
P30457	HLA class I histocompatibility antigen, A-66 α chain	9.0	8.5	−1.55
P18462	HLA class I histocompatibility antigen, A-25 α chain	9.0	8.5	−1.55
P35080	profilin-2	10.0	8.8	−1.55
P60763	ras-related C3 botulinum toxin substrate 3	15.6	7.2	−1.55
P14866	heterogeneous nuclear ribonucleoprotein L	4.4	10.1	−1.55
P60900	proteasome subunit α type-6	9.4	7.3	−1.57
P62879	guanine nucleotide-binding protein G(I)/G(S)/G(T) subunit β-2	9.4	6.5	−1.57
P06454	prothymosin α	23.4	23.0	−1.57
P0DME0	protein SETSIP	6.3	5.9	−1.57
P30050	60S ribosomal protein L12	24.2	17.1	−1.57
P19012	keratin, type I cytoskeletal 15	7.5	27.6	−1.58
Q9NQC3	reticulon-4	2.3	9.9	−1.58
P22392	nucleoside diphosphate kinase B	31.6	18.1	−1.58
P04626	receptor tyrosine-protein kinase erbB-2	1.9	8.5	−1.59
Q7Z406	myosin-14	1.8	16.5	−1.60
P35749	myosin-11	1.8	16.5	−1.60
P18206	vinculin	12.8	50.7	−1.60
P12956	X-ray repair cross-complementing protein 6	3.9	4.6	−1.61
P05783	keratin, type I cytoskeletal 18	10.0	17.8	−1.61
P07237	protein disulfide-isomerase	12.8	12.8	−1.64
O43707	α-actinin-4	15.2	49.8	−1.64
O75369	filamin-B	5.4	37.0	−1.66
P25786	proteasome subunit α type-1	15.2	10.2	−1.67
P05141	ADP/ATP translocase 2	14.4	16.7	−1.69
P12814	α-actinin-1	9.9	43.6	−1.70
P83881	60S ribosomal protein L36a	8.5	3.5	−1.70
Q969Q0	60S ribosomal protein L36a-like	8.5	3.5	−1.70
P13646	keratin, type I cytoskeletal 13	10.3	24.1	−1.72
P35241	radixin	9.4	21.8	−1.74
Q92945	far upstream element-binding protein 2	4.8	7.3	−1.75
P40121	macrophage-capping protein	6.3	4.2	−1.77
Q9H4B7	tubulin β-1 chain	6.2	11.5	−1.78
P52907	F-actin-capping protein subunit α-1	8.0	5.5	−1.81
P60842	eukaryotic initiation factor 4A-I	10.6	18.3	−1.81
Q9Y490	talin-1	8.2	52.2	−1.82
P08727	keratin, type I cytoskeletal 19	26.3	46.6	−1.84
P15880	40S ribosomal protein S2	16.0	19.5	−1.84
P0DP25	calmodulin-3	6.0	8.1	−1.86
P0DP24	calmodulin-2	6.0	8.1	−1.86
P0DP23	calmodulin-1	6.0	8.1	−1.86
P30101	protein disulfide-isomerase A3	21.2	31.3	−1.89
Q13509	tubulin β-3 chain	13.8	15.8	−1.89
Q14240	eukaryotic initiation factor 4A-II	5.4	11.6	−1.93
O60361	putative nucleoside diphosphate kinase	31.4	18.1	−1.94
Q8IVF2	protein AHNAK2	1.0	12.8	−1.95

DOI: 10.1021/acsomega.9b02512
ACS Omega 2019, 4, 21761−21777

Table 2. continued

protein ID	description	% coverage	protein score	fold change
P23396	40S ribosomal protein S3	21.4	19.5	−1.97
P80723	brain acid soluble protein 1	45.8	24.8	−2.00
P19338	nucleolin	8.3	13.7	−2.02
P35579	myosin-9	8.3	52.2	−2.03
P63000	ras-related C3 botulinum toxin substrate 1	22.9	10.1	−2.03
Q15149	plectin	4.0	47.9	−2.04
P61313	60S ribosomal protein L15	4.4	5.4	−2.05
P28070	proteasome subunit β type-4	3.8	4.0	−2.07
Q99623	prohibitin-2	4.0	3.9	−2.07
Q86V81	THO complex subunit 4	4.3	4.8	−2.07
P78371	T-complex protein 1 subunit β	9.2	16.0	−2.24
P62633	cellular nucleic acid-binding protein	11.9	7.7	−2.30
Q15185	prostaglandin E synthase 3	11.3	5.7	−2.36
Q8NFI4	putative protein FAM10A5	5.2	5.2	−2.44
P50502	Hsc70-interacting protein	5.2	5.2	−2.44
Q8IZP2	putative protein FAM10A4	7.9	5.2	−2.44
P52209	6-phosphogluconate dehydrogenase, decarboxylating	6.6	15.4	−2.51
P24844	myosin regulatory light polypeptide 9	17.4	8.2	−2.66
O14950	myosin regulatory light chain 12B	17.4	8.2	−2.66
P19105	myosin regulatory light chain 12A	17.5	8.2	−2.66
P05556	integrin β-1	6.3	19.3	−2.78
Q9BUF5	tubulin β-6 chain	12.3	14.4	−3.01

metastatic lymph nodes.[63] Xu and colleagues[64] reported CHIP activation of MAPK and AKT signaling activities and upregulation of E-cadherin, which led to epithelial−mesenchymal transition and enhanced migration and invasion potential of cells.

Cellular dynamics is a fundamental characteristic for cellular proliferation and, consequently, for tumor growth. Decreased levels of myosin regulatory light chain (MLC) and plectin after IL-12 and the combination of P-MAPA and IL-12 may be able to impair cancer cell dynamics, directly by avoiding cell proliferation and reducing their aggressiveness. The MLC phosphorylation seems to be an important marker for cancer cell functions, including cell growth, adhesion, and migration.[65,66] Leiomyosarcomas with high proliferative activity present increased MLC phosphorylation,[67,68] which is majorly measured by MLC kinase (MLCK) expression. In fact, the blockage of MLCK activities by a pharmacological inhibitor decreases breast cancer cell growth.[69,70] The expression of phosphomimetic MLC is able to increase the proliferative rate calculated by Ki-67 expression.[69] Another important protein to control cellular dynamics is plectin, playing key roles in cytoskeleton anchoring, signal transduction, and even in apoptosis induction.[71−73] Katada and colleagues[74] observed that plectin expression is significantly higher in tumor tissues compared with nontumor tissues in head and neck squamous cell carcinoma (HNSCC). Overexpression of this protein has also been reported in colorectal cancer, pancreatic cancer, and prostatic cancer.[75−77] Additionally, its upregulation is directly associated with poor prognosis and increased frequency of recurrence. Plectin also activates ERK 1/2 kinases to promote migration and invasion of HNSCC cells.[74] The depletion of plectin is able to impair cellular proliferation and migration in the MCF-7 breast cancer cell line[78] and in PC3 prostate cancer cells.[79]

Finally, treatment with P-MAPA and the association of P-MAPA and IL-12 significantly reduced the levels of the key protein vimentin (1.64- and 2.52-fold decrease vs the control group, respectively). Vimentin is an intermediate filament found in various mesenchymal cells in a wide variety of tissues, responsible for the maintenance of cell and tissue integrity.[80] In platinum-resistant ovarian cancer cell lineages, the reduction of vimentin levels by miRNA let-7g overexpression resulted in reduced epithelial-to-mesenchymal transition (EMT), decreased their migratory potential, and restored sensitivity to platinum-based chemotherapy.[81] High expression of vimentin has also been implicated in poor prognosis in a number of other cancer types, such as breast cancer, prostate cancer, colorectal cancer, and nonsmall-cell lung cancer.[82−85] Its upregulation is further associated with decreased disease-free survival and increased lymph node metastasis in colorectal cancer.[85] Vimentin is a key factor for epithelial plasticity and cytoplasm architecture maintenance during the epithelial−mesenchymal transition, and its overexpression confers elevated cancer cell motility, directional migration, and metastasis.[82,86,87] In the MDA-MB231 breast cancer cell line, the depletion of vimentin promoted reorganization of the cytoskeleton and decreased cell proliferation and motility.[87] We believe that the association of P-MAPA with IL-12 is important to disassemble part of the cytoskeleton that regulates tumor cell aggressiveness.

In summary, our present findings reveal important mechanisms by which immunotherapy with P-MAPA and IL-12 may impact OC progression and aggressiveness. The wide variety of targets exhibited herein shows that these treatments are able to attack OC cell malignant functions through different regulatory mechanisms. Future studies associating these therapies with OC standard chemotherapy (e.g., taxanes and platinum derivatives) could also bring an important approach regarding the use of these compounds as adjuvant therapeutics.

3. CONCLUSIONS

We described a number of important changes in several protein signatures that are modulated by P-MAPA and IL-12 therapies in ovarian cancer SKOV-3 cells. While P-MAPA and IL-12 alone were efficient to upregulate structural proteins (e.g., related to tight junctions), they downregulated molecules involved in cell signaling that are associated with cancer progression. Combinatory therapy with P-MAPA and IL-12 was the most efficient to distinctively regulate proteins involved in metabolic processes, such as energy and mitochondrial processes, cell oxidation, and senescence; inhibition of these activities may render cancer cells more vulnerable to structural instability, apoptosis, and metabolical dysfunctions. This approach provides reliable insights into the cellular regulation associated with OC progression and, alternatively, suggests the therapeutic use of P-MAPA and IL-12 as a complementary strategy for OC treatment.

DOI: 10.1021/acsomega.9b02512
ACS Omega 2019, 4, 21761−21777

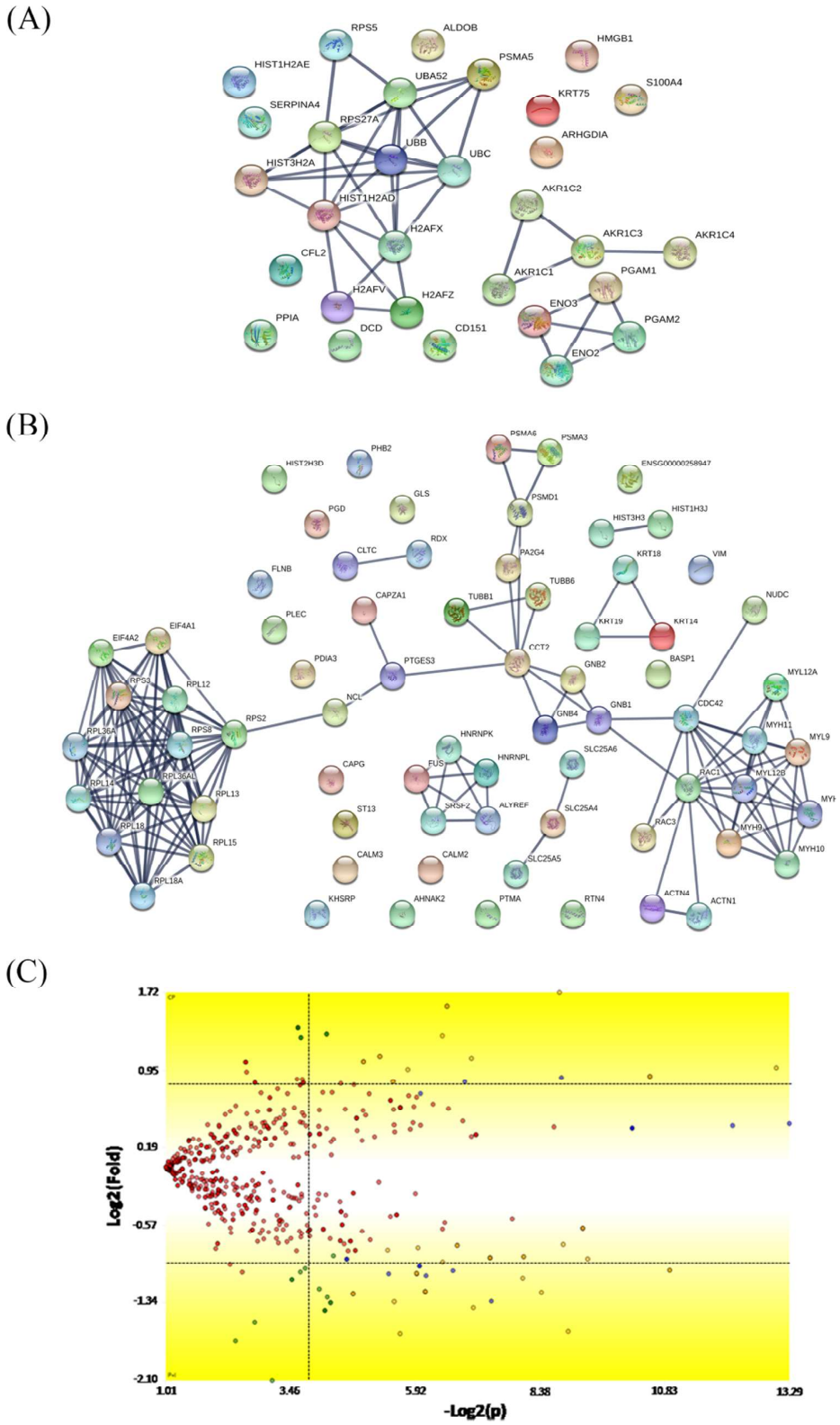

Figure 5. Mapping of the protein association network in P-MAPA + IL-12-treated SKOV-3 cells. Source of the protein−protein interaction is based on cellular processing and its related molecular systems. Thicker lines show the highest confidence score (0.900) for upregulated (A) and downregulated (B) molecules of a functional association in response to P-MAPA + IL-12 therapy in SKOV-3 cells. (C) Volcano plot indicates large magnitude fold-changes (*y*-axis) and statistical significance (*p*-value, *x*-axis); this plot indicates log 2 fold change vs −log 2 FDR-corrected *p*-value. Differentially expressed proteins are shown in the upper and lower right areas. See legends in Table 3.

DOI: 10.1021/acsomega.9b02512
ACS Omega 2019, 4, 21761−21777

Table 3. Differentially Expressed Proteins in the P-MAPA + IL-12 Group versus the Control Group

protein ID	description	% coverage	protein score	fold change
P62987	ubiquitin-60S ribosomal protein L40	26.6	15.5	2.60
P62979	ubiquitin-40S ribosomal protein S27a	21.8	15.5	2.60
P0CG47	polyubiquitin-B	14.9	15.5	2.60
Q9Y281	cofilin-2	16.9	7.7	2.46
O95678	keratin, type II cytoskeletal 75	4.9	9.2	2.10
Q04828	aldo-keto reductase family 1 member C1	8.1	8.8	2.06
P42330	aldo-keto reductase family 1 member C3	7.7	7.6	2.06
P52895	aldo-keto reductase family 1 member C2	8.1	8.8	2.06
P0CG48	polyubiquitin-C	5.0	15.5	2.05
P28066	proteasome subunit α type-5	12.0	7.7	1.98
P48509	CD151 antigen	6.7	8.3	1.95
P52565	Rho GDP-dissociation inhibitor 1	8.3	6.3	1.86
P81605	dermcidin	10.0	5.3	1.83
P15259	phosphoglycerate mutase 2	7.9	5.5	1.80
P18669	phosphoglycerate mutase 1	7.9	5.5	1.80
P09429	high mobility group protein B1	13.5	16.2	1.78
P09104	γ-enolase	10.4	18.8	1.78
P13929	β-enolase	10.4	18.8	1.78
P26447	protein S100-A4	26.7	7.6	1.77
P17516	aldo-keto reductase family 1 member C4	2.8	5.6	1.76
P46782	40S ribosomal protein S5	8.3	7.3	1.75
P05062	fructose-bisphosphate aldolase B	3.9	9.1	1.67
P62937	peptidyl-prolyl cis−trans isomerase A	18.8	18.9	1.67
B2RPK0	putative high mobility group protein B1-like 1	7.1	7.6	1.65
P29622	kallistatin	1.9	5.7	1.61
Q71UI9	histone H2A.V	12.5	17.8	1.58
P0C0S5	histone H2A.Z	12.5	17.8	1.58
P16104	histone H2AX	16.1	17.8	1.51
P20671	histone H2A type 1-D	17.7	17.8	1.51
Q7L7L0	histone H2A type 3	17.7	17.8	1.51
P04908	histone H2A type 1-B/E	17.7	17.8	1.51
P60763	ras-related C3 botulinum toxin substrate 3	10.4	5.6	−1.52
P02533	keratin, type I cytoskeletal 14	27.1	47.6	−1.52
Q9H4B7	tubulin β-1 chain	6.2	11.5	−1.53
Q71DI3	histone H3.2	14.0	7.1	−1.53
Q16695	histone H3.1t	14.0	7.1	−1.53
P68431	histone H3.1	14.0	7.1	−1.53
O94925	glutaminase kidney isoform, mitochondrial	7.9	21.8	−1.53
O43707	α-actinin-4	15.4	46.5	−1.53
P19338	nucleolin	4.7	9.7	−1.54
P62873	guanine nucleotide-binding protein G(I)/G(S)/G(T) subunit β-1	9.4	11.9	−1.54
P60953	cell division control protein 42 homolog	11.5	7.8	−1.54
O60361	putative nucleoside diphosphate kinase	31.4	13.5	−1.55
Q9HAV0	guanine nucleotide-binding protein subunit β-4	5.9	7.8	−1.55
P30050	60S ribosomal protein L12	24.2	15.6	−1.56
P06454	prothymosin α	23.4	23.5	−1.56
P40121	macrophage-capping protein	6.3	4.0	−1.57
Q9UQ80	proliferation-associated protein 2G4	12.2	12.0	−1.58
P52907	F-actin-capping protein subunit α-1	8.0	5.3	−1.58
P12814	α-actinin-1	10.3	40.8	−1.61
Q00610	clathrin heavy chain 1	4.8	21.3	−1.62
P60842	eukaryotic initiation factor 4A-I	10.6	15.9	−1.63
P30101	protein disulfide-isomerase A3	19.4	30.0	−1.64
O75369	filamin-B	5.5	34.6	−1.65
P12235	ADP/ATP translocase 1	11.1	16.5	−1.66
P12236	ADP/ATP translocase 3	11.1	16.5	−1.66
P61978	heterogeneous nuclear ribonucleoprotein K	17.3	30.1	−1.66
Q01130	serine-/arginine-rich splicing factor 2	10.0	7.4	−1.67
Q99460	26S proteasome non-ATPase regulatory subunit 1	1.0	3.3	−1.68
P63000	ras-related C3 botulinum toxin substrate 1	10.4	7.9	−1.69
Q15185	prostaglandin E synthase 3	19.4	5.5	−1.69
P62879	guanine nucleotide-binding protein G(I)/G(S)/G(T) subunit β-2	6.5	7.8	−1.71
P62241	40S ribosomal protein S8	13.0	9.8	−1.75
P05141	ADP/ATP translocase 2	14.4	20.8	−1.77
P35241	radixin	10.3	25.2	−1.77
Q14240	eukaryotic initiation factor 4A-II	5.4	11.3	−1.78
Q9Y266	nuclear migration protein nudC	8.8	9.5	−1.78
P50914	60S ribosomal protein L14	10.7	11.4	−1.84
Q13509	tubulin β-3 chain	13.8	14.8	−1.85
P0DP24	calmodulin-2	6.0	6.6	−1.86
P0DP25	calmodulin-3	6.0	6.6	−1.86
P0DP23	calmodulin-1	6.0	6.6	−1.86
Q9NQC3	reticulon-4	2.3	10.2	−1.87
P08727	keratin, type I cytoskeletal 19	33.3	54.1	−1.88
P14866	heterogeneous nuclear ribonucleoprotein L	4.4	10.8	−1.91
P35637	RNA-binding protein FUS	3.0	7.3	−1.94
P05783	keratin, type I cytoskeletal 18	11.9	22.4	−1.97
P61313	60S ribosomal protein L15	4.4	6.6	−2.00
Q86V81	THO complex subunit 4	4.3	5.1	−2.02
P23396	40S ribosomal protein S3	21.0	18.2	−2.03
P25788	proteasome subunit α type-3	11.0	6.8	−2.05
Q92945	far upstream element-binding protein 2	4.8	9.1	−2.05
P60900	proteasome subunit α type-6	12.6	11.0	−2.06
P80723	brain acid soluble protein 1	45.8	20.6	−2.10
Q8IVF2	protein AHNAK2	1.0	15.5	−2.14
P35749	myosin-11	2.2	22.4	−2.16
Q7Z406	myosin-14	2.2	22.4	−2.16
P35580	myosin-10	2.6	22.2	−2.30
Q99623	prohibitin-2	7.0	5.7	−2.34
O14950	myosin regulatory light chain 12B	6.4	6.9	−2.34
P24844	myosin regulatory light polypeptide 9	6.4	6.9	−2.34
P19105	myosin regulatory light chain 12A	6.4	6.9	−2.34
P52209	6-phosphogluconate dehydrogenase, decarboxylating	6.6	13.4	−2.35
Q8NFI4	putative protein FAM10A5	5.2	5.3	−2.38

DOI: 10.1021/acsomega.9b02512
ACS Omega 2019, 4, 21761−21777

Table 3. continued

protein ID	description	% coverage	protein score	fold change
P50502	Hsc70-interacting protein	5.2	5.3	−2.38
Q8IZP2	putative protein FAM10A4	7.9	5.3	−2.38
P15880	40S ribosomal protein S2	16.0	26.8	−2.50
P35579	myosin-9	9.7	62.2	−2.51
P08670	vimentin	31.3	88.0	−2.52
Q15149	plectin	6.4	71.7	−2.61
P83881	60S ribosomal protein L36a	16.0	7.8	−2.66
Q969Q0	60S ribosomal protein L36a-like	16.0	7.8	−2.66
P26373	60S ribosomal protein L13	14.2	17.2	−2.87
P78371	T-complex protein 1 subunit β	11.0	19.5	−3.08
Q9BUF5	tubulin β-6 chain	9.6	15.1	−3.12
Q02543	60S ribosomal protein L18a	16.5	14.2	−3.27
Q07020	60S ribosomal protein L18	30.9	20.8	−4.29

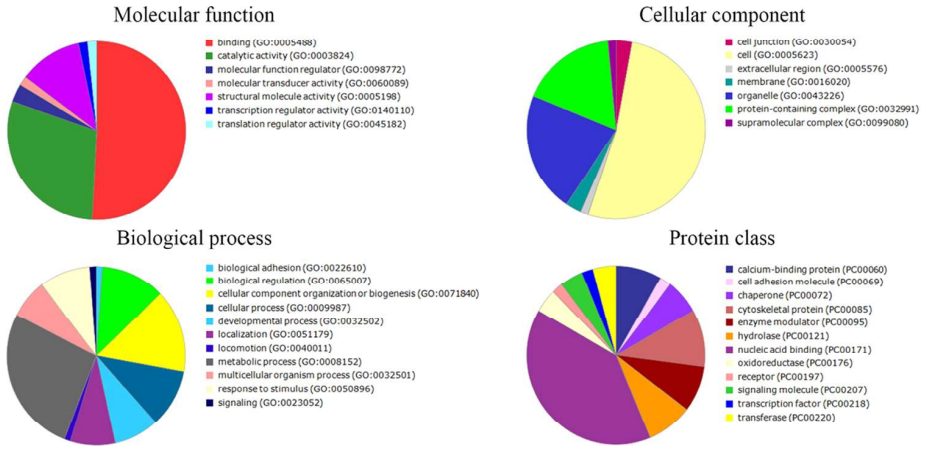

Figure 6. Pie charts of the proteins that were differentially altered in SKOV-3 cells following P-MAPA treatment. PANTHER classification indicates functionally distinct proteins according to their molecular functions, biological processes, cellular components, and class.

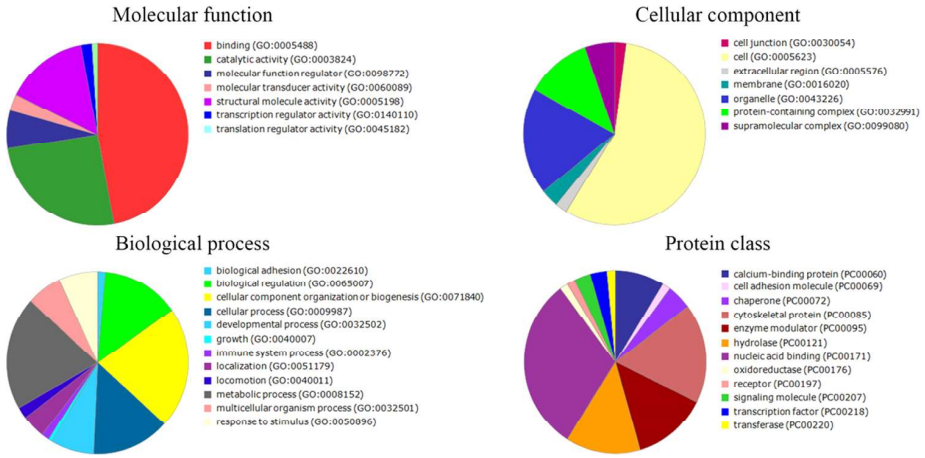

Figure 7. Pie charts of the proteins that were differentially altered in SKOV-3 cells following IL-12 treatment. PANTHER classification indicates functionally distinct proteins according to their molecular functions, biological processes, cellular components, and class.

4. EXPERIMENTAL SECTION

4.1. Cell Line and Culture. Human OC cell line, SKOV-3, was purchased from the American Type Culture Collection (ATCC, Rockville, MD). During the experiment, SKOV-3 cells were incubated with RPMI 1640 (Life Technologies, Grand Island, NY) supplemented with 10% fetal bovine serum and 1% anti-anti solution (100 mg/mL penicillin G, and 100 μg/mL streptomycin (Merck, Darmstadt, Germany)). Cells were maintained at 37 °C in a humidified atmosphere of 5% CO_2, and the culture medium was changed every 2−3 days.

4.2. P-MAPA and IL-12 Treatments. To determine the better dose−response effect, three different doses of P-MAPA (25, 50, and 100 μg/mL) were used in accordance with Fávaro.[13] Initially, 5 mg of P-MAPA was diluted in 1 mL of saline to achieve a stock solution of 5 mg/mL; this solution was then diluted in the cell culture medium to obtain the proper concentrations. For the treatment with recombinant (rh)IL-12, doses of 0.5, 1, and 2 ng/mL were used in the culture medium in accordance the method of Su and colleagues.[88] To combine P-MAPA with IL-12, the most representative dose and incubation time were chosen after performing the MTT assay. The saline solution was used as a

DOI: 10.1021/acsomega.9b02512
ACS Omega 2019, 4, 21761−21777

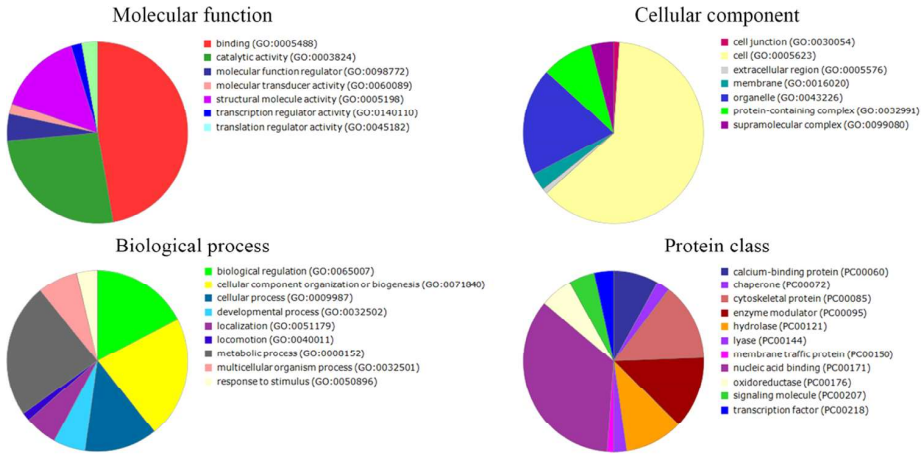

Figure 8. Pie charts of the proteins that were differentially altered in SKOV-3 cells following P-MAPA + IL-12 treatment. PANTHER classification indicates functionally distinct proteins according to their molecular functions, biological processes, cellular components, and class.

solvent vehicle control and administered in the same procedures for treatments.

4.3. MTT Assay. SKOV-3 cells were seeded in a plate at a density of 1×10^3 cells/well. Cellular activity or toxicity was first evaluated using the three concentrations of both treatments, P-MAPA and IL-12, after 0, 24, 48, and 72 h exposure. All analyses were performed in three technical and biological replicates. MTT solution was added to the wells for 4 h, and the crystals were diluted with dimethyl sulfoxide (DMSO) under agitation. The concentration was determined by an Epoch microplate reader (BioTek Instruments, Highland Park, PO) at 540 nm, with the reference curve fixed at 650 nm. The percentage (%) of crystal formation was calculated based on the control group as the reference. After the testing assay, we determined the doses of 25 μg/mL P-MAPA and 1 ng/mL IL-12 and set the period of treatment at 48 h. Since the study proposed to globally identify proteins involved in potential signaling pathways that are modulated by the treatments, we defined doses and periods capable of decreasing 10−30% cell viability; higher doses could bias the results because the increased cell death might result in loss of important proteins.

4.4. Protein Quantification. After treatments, the proteins were extracted from SKOV-3 cells in biological triplicate from each experiment and were quantified in triplicate using a colorimetric method described by Bradford (BioRad Protein Assay Kit; Cod. 500-0001). Bovine serum albumin (0.1% BSA) was used as the reference protein. After quantification, individual samples were transferred to Eppendorf LoBind tubes and diluted with 0.9% (m/v) saline solution until reaching the concentration of 50 μg/40 μL for each sample.

4.5. In-Solution Trypsin Digestion. All samples were subjected to the protocol for trypsin digestion. First, 50 μg of lyophilized proteins was diluted in 50 mM ammonium bicarbonate, and 25 μL of RapiGest SF surfactant (code 186001861, Waters Corporation) was added to the samples for 60 min at 37 °C. Then, samples were reduced and alkylated with 10 mM dithiothreitol (DTT) and 45 mM iodoacetamide (IAA) at room temperature (RT) for 20 min. Enzymatic digestion was performed using trypsin (1:100; enzyme/sample) solubilized in 50 mM ammonium bicarbonate buffer (pH 7.8) for 18 h. Hydrolysis was stopped by adding 1% (v/v) formic acid to the samples for 1 h. Samples were incubated for 90 min at RT and then centrifuged at 14 000g for 30 min at 6 °C. Supernatants were removed into a new tube and subjected to desalting columns Peptide Cleanup C18 Spin (code 5188-2750 Agilent Technologies). After peptides were dried in vacuum (SpeedVac; Thermo Scientific), they were dissolved in 3% acetonitrile (ACN) with 0.1% formic acid solution before analysis.

4.6. Peptide Sequencing for Mass Spectrometry. Label-free analysis was performed using a liquid nanocromatograph (Ultimate 3000 LC Dionex, Germering, Germany) coupled to a quadrupole-orbitrap model mass spectrometer Q-Exactive (ThermoFisher Scientific, Bremen, Germany). The chromatograph was equipped with a binary system of pumps and an automatic sample applicator. The mobile phase consisted of 0.1% (v/v) formic acid in water LCMS (solvent A) and 0.1% (v/v) formic acid in 80% (v/v) ACN (solvent B). The peptides were loaded in a precolumn C18, 30 μm × 5 mm (code 164649, ThermoFisher Scientific), and desalting was carried out in an isocratic gradient of 4% B for 3 min at a flow rate of 300 nL/min. Then, peptides were fractioned using the analytical column Reprosil-Pur C18-AQ, 3 μm, 120 Å, 105 mm (code 1PCH7515-105H354-NV, PICOCHIP) using a linear gradient of 4−55% B for 30 min, 55−90% B for 1 min, maintained at 90% B for 5 min, and recalibrated at 4% B for 20 min (flow rate of 300 nL/min). Positive ionization was obtained in a Nanospray ion source (PICOCHIP) with the DDA method. Mass spectra were acquired in the mass range of m/z 200−2000, resolution of 70.000, and 100 ms for injection time. The fragmentation chamber was conditioned with collision energy between 29 and 35%, with resolution of 17.500, 50 ms of injection time, 4.0 m/z of MS/MS isolation window, and dynamic exclusion of 10 s. All samples were quantified in biological and technical triplicate. Spectrometry data were acquired using Thermo Xcalibur software (version 4.0.27.19, ThermoFisher Scientific Inc.).

4.7. Data Analysis. For proteomic analyses, the raw data.RAW was subjected to software PatternLab (version 4.0.0.84; Carvalho and colleagues)[89] to identify and determine which proteins were differentially expressed. The parameters used were the Swiss-Prot database (*Homo sapiens* taxonomy), trypsin as the proteolytic enzyme, permission of two lost cleavages, fixed modifications of cysteine carbamidomethylation and methionine oxidation as variable modification, and

DOI: 10.1021/acsomega.9b02512
ACS Omega 2019, 4, 21761−21777

tolerance errors of MS 40 ppm and MS/MS 0.0200 ppm. The false discovery rate (FDR) was set at ≤1%. We used only proteins obtained in all three runs, and the spectral counts for each protein were normalized by the weighted average of replicates of each sample. Missing data were analyzed by multiple imputation according to Royston,[90] and the standard errors were computed according to the "Rubin rules".[91] Only proteins that showed statistical significance at $p < 0.05$ and a protein ratio less than 1.5-fold change or greater than 1.5-fold change were used. Results were compared using Student's t test to set the differences between the groups ($p < 0.05$). Additional analyses of cellular components, molecular function, and biological processes were determined through Protein Annotation Through Evolutionary Relationship (PANTHER) (http://pantherdb.org/) classification, and network interactions between proteins were obtained using STRING software (http://string-db.org/) under the basic parameters of cutoff score of 0.900 (highest confidence), evidence as network edges, and PPI enrichment p-value of $<1.0 \times 10^{-16}$.

AUTHOR INFORMATION

Corresponding Author

*E-mail: luiz-gustavo.chuffa@unesp.br. Phone: +55 (14) 3880-0027.

ORCID

Luiz Gustavo de Almeida Chuffa: 0000-0002-0199-3396

Author Contributions

L.G.d.A.C., L.A.L.J.: collected and analyzed the data, drafted the manuscript, and conceived the main idea of the study. L.D.d.S., R.F.D., H.S.S., W.J.F., M.M., F.E.M., I.d.S.N., and M.S.C.: participated in the acquisition of the data and in the design and intellectual conception of the study. All authors approved the final version of the manuscript.

Funding

We would like to extend special thanks to Fundação de Amparo à Pesquisa do Estado de São Paulo (FAPESP, Grant numbers: 2016/03993-9; 2019/00906-6), CAPES, and PROPG/PROPE 12/2019 for providing financial support.

Notes

The authors declare no competing financial interest.

ACKNOWLEDGMENTS

We are grateful to Mister Bruno Rossini for his excellent technical support, and special thanks to the Center for the Study of Venoms and Venomous Animals (CEVAP) from UNESP, Botucatu, São Paulo, Brazil.

REFERENCES

(1) Cannistra, S. A. Cancer of the ovary. *N. Engl. J. Med.* **2004**, *35*, 2519−2565.

(2) Siegel, R. L.; Miller, K. D.; Jemal, A. Cancer statistics, 2019. *CA Cancer J. Clin.* **2019**, *69*, 7−34.

(3) Tessitore, A.; Gaggiano, A.; Cicciarelli, G.; Verzella, D.; Capece, D.; Fischietti, M.; Zazzeroni, F.; Alesse, E. Serum biomarkers identification by mass spectrometry in high-mortality tumors. *Int. J. Proteomics* **2013**, *2013*, No. 125858.

(4) Jessmon, P.; Boulanger, T.; Zhou, W.; Patwardhan, P. Epidemiology and treatment patterns of epithelial ovarian cancer. *Expert. Rev. Anticancer Ther.* **2017**, *17*, 427−437.

(5) Chuffa, L. G. A.; Seiva, F. R.; Fávaro, W. J.; Teixeira, G. R.; Amorim, J. P.; Mendes, L. O.; Fioruci, B. A.; Pinheiro, P. F.; Fernandes, A. A.; Franci, J. A.; Delella, F. K.; Martinez, M.; Martinez, F. E. Melatonin reduces LH, 17 beta-estradiol and induces differential regulation of sex steroid receptors in reproductive tissues during rat ovulation. *Reprod. Biol. Endocrinol.* **2011a**, *9*, 108.

(6) Chuffa, L. G.; Amorim, J. P.; Teixeira, G. R.; Mendes, L. O.; Fioruci, B. A.; Pinheiro, P. F.; Seiva, F. R.; Novelli, E. L.; Mello Júnior, W.; Martinez, M.; Martinez, F. E. Long-term melatonin treatment reduces ovarian mass and enhances tissue antioxidant defenses during ovulation in the rat. *Braz. J. Med. Biol. Res.* **2011b**, *44*, 217−223.

(7) Chuffa, L. G.; Fioruci-Fontanelli, B. A.; Mendes, L. O.; Fávaro, W. J.; Pinheiro, P. F.; Martinez, M.; Martinez, F. E. Characterization of chemically induced ovarian carcinomas in an ethanol-preferring rat model: influence of long-term melatonin treatment. *PLoS One* **2013**, *8*, No. e81676.

(8) Chuffa, L. G.; Fioruci-Fontanelli, B. A.; Mendes, L. O.; Ferreira Seiva, F. R.; Martinez, M.; Fávaro, W. J.; Domeniconi, R. F.; Pinheiro, P. F.; Delazari Dos Santos, L.; Martinez, F. E. Melatonin attenuates the TLR4-mediated inflammatory response through MyD88- and TRIF-dependent signaling pathways in an in vivo model of ovarian cancer. *BMC Cancer* **2015**, *6*, 15−34.

(9) Chuffa, L. G. A.; Alves, M. S.; Martinez, M.; Camargo, I. C.; Pinheiro, P. F.; Domeniconi, R. F.; Júnior, L. A.; Martinez, F. E. Apoptosis is triggered by melatonin in an in vivo model of ovarian carcinoma. *Endocr. Relat. Cancer* **2016**, *23*, 65−76.

(10) Chuffa, L. G.; Lupi Júnior, L. A.; Seiva, F. R.; Martinez, M.; Domeniconi, R. F.; Pinheiro, P. F.; Dos Santos, L. D.; Martinez, F. E. Quantitative proteomic profiling reveals that diverse metabolic pathways are influenced by melatonin in an in vivo model of ovarian carcinoma. *J. Proteome Res.* **2016**, *15*, 3872−3882.

(11) de Almeida Chuffa, L. G.; de Moura Ferreira, G.; Lupi, L. A.; da Silva Nunes, I.; Fávaro, W. J. P-MAPA immunotherapy potentiates the effect of cisplatin on serous ovarian carcinoma through targeting TLR4 signaling. *J. Ovarian Res.* **2018**, *11*, No. 8.

(12) Kelly, M. G.; Alvero, A. B.; Chen, R.; Silasi, D. A.; Abrahams, V. M.; Chan, S.; Visintin, I.; Rutherford, T.; Mor, G. TLR-4 signaling promotes tumor growth and paclitaxel chemoresistance in ovarian cancer. *Cancer Res.* **2006**, *66*, 3859−3868.

(13) Fávaro, W. J.; Nunes, O. S.; Seiva, F. R.; Nunes, I. S.; Woolhiser, L. K.; Durán, N.; Lenaerts, A. J. Effects of P-MAPA immunomodulator on toll-like receptors and p53: potential therapeutic strategies for infectious diseases and cancer. *Infect. Agent. Cancer* **2012**, *7*, 14.

(14) Garcia, P. V.; Seiva, F. R.; Carniato, A. P.; de Mello Júnior, W.; Duran, N.; Macedo, A. M.; de Oliveira, A. G.; Romih, R.; da Silva Nunes, I.; da Silva Nunes, O.; Fávaro, W. J. Increased toll-like receptors and p53 levels regulate apoptosis and angiogenesis in non-muscle invasive bladder cancer: mechanism of action of P-MAPA biological response modifier. *BMC Cancer* **2016**, *16*, 422.

(15) Trinchieri, G. Interleukin-12 and the regulation of innate resistance and adaptive immunity. *Nat. Rev. Immunol.* **2003**, *3*, 133−146.

(16) Cohen, C. A.; Shea, A. A.; Heffron, C. L.; Schmelz, E. M.; Roberts, P. C. Interleukin-12 immunomodulation delays the onset of lethal peritoneal disease of ovarian cancer. *J. Interferon Cytokine Res.* **2016**, *36*, 62−73.

(17) Hurteau, J. A.; Blessing, J. A.; De Cesare, S. L.; Creasman, W. T. Evaluation of recombinant human interleukin-12 in patients with recurrent or refractory ovarian cancer: a gynecologic oncology group study. *Gynecol. Oncol.* **2001**, *82*, 7−10.

(18) Lenzi, R.; Edwards, R.; June, C.; Seiden, M. V.; Garcia, M. E.; Rosenblum, M.; Freedman, R. S. Phase II study of intraperitoneal recombinant interleukin-12 (rhIL-12) in patients with peritoneal carcinomatosis (residual disease <1 cm) associated with ovarian cancer or primary peritoneal carcinoma. *J. Transl. Med.* **2007**, *5*, 66.

(19) Odunsi, K.; Wollman, R. M.; Ambrosone, C. B.; Hutson, A.; McCann, S. E.; Tammela, J.; Geisler, J. P.; Miller, G.; Sellers, T.; Cliby, W.; Qian, F.; Keitzm, B.; Intengan, M.; Lele, S.; Alderfer, J. L. Detection of epithelial ovarian cancer using 1H-NMR-based metabonomics. *Int. J. Cancer* **2005**, *113*, 782−788.

DOI: 10.1021/acsomega.9b02512
ACS Omega 2019, 4, 21761−21777

(20) Zhang, T.; Wu, X.; Ke, C.; Yin, M.; Li, Z.; Fan, L.; Zhang, W.; Zhang, H.; Zhao, F.; Zhou, X.; Lou, G.; Li, K. Identification of potential biomarkers for ovarian cancer by urinary metabolomic profiling. *J. Proteome Res.* **2013**, *12*, 505−512.
(21) Shender, V. O.; Pavlyukov, M. S.; Ziganshin, R. H.; Arapidiz, G. P.; Kovalchukz, S. I.; Anikanov, N. A.; Altukhov, I. A.; Alexeev, D. G.; Butenko, I. O.; Shavarda, A. L.; Khomyakova, E. B.; Evtushenko, E.; Ashrafyan, L. A.; Antonova, I. B.; Kuznetcov, I. N.; Gorbachev, A. Y.; Shakhparonov, M. I.; Govorun, V. M. Proteome-metabolome profiling of ovarian cancer ascites reveals novel components involved in intercellular communication. *Mol. Cell. Proteomics* **2014**, *13*, 3558−3571.
(22) Horak, P.; Pils, D.; Kaider, A.; Pinter, A.; Elandt, K.; Sax, C.; Zielinski, C. C.; Horvat, R.; Zeillinger, R.; Reinthaller, A.; Krainer, M. Perturbation of the tumor necrosis factor-related apoptosis-inducing ligand cascade in ovarian cancer: overexpression of FLIPL and deregulation of the functional receptors DR4 and DR5. *Clin. Cancer Res.* **2005**, *11*, 8585−8591.
(23) Le Moguen, K.; Lincet, H.; Deslandes, E.; Hubert-Roux, M.; Lange, C.; Poulain, L.; Gauduchon, P.; Baudin, B. Comparative proteomic analysis of cisplatin sensitive IGROV1 ovarian carcinoma cell line and its resistant counterpart IGROV1−R10. *Proteomics* **2006**, *6*, 5183−5192.
(24) Hershko, A. Ubiquitin: roles in protein modification and breakdown. *Cell* **1983**, *34*, 11−12.
(25) Han, X. J.; Lee, M. J.; Yu, G. R.; Lee, Z. W.; Bae, J. Y.; Bae, Y. C.; Kang, S. H.; Kim, D. G. Altered dynamics of ubiquitin hybrid proteins during tumor cell apoptosis. *Cell. Death Dis.* **2012**, *3*, No. e255.
(26) Zhou, Q.; Hou, Z.; Zuo, S.; Zhou, X.; Feng, Y.; Sun, Y.; Yuan, X. LUCAT1 promotes colorectal cancer tumorigenesis by targeting the ribosomal protein L40-MDM2-p53 pathway through binding with UBA52. *Cancer Sci.* **2019**, *110*, 1194−1207.
(27) Xu, L.; Zhang, Y.; Qu, X.; Che, X.; Guo, T.; Li, C.; Ma, R.; Fan, Y.; Ma, Y.; Hou, K.; Li, D.; Hu, X.; Liu, B.; Yu, R.; Yan, H.; Gong, J.; Liu, Y. DR5-Cbl-b/c-Cbl-TRAF2 complex inhibits TRAIL-induced apoptosis by promoting TRAF2-mediated polyubiquitination of caspase-8 in gastric cancer cells. *Mol Oncol.* **2017**, *11*, 1733−1751.
(28) Cao, H. H.; Zhang, S. Y.; Shen, J. H.; Wu, Z. Y.; Wu, J. Y.; Wang, S. H.; Li, E. M.; Xu, L. Y. A three-protein signature and clinical outcome in esophageal squamous cell carcinoma. *Oncotarget* **2015**, *6*, 5435−5448.
(29) Derycke, L.; Stove, C.; Vercoutter-Edouart, A. S.; De Wever, O.; Dollé, L.; Colpaert, N.; Depypere, H.; Michalski, J. C.; Bracke, M. The role of non-muscle myosin IIA in aggregation and 5448 invasion of human MCF-7 breast cancer cells. *Int. J. Dev. Biol.* **2011**, *55*, 835−840.
(30) Liang, S.; He, L.; Zhao, X.; Miao, Y.; Gu, Y.; Guo, C.; Xue, Z.; Dou, W.; Hu, F.; Wu, K.; Nie, Y.; Fan, D. MicroRNA let-7f inhibits tumor invasion and metastasis by targeting MYH9 in human gastric cancer. *PLoS One* **2011**, *6*, No. e18409.
(31) Xia, Z. K.; Yuan, Y. C.; Yin, N.; Yin, B. L.; Tan, Z. P.; Hu, Y. R. Nonmuscle myosin IIA is associated with poor prognosis of esophageal squamous cancer. *Dis. Esophagus* **2012**, *25*, 427−436.
(32) Brackley, K. I.; Grantham, J. Subunits of the chaperonin CCT interact with F-actin and influence cell shape and cytoskeletal assembly. *Exp. Cell Res.* **2010**, *316*, 543−553.
(33) Huang, X.; Wang, X.; Cheng, C.; Cai, J.; He, S.; Wang, H.; Liu, F.; Zhu, C.; Ding, Z.; Huang, X.; Zhang, T.; Zhang, Y. Chaperonin containing TCP1, subunit 8 (CCT8) is upregulated in hepatocellular carcinoma and promotes HCC proliferation. *APMIS* **2014**, *122*, 1070−1079.
(34) Qiu, X.; He, X.; Huang, Q.; Liu, X.; Sun, G.; Guo, J.; Yuan, D.; Yang, L.; Ban, N.; Fan, S.; Tao, T.; Wang, D. Overexpression of CCT8 and its significance for tumor cell proliferation, migration and invasion in glioma. *Pathol. Res. Pract.* **2015**, *211*, 717−725.
(35) Yang, X.; Ren, H.; Shao, Y.; Sun, Y.; Zhang, L.; Li, H.; Zhang, X.; Yang, X.; Yu, W.; Fu, J. Chaperonin-containing T-complex protein 1 subunit 8 promotes cell migration and invasion in human esophageal squamous cell carcinoma by regulating α-actin and β-tubulin expression. *Int. J. Oncol.* **2018**, *52*, 2021−2030.
(36) Fusaro, G.; Dasgupta, P.; Rastogi, S.; Joshi, B.; Chellappan, S. Prohibitin induces the transcriptional activity of p53 and is exported from the nucleus upon apoptotic signaling. *J. Biol. Chem.* **2003**, *278*, 47853−47861.
(37) Thuaud, F.; Ribeiro, N.; Nebigil, C. G.; Désaubry, L. Prohibitin ligands in cell death and survival: mode of action and therapeutic potential. *Chem. Biol.* **2013**, *20*, 316−331.
(38) Jia, L.; Yi, X. F.; Zhang, Z. B.; Zhuang, Z. P.; Li, J.; Chambers, S. K.; Kong, B. H.; Zheng, W. Prohibitin as a novel target protein of luteinizing hormone in ovarian epithelial carcinogenesis. *Neoplasma* **2011**, *58*, 104−109.
(39) Gregory-Bass, R. C.; Olatinwo, M.; Xu, W.; Matthews, R.; Stiles, J. K.; Thomas, K.; Liu, D.; Tsang, B.; Thompson, W. E. Prohibitin silencing reverses stabilization of mitochondrial integrity and chemoresistance in ovarian cancer cells by increasing their sensitivity to apoptosis. *Int. J. Cancer* **2008**, *122*, 1923−1930.
(40) Kim, J.-W.; Akiyama, M.; Park, J.-H.; Lin, M.-L.; Shimo, A.; Ueki, T.; Daigo, Y.; Tsunoda, T.; Nishidate, T.; Nakamura, Y.; Katagiri, T. Activation of an estrogen/estrogen receptor signaling by BIG3 through its inhibitory effect on nuclear transport of PHB2/REA in breast cancer. *Cancer Sci.* **2009**, *100*, 1468−1478.
(41) Mengwasser, J.; Piau, A.; Schlag, P.; Sleeman, J. P. Differential immunization identifies PHB1/PHB2 as blood-borne tumor antigens. *Oncogene* **2004**, *23*, 7430−7435.
(42) Martín, B.; Sanz, R.; Aragüés, R.; Oliva, B.; Sierra, A. Functional clustering of metastasis proteins describes plastic adaptation resources of breast-cancer cells to new microenvironments. *J. Proteome Res.* **2008**, *7*, 3242−3253.
(43) Maciver, S. K.; Hussey, P. J. The ADF/cofilin family: Actin remodeling proteins. *Genome Biol.* **2002**, *3*, No. reviews3007.1.
(44) Wang, Y.; Kuramitsu, Y.; Ueno, T.; Suzuki, N.; Yoshino, S.; Iizuka, N.; Zhang, X.; Oka, M.; Nakamura, K. Differential expression of up-regulated cofilin-1 and down-regulated cofilin-2 characteristic of pancreatic cancer tissues. *Oncol. Rep.* **2011**, *26*, 1595−1599.
(45) Li, G. B.; Cheng, Q.; Liu, L.; Zhou, T.; Shan, C. Y.; Hu, X. Y.; Zhou, J.; Liu, E. H.; Li, P.; Gao, N. Mitochondrial translocation of cofilin is required for allyl isothiocyanate-mediated cell death via ROCK1/PTEN/PI3K signaling pathway. *Cell Commun. Signal* **2013**, *11*, 50.
(46) Li, G.; Zhou, J.; Budhraja, A.; Hu, X.; Chen, Y.; Cheng, Q.; Liu, L.; Zhou, T.; Li, P.; Liu, E.; Gao, N. Mitochondrial translocation and interaction of cofilin and Drp1 are required for erucin-induced mitochondrial fission and apoptosis. *Oncotarget* **2015**, *6*, 1834−1849.
(47) Hensley, P. J.; Zetter, D.; Horbinski, C. M.; Strup, S. E.; Kyprianou, N. Association of epithelial-mesenchymal transition and nuclear cofilin with advanced urothelial cancer. *Hum. Pathol.* **2016**, *57*, 68−77.
(48) Maimaiti, Y.; Tan, J.; Liu, Z.; Guo, Y.; Yan, Y.; Nie, X.; Huang, B.; Zhou, J.; Huang, T. Overexpression of cofilin correlates with poor survival in breast cancer: A tissue microarray analysis. *Oncol. Lett.* **2017**, *14*, 2288−2294.
(49) Pappa, K. I.; Lygirou, V.; Kontostathi, G.; Zoidakis, J.; Makridakis, M.; Vougas, K.; Daskalakis, G.; Polyzos, A.; Anagnou, N. P. Proteomic analysis of normal and cancer cervical cell lines reveals deregulation of cytoskeleton-associated proteins. *Cancer Genomics Proteomics* **2017**, *14*, 253−266.
(50) Cairns, R. A.; Harris, I. S.; Mak, T. W. Regulation of cancer cell metabolism. *Nat. Rev. Cancer* **2011**, *11*, 85−95.
(51) Lin, R.; Elf, S.; Shan, C.; Kang, H. B.; Ji, Q.; Zhou, L.; Hitosugi, T.; Zhang, L.; Zhang, S.; Seo, J. H.; Xie, J.; Tucker, M.; Gu, T. L.; Sudderth, J.; Jiang, L.; Mitsche, M.; De Berardinis, R. J.; Wu, S.; Li, Y.; Mao, H.; Chen, P. R.; Wang, D.; Chen, G. Z.; Hurwitz, S. J.; Lonial, S.; Arellano, M. L.; Khoury, H. J.; Khuri, F. R.; Lee, B. H.; Lei, Q.; Brat, D. J.; Ye, K.; Boggon, T. J.; He, C.; Kang, S.; Fan, J.; Chen, J. 6-Phosphogluconate dehydrogenase links oxidative PPP, lipogenesis and tumour growth by inhibiting LKB1-AMPK signalling. *Nat. Cell Biol.* **2015**, *17*, 1484−1496.

DOI: 10.1021/acsomega.9b02512
ACS Omega 2019, 4, 21761−21777

(52) Zheng, W.; Feng, Q.; Liu, J.; Guo, Y.; Gao, L.; Li, R.; Xu, M.; Yan, G.; Yin, Z.; Zhang, S.; Liu, S.; Shan, C. Inhibition of 6-phosphogluconate dehydrogenase reverses cisplatin resistance in ovarian and lung cancer. *Front. Pharmacol.* **2017**, *8*, 421.
(53) Yang, X.; Peng, X.; Huang, J. Inhibiting 6-phosphogluconate dehydrogenase selectively targets breast cancer through AMPK activation. *Clin. Transl. Oncol.* **2018**, *20*, 1145−1152.
(54) Guo, H.; Xiang, Z.; Zhang, Y.; Sun, D. Inhibiting 6-phosphogluconate dehydrogenase enhances chemotherapy efficacy in cervical cancer via AMPK-independent inhibition of RhoA and Rac1. *Clin. Transl. Oncol.* **2019**, *21*, 404−411.
(55) Ma, L.; Cheng, Q. Inhibiting 6-phosphogluconate dehydrogenase reverses doxorubicin resistance in anaplastic thyroid cancer via inhibiting NADPH-dependent metabolic reprogramming. *Biochem. Biophys. Res. Commun.* **2018**, *498*, 912−917.
(56) Cao, Z.; Li, G.; Shao, Q.; Yang, G.; Zheng, L.; Zhang, T.; Zhao, Y. CHIP: A new modulator of human malignant disorders. *Oncotarget* **2016**, *7*, 29864−29874.
(57) Kurozumi, S.; Yamaguchi, Y.; Hayashi, S.; Hiyoshi, H.; Suda, T.; Gohno, T.; Matsumoto, H.; Takei, H.; Horiguchi, J.; Takeyoshi, I.; Oyama, T.; Kurosumi, M. Prognostic value of the ubiquitin ligase carboxyl terminus of the Hsc70-interacting protein in postmenopausal breast cancer. *Cancer Med.* **2016**, *5*, 1873−1882.
(58) Wang, S.; Wu, X.; Zhang, J.; Chen, Y.; Xu, J.; Xia, X.; He, S.; Qiang, F.; Li, A.; Shu, Y.; Røe, O. D.; Li, G.; Zhou, J. W. CHIP functions as a novel suppressor of tumour angiogenesis with prognostic significance in human gastric cancer. *Gut* **2013**, *62*, 496−508.
(59) Choi, Y. N.; Lee, S. K.; Seo, T. W.; Lee, J. S.; Yoo, S. J. C-Terminus of Hsc70-interacting protein regulates profilin1 and breast cancer cell migration. *Biochem. Biophys. Res. Commun.* **2014**, *446*, 1060−1066.
(60) Esser, C.; Scheffner, M.; Hohfeld, J. The chaperone-associated ubiquitin ligase CHIP is able to target p53 for proteasomal degradation. *J. Biol. Chem.* **2005**, *280*, 27443−27448.
(61) Narayan, V.; Pion, E.; Landre, V.; Muller, P.; Ball, K. L. Docking-dependent ubiquitination of the interferon regulatory factor-1 tumor suppressor protein by the ubiquitin ligase CHIP. *J. Biol. Chem.* **2011**, *286*, 607−619.
(62) Oh, K. H.; Yang, S. W.; Park, J. M.; Seol, J. H.; Iemura, S.; Natsume, T.; Murata, S.; Tanaka, K.; Jeon, Y. J.; Chung, C. H. Control of AIF-mediated cell death by antagonistic functions of CHIP ubiquitin E3 ligase and USP2 deubiquitinating enzyme. *Cell Death Differ.* **2011**, *18*, 1326−1336.
(63) Wen, J.; Luo, K. J.; Hu, Y.; Yang, H.; Fu, J. H. Metastatic lymph node CHIP expression is a potential prognostic marker for resected esophageal squamous cell carcinoma patients. *Ann. Surg. Oncol.* **2013**, *20*, 1668−1675.
(64) Xu, J.; Zhou, J.; Dai, H.; Liu, F.; Li, W.; Wang, W.; Guo, F. CHIP functions as an oncogene by promoting colorectal cancer metastasis via activation of MAPK and AKT signaling and suppression of E-cadherin. *J. Transl. Med.* **2018**, *16*, 169.
(65) Xia, D.; Stull, J. T.; Kamm, K. E. Myosin phosphatase targeting subunit 1 affects cell migration by regulating myosin phosphorylation and actin assembly. *Exp. Cell Res.* **2005**, *304*, 506−517.
(66) Su, L.; Nalle, S. C.; Shen, L.; Turner, E. S.; Singh, G.; Breskin, L. A.; Khramtsova, E. A.; Khramtsova, G.; Tsai, P. Y.; Fu, Y. X.; Abraham, C.; Turner, J. R. TNFR2 activates MLCK- dependent tight junction dysregulation to cause apoptosis-mediated barrier loss and experimental colitis. *Gastroenterology* **2013**, *145*, 407−415.
(67) Hanahan, D.; Weinberg, R. A. Hallmarks of cancer: the next generation. *Cell* **2011**, *144*, 646−674.
(68) Li, H. S.; Lin, Q.; Wu, J.; Jiang, Z. H.; Zhao, J. B.; Pan, J.; He, W. Q.; Zha, J. M. Myosin regulatory light chain phosphorylation is associated with leiomyosarcoma development. *Biomed. Pharmacother.* **2017**, *92*, 810−818.
(69) Yamashiro, S.; Yamakita, Y.; Totsukawa, G.; Goto, H.; Kaibuchi, K.; Ito, M.; Hartshorne, D. J.; Matsumura, F. Myosin phosphatase-targeting subunit 1 regulates mitosis by antagonizing polo-like kinase 1. *Dev. Cell* **2008**, *14*, 787−797.
(70) Zhou, X.; Liu, Y.; You, J.; Zhang, H.; Zhang, X.; Ye, L. Myosin light-chain kinase contributes to the proliferation and migration of breast cancer cells through cross-talk with activated ERK1/2. *Cancer Lett.* **2008**, *270*, 312−327.
(71) Andra, K.; Nikolic, B.; Stocher, M.; Drenckhahn, D.; Wiche, G. Not just scaffolding: plectin regulates actin dynamics in cultured cells. *Genes Dev.* **1998**, *12*, 3442−3451.
(72) Wiche, G. Role of plectin in cytoskeleton organization and dynamics. *J. Cell Sci.* **1998**, *111*, 2477−2486.
(73) Stegh, A. H.; Herrmann, H.; Lampel, S.; Weisenberger, D.; Andrä, K.; Seper, M.; Wiche, G.; Krammer, P. H.; Peter, M. E. Identification of the cytolinker plectin as a major early in vivo substrate for caspase 8 during CD95- and tumor necrosis factor receptor-mediated apoptosis. *Mol. Cell. Biol.* **2000**, *20*, 5665−5679.
(74) Katada, K.; Tomonaga, T.; Satoh, M.; Matsushita, K.; Tonoike, Y.; Kodera, Y.; Hanazawa, T.; Nomura, F.; Okamoto, Y. Plectin promotes migration and invasion of cancer cells and is a novel prognostic marker for head and neck squamous cell carcinoma. *J. Proteomics* **2012**, *75*, 1803−1815.
(75) Nagle, R. B.; Hao, J.; Knox, J. D.; Dalkin, B. L.; Clark, V.; Cress, A. E. Expression of hemidesmosomal and extracellular matrix proteins by normal and malignant human prostate tissue. *Am. J. Pathol.* **1995**, *146*, 1498−1507.
(76) Lee, K. Y.; Liu, Y. H.; Ho, C. C.; Pei, R. J.; Yeh, K. T.; Cheng, C. C.; Lai, Y. S. An early evaluation of malignant tendency with plectin expression in human colorectal adenoma and adenocarcinoma. *J. Med.* **2004**, *35*, 141−149.
(77) Kelly, K. A.; Bardeesy, N.; Anbazhagan, R.; Gurumurthy, S.; Berger, J.; Alencar, H.; Depinho, R. A.; Mahmood, U.; Weissleder, R. Targeted nanoparticles for imaging incipient pancreatic ductal adenocarcinoma. *PLoS Med.* **2008**, *5*, No. e85.
(78) Boczonadi, V.; McInroy, L.; Maatta, A. Cytolinker cross-talk: periplakin N-terminus interacts with plectin to regulate keratin organisation and epithelial migration. *Exp. Cell Res.* **2007**, *313*, 3579−3591.
(79) Burch, T. C.; Watson, M. T.; Nyalwidhe, J. O. Variable metastatic potentials correlate with differential plectin and vimentin expression in syngeneic androgen independent prostate cancer cells. *PLoS One* **2013**, *8*, No. e65005.
(80) Coulombe, P. A.; Wong, P. Cytoplasmic intermediate filaments revealed as dynamic and multipurpose scaffolds. *Nat. Cell Biol.* **2004**, *6*, 699−706.
(81) Biamonte, F.; Santamaria, G.; Sacco, A.; Perrone, F. M.; Di Cello, A.; Battaglia, A. M.; Salatino, A.; Di Vito, A.; Aversa, I.; Venturella, R.; Zullo, F.; Costanzo, F. MicroRNA let-7g acts as tumor suppressor and predictive biomarker for chemoresistance in human epithelial ovarian cancer. *Sci. Rep.* **2019**, *9*, No. 5668.
(82) Satelli, A.; Li, S. Vimentin in cancer and its potential as a molecular target for cancer therapy. *Cell Mol. Life Sci.* **2011**, *68*, 3033−3046.
(83) Lehtinen, L.; Ketola, K.; Makela, R.; Mpindi, J. P.; Viitala, M.; Kallioniemi, O.; Iljin, K. High-throughput RNAi screening for novel modulators of vimentin expression identifies MTHFD2 as a regulator of breast cancer cell migration and invasion. *Oncotarget* **2013**, *4*, 48−63.
(84) Tadokoro, A.; Kanaji, N.; Liu, D.; Yokomise, H.; Haba, R.; Ishii, T.; Takagi, T.; Watanabe, N.; Kita, N.; Kadowaki, N.; Bandoh, S. Vimentin Regulates Invasiveness and Is a Poor Prognostic Marker in Non-small Cell Lung Cancer. *Anticancer Res.* **2016**, *36*, 1545−1551.
(85) Du, L.; Li, J.; Lei, L.; He, H.; Chen, E.; Dong, J.; Yang, J. High vimentin expression predicts a poor prognosis and progression in colorectal cancer: a study with meta-analysis and TCGA database. *Biomed. Res. Int.* **2018**, *2018*, No. 6387810.
(86) Franke, W. W.; Grund, C.; Kuhn, C.; Jackson, B. W.; Illmensee, K. Formation of cytoskeletal elements during mouse embryogenesis. III. Primary mesenchymal cells and the first appearance of vimentin filaments. *Differentiation* **1982**, *23*, 43−59.

DOI: 10.1021/acsomega.9b02512
ACS Omega 2019, 4, 21761−21777

(87) Liu, C. Y.; Lin, H. H.; Tang, M. J.; Wang, Y. K. Vimentin contributes to epithelial-mesenchymal transition cancer cell mechanics by mediating cytoskeletal organization and focal adhesion maturation. *Oncotarget* **2015**, *6*, 15966−15983.
(88) Su, W.; Ito, T.; Oyama, T.; Kitagawa, T.; Yamori, T.; Fujiwara, H.; Matsuda, H. The direct effect of IL-12 on tumor cells: IL-12 acts directly on tumor cells to activate NF-kappaB and enhance IFN-gamma-mediated STAT1 phosphorylation. *Biochem. Biophys. Res. Commun.* **2001**, *280*, 503−512.
(89) Carvalho, P. C.; Lima, D. B.; Leprevost, F. V.; Santos, M. D.; Fischer, J. S.; Aquino, P. F.; Moresco, J. J.; Yates, J. R., 3rd; Barbosa, V. C. Integrated analysis of shotgun proteomic data with PatternLab for proteomics 4.0. *Nat. Protoc.* **2016**, *11*, 102−117.
(90) Royston, P. Multiple imputation of missing values. *Stata J.* **2004**, 227−241.
(91) Rubin, D. B. *Multiple Imputation for Non-response in Surveys*; John Wiley & Sons: New York, 1987.

DOI: 10.1021/acsomega.9b02512
ACS Omega 2019, 4, 21761−21777

Conclusões

O presente estudo avaliou o efeito das imunoterapias com P-MAPA e IL-12, isolados ou combinados, na agressividade e na via de sinalização dos TLRs. Foi observado que ambos os tratamentos produzem efeitos anti-tumorigênicos nas células SKOV-3, como redução da viabilidade, metabolismo e motilidade celular. O P-MAPA é capaz de diminuir o potencial invasivo das células tumorais e de aumentar a sensibilidade das mesmas ao tratamento com paclitaxel. A terapia combinada com P-MAPA e IL-12 apresenta um potente efeito na via de sinalização dos TLRs, sendo capaz de diminuir os níveis de moléculas adaptadoras e produtos finais envolvidos na indução da inflamação e, potencialmente, na quimiorresistência das células de câncer de ovário. Particularmente, o tratamento com P-MAPA e P-MAPA+IL-12 estimula a secreção de mediadores pró e anti-inflamatórios, sendo capaz de modular eficientemente a imunogenicidade do microambiente tumoral. Adicionalmente, através da estratégia de análise proteômica global, observa-se que o P-MAPA e IL-12 isolados regulam os níveis de proteínas estruturais e de sinalização celular tradicionalmente envolvidas na progressão do câncer. A associação dos dois compostos também promove a modulação de importantes proteínas envolvidas em diversos processos celulares, como oxidação celular, senescência, processos metabólicos e energéticos, alterações estas que podem levar à instabilidade das células tumorais, disfunções metabólicas e resultar no aumento dos índices de morte celular. Este trabalho descreve uma série de efeitos importantes dos compostos P-MAPA e IL-12 que os tornam potenciais candidatos a estudos mais aprofundados de seus papéis como agentes adjuvantes para o tratamento do câncer de ovário, uma vez que, além de seu conhecido efeito na modulação do sistema imune, também influenciam diretamente as células tumorais ovarianas, favorecendo a eficácia dos tratamentos mais tradicionais e reduzindo a sua agressividade.

Referências bibliográficas

AHMED, A.A.; ETEMADMOGHADAM, D.; TEMPLE, J.; LYNCH, A.G.; RIAD, M.; SHARMA, R.; *et al*. Driver mutations in TP53 are ubiquitous in high grade serous carcinoma of the ovary. **The Journal of Pathology**, v.221; v.49-56, 2010.

AKIRA, S.; TAKEDA, K. Toll-like receptor signalling. **Nature Reviews Immunology**, v.4, p.499-511, 2004.

AMERICAN TYPE CULTURE COLLECTION. SK-OV-3 [SKOV-3; SKOV3] (ATCC® HTB-77™) Product Sheet. Disponível em: https://www.atcc.org/products/all/HTB-77.aspx#characteristics. Acesso em: 08 de agosto de 2019.

BASITH, S.; MANAVALAN, B.; LEE, G.; KIM, S.G.; CHOI, S. Toll-like receptormodulators: a patent review (2006–2010). **Expert Opinion on Therapeutic Patents**, v.21, 927-944, 2011.

BAST, R.C. JR.; HENNESSY, B.; MILLS, G.B. The biology of ovarian cancer: New opportunities for translation. **Nature Reviews Cancer**, v.9, p.415-428, 2009.

BEREK, J.S.; KEHOE, S.T.; KUMAR, L.; FRIEDLANDER, M. Cancer of the ovary, fallopian tube, and peritoneum. **International Journal of Gynecology & Obstetrics**, v.143, p.59-78, 2018.

BOYD, J. Specific keynote: hereditary ovarian cancer: what we know. **Gynecologic Oncology**, v.88, p.S8e10, 2003.

CHEN, S.S.; MICHAEL, A.; BUTLER-MANUEL, S.A. Advances in the treatment of ovarian cancer: a potential role of antiinflammatory phytochemicals. **Discovery Medicine**, v.13, p.7-17, 2012.

CHUFFA, L.G.: DE MOURA FERREIRA, G.: LUPI, L.A.; DA SILVA NUNES, I.; FÁVARO, W.J. P-MAPA immunotherapy potentiates the effect of cisplatin on serous ovarian carcinoma through targeting TLR4 signaling. **Journal of Ovarian Research**, v.11, p.8, 2018.

COLOMBO, M.P.; TRINCHIERI, G. Interleukin-12 in anti-tumor immunity and immunotherapy. **Cytokine & Growth Factor Reviews**, v.13, p.155-168, 2002.

CUI, J.; SHIN, T.; KAWANO, T.; SATO, H.; KONDO, E.; TOURA, I.; *et al.* Requirement for Valpha14 NKT cells in IL-12-mediated rejection of tumors. **Science**, v.278, p.1623-1626, 1997.

D'ADHEMAR, C.J.; SPILLANE, C.D.; GALLAGHER, M.F.; BATES, M.; COSTELLO, K.M.; BARRY-O'CROWLEY, J.; *et al*. The MyD88+ phenotype is an adverse prognostic factor in epithelial ovarian cancer. **PLoS One**, v.9, p.e100816, 2014.

DAJON, M.; IRIBARREN, K.; CREMER, I. Toll-like receptor stimulation in cancer: A pro- and anti-tumor double-edged sword. **Immunobiology**, v.222, p.89-100, 2017.

DANGELO, J.G.; FATTINI, C.A. Anatomia humana sistêmica e segmentar. 3 ed. São Paulo: Editora Atheneu, 2007.

DUSKA, L.R.; KOHN, E.C. The new classifications of ovarian, fallopian tube, and primary peritoneal cancer and their clinical implications. **Annals of Oncology**, v.28, p.viii8-viii12, 2017.

FARMABRASILIS. P-MAPA, Propriedades gerais da molécula. Disponível em: http://www.farmabrasilis.org/todos_conteudos_interna.php?idioma=br&id=108. Acesso em: 08 de agosto de 2019.

FÁVARO, W.J.; NUNES, O.S.; SEIVA, F.R.; NUNES, I.S.; WOOLHISER, L.K.; DURÁN, N.; *et al*. Effects of P-MAPA Immunomodulator on toll-like receptors and p53: potential therapeutic strategies for infectious diseases and cancer. **Infectious Agents and Cancer**, v.7, p.14, 2012.

FITZGERALD, K.A.; ROWE, D.C.; BARNES, B.J.; CAFFREY, D.R.; VISINTIN, A.; LATZ, E.; *et al*. LPS-TLR4 signaling to IRF-3/7 and NF-kappaB involves the toll adapters TRAM and TRIF. **Journal of Experimental Medicine**, v.198, p.1043-1055, 2003.

GATA, V.; FLORIN LAURENTIU, I. The role of Toll-like receptors in ovarian cancer. **Journal of the Balkan Union of Oncology**, v.22, p.1092-1096, 2017.

HOPKINS, P.A., SRISKANDAN, S. Mammalian Toll-like receptors: to immunityand beyond. **Clinical and Experimental Immunology**, v.140, p.395-407, 2005.

HUANG, B.; ZHAO, J.: LI, H.; HE, K.L.; CHEN, Y.; CHEN, S.H.; *et al*. Toll-like receptors on tumor cells facilitate evasion of immune surveillance. **Cancer Research**, v.65, p.5009-5014, 2005.

HURTEAU, J.A.; BLESSING, J.A.;DeCESARE, S.L., CREASMAN, W.T. Evaluation of recombinant human interleukin-12 in patients with recurrent or refractory ovarian cancer: a gynecologic oncology group study. **Gynecologic Oncology**, v.82, p.7-10, 2001.

INSTITUTO NACIONAL DO CÂNCER. Estatísticas de câncer. Disponível em: https://www.inca.gov.br/numeros-de-cancer. Acesso em: 24 de julho de 2019.

JESSMON, P.; BOULANGER, T.; ZHOU, W.; PATWARDHAN, P. Epidemiology and treatment patterns of epithelial ovarian cancer. **Expert Review of Anticancer Therapy**, v.17, p.427-437, 2017.

JONES, S.; WANG, T.L.; SHIH, I.M.; MAO, T.L.; NAKAYAMA, K.; RODEN, R.; *et al.* Frequent mutations of chromatin remodeling gene ARID1A in ovarian clear cell carcinoma. **Science**, v.330, p.228-231, 2010.

JUNQUEIRA, L.C.U; CARNEIRO, J. Histologia básica. 12 ed. Rio de Janeiro: Guanabara Koogan, 2013.

KAWAI, T.; AKIRA, S. The role of pattern-recognition receptors in innateimmunity: update on Toll-like receptors. **Nature Immunology**, v.11, p.373-384, 2010.

KAWANO, T.; CUI, J.; KOEZUKA, Y.; TOURA, I.; KANEKO, Y.; MOTOKI, K.; *et al*. CD1d-restricted and TCR-mediated activation of valpha14 NKT cells by glycosylceramides. **Science**, v.278, p.1626-1629, 1997.

KRISHNAN, V.; BEREK, J.S.; DORIGO, O. Immunotherapy in ovarian cancer. **Current Problems in Cancer**, v.41, p.48-63, 2017.

KROEGER, P.T. JR.; DRAPKIN, R. Pathogenesis and heterogeneity of ovarian cancer. **Current Opinion in Obstetrics and Gynecology**, v.29, p.26-34, 2017.

KURMAN, R.J.; SHIH, I.M. Molecular pathogenesis and extraovarian origin of epithelial ovarian cancer--shifting the paradigm. **Human Pathology**, v.42, p.918-931, 2011.

LA VECCHIA, C. Ovarian cancer: epidemiology and risk factors. **European Journal of Cancer Prevention**, v.26, p.55-62, 2017.

LEDERMANN, J.A.; RAJA, F.A.; FOTOPOULOU, C.; GONZALEZ-MARTIN, A.; COLOMBO, N.; SESSA, C.; ESMO GUIDELINES WORKING GROUP. Newly diagnosed and relapsed epithelial ovarian carcinoma: ESMO clinical practice guidelines for diagnosis, treatment and follow-up. **Annals of Oncology**, v.S6, p.24-32, 2013.

LI, Q.; VERMA, I.M. NF-κB regulation in the immune system. **Nature Reviews Immunology**, v.2, p.725-734, 2002.

LISIO, M.A.; FU, L.; GOYENECHE, A.; GAO, Z.H.; TELLERIA, C. High-grade serous ovarian cancer: basic sciences, clinical and therapeutic standpoints. **International Journal of Molecular Sciences**, v.20, p.E952, 2019.

LUAN, N.N.; WU, Q.J.; GONG, T.T.; VOGTMANN, E.; WANG, Y.L.; LIN, B. Breastfeeding and ovarian cancer risk: a meta-analysis of epidemiologic studies. **The American Journal of Clinical Nutrition**, v.98, p.1020e31, 2013.

LUPI, L.A.; DELELLA, F.K.; CUCIELO, M.S.; ROMAGNOLI, G.G.; KANENO, R.; NUNES, I.D.S.; *et al*. P-MAPA and interleukin-12 reduce cell migration/invasion and attenuate the toll-like receptor-mediated inflammatory response in ovarian cancer SKOV-3 Cells: a preliminary study. **Molecules**, v.25, p.E5, 2019.

MA, X.; CHOW, J.M.; GRI, G.; CARRA, G.; GEROSA, F.; WOLF, S.F.; *et al*. The interleukin 12 p40 gene promoter is primed by interferon gamma in monocytic cells. **Journal of Experimental Medicine**, v.183, p.147-157, 1996.

MARKMAN, M. Optimizing primary chemotherapy in ovarian cancer. **Hematology/Oncology Clinics of North America**, v.17, p.957-968, 2003.

MATULONIS, U.A.; SOOD, A.K.; FALLOWFIELD, L.; HOWITT, B.E.; SEHOULI, J.; KARLAN, B.Y. Ovarian cancer. **Nature Reviews Disease Primers**, v.2, p.16061, 2016.

MEDZHITOV, R., PRESTON-HURLBURT, P., JANEWAY, C.A. A human homologue ofthe Drosophila Toll protein signals activation of adaptive immunity. **Nature**, v.388, p.394-397, 1997.

MUCCIOLI, M.; SPRAGUE, L.; NANDIGAM, H.; PATE, M.; BENENCIA, F. Toll-like receptors as novel therapeutic targets for ovarian cancer. **ISRN Oncology**, v.2012, p.642141, 2012.

NEWTON, K.; DIXIT, V.M. Signaling in innate immunity and inflammation. **Cold Spring Harbor Perspectives in Biology**, v.4, p.a006049, 2012.

PATEL, H.; SHAW, S.G.; SHI-WEN, X.; ABRAHAM, D.; BAKER, D.M.; TSUI, J.C. Toll-like receptors in ischaemia and its potential role in the pathophysiology of muscle damage in critical limb ischaemia. **Cardiology Research and Practice**, v.2012, p.121237, 2012.

ROCK, F.L.; HARDIMAN, G.; TIMANS, J.C.; KASTELEIN, R.A.; BAZAN, J.F. A family of human receptors structurally related to Drosophila Toll. **Proceedings of the National Academy of Sciences**, v.95, p.588-593, 1998.

SATO, Y.; GOTO, Y.; NARITA, N.; HOON, D.S. Cancer cells expressing toll-like receptors and the tumor microenvironment. **Cancer Microenvironment**, v.2, p.205-214, 2009.

SHIH, I.M.; KURMAN, R.J. Ovarian tumorigenesis- a proposed model based on morphological and molecular genetic analysis. **The American Journal of Pathology**, v.164, p.1511-1518, 2004.

SIEGEL, R.L.; MILLER, K.D.; JEMAL, A. Cancer statistics, 2019. **CA: A Cancer Journal for Clinicians**, v.69, p.7-34, 2019.

SILVER, D.F.; HEMPLING, R.E.: PIVER, M.S.; REPASKY, E.A. Effects of IL-12 on human ovarian tumors engrafted into SCID mice. **Gynecologic Oncology**, v.72, p.154-160, 1999.

SMYTH, M.J.; CROWE, N.Y.; HAYAKAWA, Y.; TAKEDA, K.; YAGITA, H.; GODFREY, D.I. NKT cells - conductors of tumor immunity? **Current Opinion in Immunology**, v.14, p.165-171, 2002.

STRATTON, J.F.; PHAROAH, P.; SMITH, S.K.; EASTON, D.; PONDER, B.A. A systematic review and meta-analysis of family history and risk of ovarian cancer. **British Journal of Obstetrics and Gynaecology**, v.105, p.493e9, 1998.

TAKEDA, K.; AKIRA, S. Toll-like receptors. **Current Protocols in Immunology**, v.109, p.1-10, 2015.

TRINCHIERI, G. Interleukin-12: a proinflammatory cytokine with immunoregulatory functions that bridge innate resistance and antigen specific adaptive immunity. **Annual Review of Immunology**, v.13, p.251-276, 1995.

USACH, I.; BLANSIT, K.; CHEN, L.M.; UEDA, S.; BROOKS, R.; KAPP, D.S.; CHAN, J.K. Survival differences in women with serous tubal, ovarian, peritoneal, and uterine carcinomas. **American Journal of Obstetrics and Gynecology**, v.212, p.188.e181-188.e186, 2015.

WEBB, P.M.; JORDAN, S.J. Epidemiology of epithelial ovarian cancer. **Best Practice & Research: Clinical Obstetrics & Gynaecology**, v.41, p.3-14, 2017.

WENTZENSEN, N.; POOLE, E.M.; TRABERT, B.; WHITE, E.; ARSLAN, A.A.; PATEL, A.V.; *et al.* Ovarian cancer risk factors by histologic subtype: an analysis from the Ovarian Cancer Cohort Consortium. **Journal of Clinical Oncology**, v.34, p.2888e98, 2016.

WIEGAND, K.C.; SHAH, S.P.; AL-AGHA, O.M.; ZHAO, Y.; TSE, K.; ZENG, T.; *et al*. ARID1A mutations in endometriosis-associated ovarian carcinomas. **The New England Journal of Medicine**, v.363, p.1532-1543, 2010.

YANG, J.M.; HUNG, C.M.; FU, C.N.; LEE, J.C.; HUANG, C.H.; YANG, M.H.; *et al*. Hispidulin sensitizes human ovarian cancer cells to TRAIL-induced apoptosis by AMPK

activation leading to Mcl-1 block in translation. **Journal of Agricultural and Food Chemistry**, v.58, p.10020-10026, 2010.

ZHOU, M.; MCFARLAND-MANCINI, M.M.; FUNK, H.M.; HUSSEINZADEH, N.; MOUNAJJED, T.; DREW, A.F. Toll-like receptor expression in normal ovary and ovarian tumors. **Cancer Immunology, Immunotherapy**, v.58, p.1375-1385, 2009.

ZHU, Y.; HUANG, J.M.; ZHANG, G.N.; ZHA, X.; DENG BF. Prognostic significance of MyD88 expression by human epithelial ovarian carcinoma cells. **Journal of Translational Medicine**, v.10, p.77, 2012.